FINITE ELEMENT ANALYSIS OF
CORNERING CHARACTERISTICS OF ROTATING TIRES

A THESIS SUBMITTED TO

THE GRADUATE SCHOOL OF NATURAL AND APPLIED SCIENCES

OF

THE MIDDLE EAST TECHNICAL UNIVERSITY

BY

MEHMET AKİF ERŞAHİN

IN PARTIAL FULFILLMENT OF THE REQUIREMENTS FOR THE DEGREE

OF

DOCTOR OF PHILOSOPHY

IN

THE DEPARTMENT OF MECHANICAL ENGINEERING

SEPTEMBER 2003

Approval of the Graduate School of Natural and Applied Sciences

———————————————
Prof. Dr. Canan ÖZGEN
Director

I certify that this thesis satisfies all the requirements as a thesis for the degree of Doctor of Philosophy.

———————————————
Prof. Dr. Kemal İDER
Head of Department

This is to certify that we have read this thesis and that in our opinion it is fully adequate, in scope and quality, as a thesis for the degree of Doctor of Philosophy.

———————————————
Prof. Dr. Y. Samim ÜNLÜSOY
Supervisor

Examining Committee Members

Prof. Dr. Y. Samim ÜNLÜSOY   ———————————————

Prof. Dr. A. Erman TEKKAYA   ———————————————

Asst.Prof. Dr. Ergin TÖNÜK   ———————————————

Dr. Engin KARAESMEN   ———————————————

Asst.Prof. Dr. Şebnem ÖZÜPEK   ———————————————

ABSTRACT

FINITE ELEMENT ANALYSIS OF
CORNERING CHARACTERISTICS OF ROTATING TIRES

Erşahin, Mehmet Akif

Ph. D., Department of Mechanical Engineering

Supervisor: Prof. Dr. Y. Samim Ünlüsoy

September 2003, 157 pages

A finite element model is developed to obtain the cornering force characteristics for rotating pneumatic tires which combines accuracy together with substantially reduced computational effort.

For cord reinforced rubber sections such as the body plies and breaker belts, continuum elements with orthotropic material properties are used to improve solution times. Drastic reductions in computational effort are then obtained by replacing the continuum elements with truss elements which do not require orientation of element coordinate system to model textile body plies. With these simplifications, new model can be used produce a complete carpet plot of cornering force characteristics in substantially reduced solution times.

The finite element model is used to obtain the cornering force characteristics of a tire, simulating the experiments on a tire test rig where the tire rotates on a flywheel. Results from both models are compared with each other and with the experimental results. It is concluded that the model developed provides results at least as accurate as the previously published models with a clear superiority in stability of solution.

Keywords: Pneumatic Tire, Cornering Force Characteristics, Cord Rubber Modeling, Finite Element Analysis

ÖZ

OTOMOBİL LASTİKLERİNİN YANAL KUVVET KARAKTERİSTİKLERİNİN SONLU ELEMANLAR YÖNTEMİYLE ANALİZİ

Erşahin, Mehmet Akif

Doktora, Makina Mühendisliği Bölümü

Tez Yöneticisi: Prof. Dr. Y. Samim Ünlüsoy

Pnömatik otomobil lastiklerinin yanal kuvvet karakteristiklerini elde etmek amacına yönelik, hassas ve hızlı çözümler verecek bir sonlu elemanlar modeli geliştirilmiştir.

Otomobil lastiğinin çelik tel ve tekstil ipliklerle güçlendirilmiş kuşak ve gövde katları, ortotropik malzeme özellikleri taşıyan katı elemanlar kullanılarak modellenerek çözüm süreleri kısaltılmıştır. Tekstil gövde katları, daha sonra, koordinat sistemi transformasyonuna gerek kalmadan çözüm yapabilmek ve çözüm süresini önemli oranda azaltabilmek için eğilme rijitliği olmayan çubuk elemanlar kullanan bir model geliştirilmiştir. Gerçekleştirilen basitleştirmeler sonucu, yeni modelle tam bir yanal kuvvet karakteristikleri takımının hesaplanmasında önemli ölçüde zaman kazanmak mümkün olmaktadır.

Sonlu elemanlar modeli volan üzerinde dönen bir lastiğin yanal kuvvet karakteristiklerinin elde edilmesinde kullanılarak, lastik deney aygıtında yapılan testlerin simülasyonu yapılmıştır. Her iki modelden elde edilen sonuçlar birbirleri ile ve deneysel sonuçlarla karşılaştırılmıştır. Karşılaştırmalar sonucunda geliştirilen modelin, en az literatürde mevcut modeller kadar hassas sonuçlar verirken, çözüm stabilitesi yönünden ise hepsinden üstün olduğu sonucuna varılmıştır.

Anahtar Kelimeler: Otomobil Lastiği, Yanal Kuvvet Karakteristikleri, İplik Kauçuk Modelleme, Sonlu Elemanlar Analizi

To the Memory of my Grandmother
Hayriye Erşahin
And to the New Life of my Little Niece
Pelin Erşahin

ACKNOWLEDGMENTS

TABLE OF CONTENTS

LIST OF TABLES

TABLE

LIST OF FIGURES

LIST OF SYMBOLS

E	Young's Modulus
E_1	Young's Modulus in Direction 1
E_2	Young's Modulus in Direction 2
E_3	Young's Modulus in Direction 3
E_c	Young's Modulus of Cord
E_r	Young's Modulus of Rubber
E_f	Young's Modulus of Fiber
E_m	Young's Modulus of Matrix
C_{ij}	Stifness Matrix
S_{ij}	Compliance Matrix
G	Shear Modulus
G_{12}	Shear Modulus in 12 Plane
G_{13}	Shear Modulus in 13 Plane
G_{23}	Shear Modulus in 23 Plane
G_c	Shear Modulus of Cord
G_r	Shear Modulus of Rubber
K	Bulk Modulus

υ	Poisson's Ratio
L	Length
ΔL	Elongation
σ	Stress
σ_n	Normal Contact Stress
σ_i	Stress Contracted Notation
σ_{fr}	Tangential Friction Stress
ε	Engineering Strain
θ	Cord Angle
F	Force
W	Strain Energy Density Function
t	Thickness
γ	Shear Strain
v_c	Volume Fraction of Cord
v_r	Volume Fraction of Rubber
v_f	Volume Fraction of Fiber
v_m	Volume Fraction of Matrix
V	Strain Energy
α	Slip Angle
F_c	Cornering Force
F_t	Traction Force

F_n	Normal Force
SAT	Self Aligning Torque
μ	Friction Coefficient
I_1	First Strain Invariant
I_2	Second Strain Invariant
I_3	Third Strain Invariant
λ	Extension Ratio
C_{10}	Mooney-Rivlin Constant
C_{01}	Mooney-Rivlin Constant
p	Pressure

CHAPTER 1

INTRODUCTION

In this Chapter, a brief history of tires will be presented and construction, types, and nomenclature of pneumatic tires will be explained. The main idea, goals and contents of the study will also be introduced briefly.

1.1 History of Tire

Tires began originally as a durable material circling a fragile wheel such as a steel hoop on a spoked wooden wagon wheel. So when inventors came up with better tires, these were not similar to the pneumatic rubber tires we know today. They were treated more as an outer layer on a wheel rather than as an independent structure.

Vulcanization discovered in 1839 by Charles Goodyear, made rubber a durable and elastic engineering material, good enough for tires for the first time. But the earliest air-filled tires did not include direct use of rubber. They were buggy tires invented by Robert William Thomson, a Scottish engineer who in 1845 patented a riveted leather wrap bolted to the wheel rims, supported by an inflated rubber-coated canvas inner tube. That patent's description of the function of a pneumatic tire still applies. It reads in part: "the application of elastic bearings around the tires of the wheels of carriages…a hollow belt composed of some air or water tight material…inflating it with air whereby the wheels will, in every part of their revolution, present a cushion of air to the ground." Not until the 1888 patent issued to John Boyd Dunlop, a British veterinary surgeon

however, did inflated rubber tires come into their own, at first for bicycles and tricycles (including that of Dunlop's nine-year old son, whose bumpy rides had inspired the invention). Carriages and wagons also used pneumatic fires, and when automobiles came along, the first ones fitted to them were so called clincher tires. These had "beads," or inner rims, made of rubber and formed with a barb to let a mechanical fastener hold them on. Soon after, other inventors brought forward the idea of using a wire cable to form the bead of the tire, with that bead nesting inside a flange on the outer rim of the wheel - the so called straight sided tire. At about the same time, tire treads began thickening and being patterned for better traction.

In the 1930s, new, synthetic materials such as rayon replaced cotton in the tires' plies, greatly improving the strength of their cord reinforcement. Synthetic rubber for increased durability emerged in Germany in the late 1930s. Then tubeless tires a wartime project of B. F. Goodrich for which a patent was granted in 1952, melded all of the Pneumatic tire's features into the angle, durable unit today's drivers are familiar with.

The concept of radial tires had been introduced in 1914, when two Englishmen named Gray and Sloper, of the Palmer Tyre Company, had received a patent for the idea. Gray and Sloper, had crossed cables around the perimeter of the tire radially, or straight out from the rim, to try to stiffen the tire sidewall Their tire was never put into production (it seems to have had inherent design flaws, and in any case the technology for bonding steel to rubber was not yet developed), but the idea lingered, particularly at Michelin. By the late 1930s the company was using rubber-encapsulated steel cord to reinforce bias-ply tires for trucks, selling the tires under the name Metallic. During the German occupation in World War II, a Michelin engineer named Marius Mignol worked with existing steel technology to fashion what he called a "cold" tire because it reduced the heat generated by internal friction. He achieved this by placing steel

plies radially across the tire. Although Mignol's experimental tire was not roadworthy, it ran cooler and with less rolling resistance than conventional tires. It had no directional control or stability, however, until he fitted an additional layer of steel belts lengthwise along its circumference. In mock derision, his fellow engineers called the resulting network of steel, a *cage á mouches*, or flying cage, because it looked like wire screening.

Michelin applied for a patent on die invention in 1946; it was granted in 1951. After refining its components further and testing the market, Michelin introduced its "X" tire in two sizes at the *Salon de I'Automobile* in Paris in October 1949. The company's part ownership of the automaker Citroen allowed it to put the near tire turn production on the innovative front wheel drive 11-CV cu. Even Michelin's own engineers could hardly believe what they had stumbled onto. Their innovation at least doubled the tread life of conventional tires and premised improvement far beyond that.

The radial's key advantage, they found, was that it could set its tread on the ground without the squirm and friction of a bias tire. The constraint of the steel belts, which would neither elongate nor compress, kept the tread from distorting and radial cording made the sidewalls more flexible increasing the tread's ability to conform to the road.The tire's reduced friction and squirm not only lessened wear but also produced fuel savings of more than 3 percent.

In 1962, a Ford engineer named Jacques Bajer and his team put together an experimental piece of test equipment they called a tire-uniformity machine to retrieve dynamic data on what went on as a wheel rolled under pressure. Such machines have since become common place and refined. Bajer stressed the need to analyze tire, vehicle and road together rather than think of the tire alone. His persistence led to a string of Society of Automotive Engineers; publications

explaining numerical analyses of skid and rolling resistance, wet traction, nonuniformity among tires and the behavior of radial tires on American cars.

1.2 Tire Construction

A view of the elements of construction of a typical radial passenger car tire is shown in Figure 1.1.
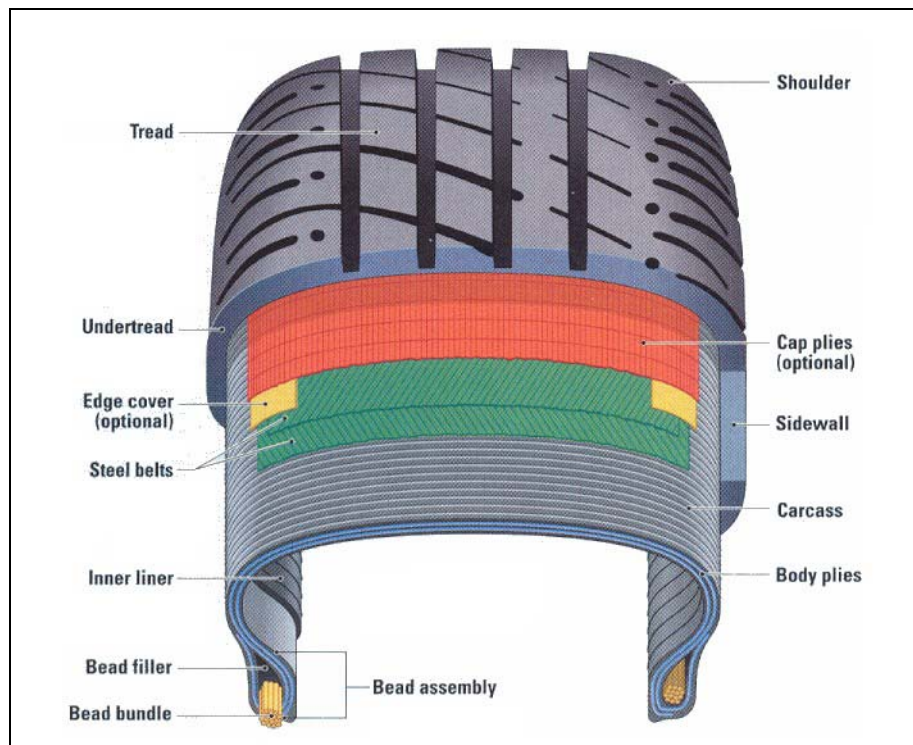
Figure 1.1 Section View of a Typical Radial Passenger Car Tire (Invention & Technology, 2001)

The main parts of the pneumatic tire, their functions and construction are given below.

The tread, usually attracts the most attention. The material used is referred to as tread compound, which varies from one tire design to the next. A winter tire, for example, has a compound that provides maximum traction in cold

weather. Racing tires, at the other extreme, use a compound designed for very high temperature ranges. The great majority of tires are built with an all season compound that delivers traction in the broad middle range of every day driving conditions. In addition, this compound must deliver good wear. The tread block provides traction at its leading and trailing edge. Within the block, sipes are often molded or cut to provide additional traction. Grooves are built into tread designs for channeling away water. Shoulder designs provide protection as well as additional traction during hard cornering. A detailed picture of the tread is given in Figure 1.2.
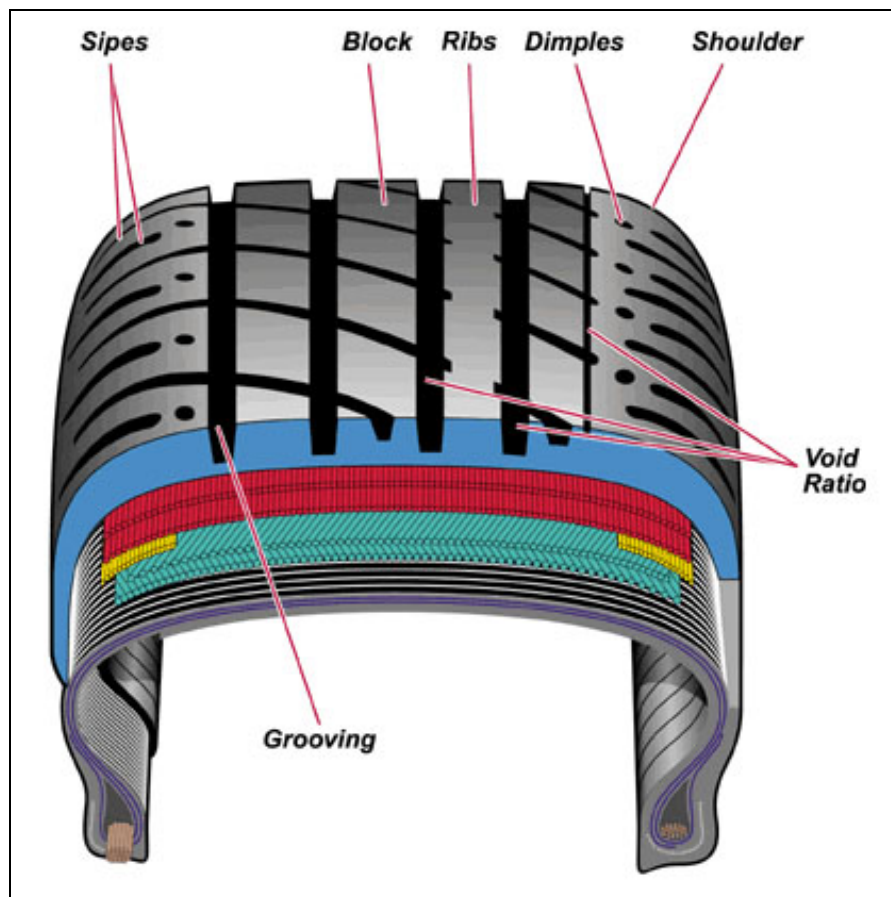
Figure 1.2 Tread Pattern (Invention & Technology, 2001)

Bead is the portion of the tire that helps keep it in contact with the rim of the wheel. It provides the air seal and is constructed of a heavy band of steel wire

called Bead Bundle. It is encased in the tire carcass around the inner circumference

Carcass can be named as "tire's load bearing frame work". The carcass's function is to maintain the shape of the tire and it must be strong enough to hold the air pressure of the tire and withstand external loads.

Body plies are rubberized fabric and cords wrapped around the beads forming the carcass or body of the tire.The cords are usually made of rayon, nylon, and glass fiber for the body plies. The plies determine the strength of the tire structure.

Layers of circumferential belts, commonly called breaker belts, are used to stiffen the tread and strengthen the plies; they lie between the tread and the inner plies. Steel cords used in breaker belts provide a stable foundation for better tread wear and traction, and also protect the casing against impacts and punctures. They provide circumferential rigidity to prevent elongation under the effect of centrifugal force, and thus ensure an almost constant tire diameter under all conditions. They also provide lateral rigidity. By restricting tread movement during contact with the road, the belt plies improve tread life. To make the steel plies, the metal wires must be firmly bonded into the rubber. Perfect bonding between these two highly dissimilar materials is difficult to achieve but essential.

1.3 Tire Classification

There are many construction and design variations in tires. But tires are mainly grouped according to the direction of cords used in the plies of carcass construction. There are two basic types, Cross Ply and Radial Ply. Cross ply tires are called Bias or Diagonal belted in United States.

1.3.1 Cross Ply Tires

A cross-ply tire is one of the older designs, and it does not have breaker belts. The position of the cords in a bias-ply tire allows the body of the tire to flex easily. This design improves the cushioning action, which provides a smooth ride on rough roads. A bias-ply tire has the plies running at an angle from bead to bead. The cord angle is also reversed from ply to ply, forming a criss-cross pattern. The tread is bonded directly to the top ply. Figure 1.3 shows the cross ply construction.
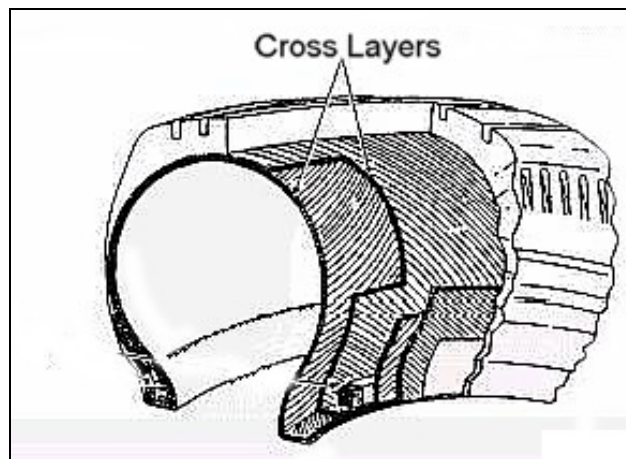
Figure 1.3 Cross Ply Tire Construction

A major disadvantage of a bias-ply tire is that the weakness of the plies and tread reduce traction at high speeds and increase rolling resistance. This makes the tire scrub or squirm, decreasing traction, operator control and accelerating tread wear. Since the tread is subjected to any flexing that occurs, the footprint, or contact patch, distorts. This distortion causes abrasion from the ground surface, which reduces the life of the tire. All of these factors significantly increase fuel consumption. The only way to increase the strength of bias-ply tires is to increase the number of plies and bead wires. Increasing number of plies increases tire mass.

When it is not carrying a load, the cross-ply tire presents a very rounded profile to the ground, with only a small elliptical area making contact. As load is applied, the tire flattens. The greater the load the more the shoulders flatten to the ground, while the tread in the middle tends to lift up. Grip is reduced overall. When subjected to a lateral force, the structure of the cross-ply tire cannot remain flat on the ground because of its rigid sidewalls. One of the shoulders is compacted against the ground while the other tends to lose contact with it. There is a strong drift effect. Due to the disadvantages explained, the cross-ply tire construction has become obselete for automobiles, even though it is still in use for commercial vehicles as a cheaper alternative.

As a transiton product between cross ply tire and radial tire, belted cross ply tires, or namely Bias Belted Tires are introduced. The bias belted tire is a cross-ply tire with breaker belts added to increase tread stiffness. The belts and plies run at different angles. The belts do not run around to the sidewalls but lie only under the tread area. A bias belted tire provides a smooth ride, good traction, and offers some reduction in rolling resistance over a bias-ply tire. Figure 1.4 shows carcass construction for a typical Bias Belted Tire. Bias belted tires have not been used except in the United States.
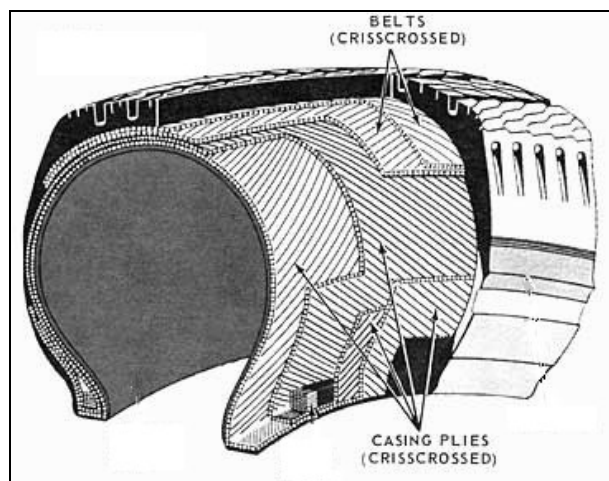
Figure 1.4 Bias Belted Carcass Construction

1.3.2   Radial Ply Tires

The radial tire is constructed in two parts. First, a single layer of rubber-
coated textile belts arch from one bead to the other to form the tire casing.
Second, numerous rubber-coated steel coreded breaker belts are placed in the
crown, under the tread, to form a strong stabilizing unit. Figure 1.5 shows the
components and layer orientations for a radial tire. Figures 1.1 and 1.2 are also
clear examples for radial tire construction.
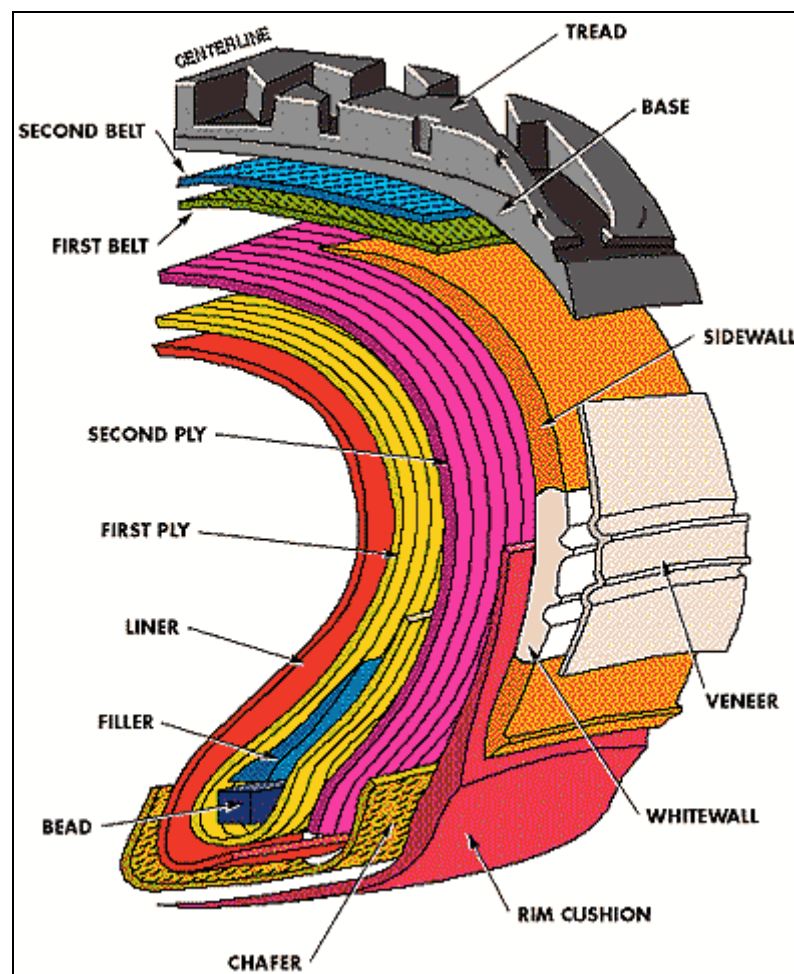
Figure 1.5 Construction of a Radial Tire

Even without a load, the radial tire is almost flat on the ground. The
contact area is already very wide. As load is applied this area grows longer

9

without losing any of its width. The tread blocks remain flat against the road surface and grip is maximized. When rolling, the flexibility of the sidewalls allows them to absorb a lot of the bumps. The sidewalls of the radial tire are highly flexible; they are going to stretch in proportion to the increase in force. The sidewalls act like a moving hinge between the wheel and the crown allowing the latter to remain flat against the ground. The path of the tire therefore remains constant even when subject to lateral loads.

To increase a radial tire's strength, larger diameter steel cables are used in the breaker belts. These steel cables help reduce punctures, tears and flats. They also help distribute heat, resulting in a cooler running tire, improving fuel economy. The stabilizing steel belts and radial construction minimize tread distortion. As the sidewalls deflect, the belts hold the tread firmly on the ground, minimizing tread scrub and greatly increasing tread life.

1.4 Tire Designation

Sidewall of the tire gives the information about the tire construction, dimensions, load carrying capacity, speed rating, and manufacturer production codes. ISO Metric Tire Designation is shown in Figure 1.6. Although there are different type of tire designations, ISO Metric Designation is the most recent and common one for automobile tires.

Figure 1.6 International Standarts Organisation Metric Tire Designation

In Fig. 1.6,

185   : Nominal Section Width (measured in millimeters),

55   : Aspect Ratio (ratio of the height of the tire's cross section, to its width),

R   : Carcass construction (R for Radial),

15   : Rim Diameter (measured in inches),

92   : Load Rating (Service Description, from Load Index table),

V   : Speed Rating (Service Description, from Speed Symbol table).

Aspect ratio of a tire is determined by dividing a tire's section height by its section width. It is often referred to as the profile of the tire. The aspect ratio affects steering stability. Generally, the shorter the sidewall, or the lower the aspect ratio, the less time it takes to transmit the steering input from the wheel to the tread. The result is quicker steering response. Aspect ratio also affects the tread contact patch. The lower aspect ratio increase response, steering feel, and stability, but degrade ride comfort. The lower aspect ratio responds to lateral force more effectively than a tire with a higher aspect ratio.

To specify carcass construction, R is used for Radial, B is used for Bias Belted and D is used for cross ply (diagonal) tires.

Load Rating is used to identify a given size tire with its load and inflation limits when used in a specific type of service. The load index of a tire and proper inflation pressure determines how much of a load the tire can carry safely. Speed ratings signify the safe top speed under perfect condition..

1.5 Tire Dynamics

In addition to supporting the vehicle and damping out road irregularities, the tires provide the longitudinal and lateral forces necessary to change the speed and direction of the vehicle. These forces are produced by the deformation of the tire where it contacts the road during acceleration, braking, and cornering. Society of Automotive Engineers (SAE) Tire Axis System is shown Figure 1.7.
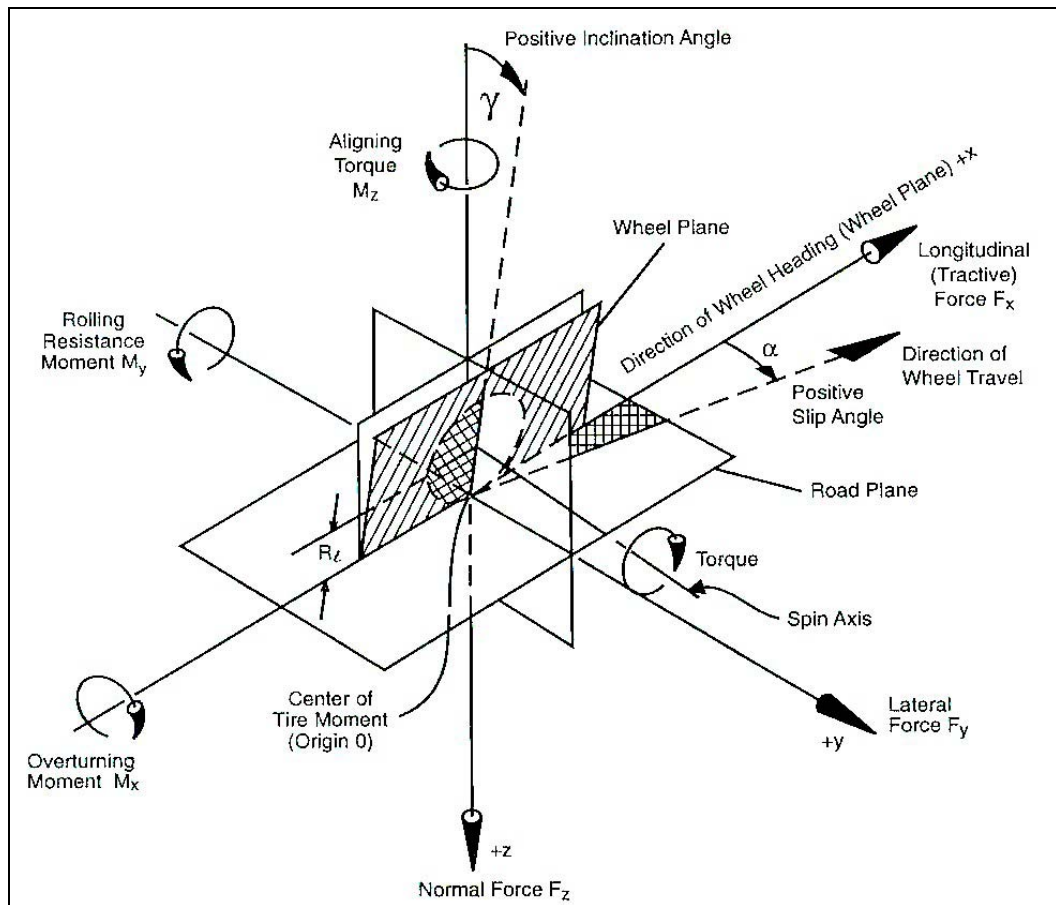
Figure 1.7 SAE Tire Axis System

In the absence of side forces, a rolling tire travels straight ahead along the wheel plane.During a cornering maneuver, however, the tire contact patch "slips" laterally while rolling such that its motion is no longer in the direction of the

wheel plane. The angle between its direction of motion and the wheel plane is referred to as the slip angle. This lateral "slip" generates a lateral force, at the tire-ground interface. This force is called cornering force. Because the force acts slightly behind the center of the wheel, it produces an aligning moment, called self aligning moment in terminology, which tends to realign the wheel in the direction of rolling. The distance between the tire axis and line of action of the cornering force is called pneumatic trail. Slip angle mechanism and the deflected shape of the tire going under deformation are given in Figures 1.8 and 1.9.
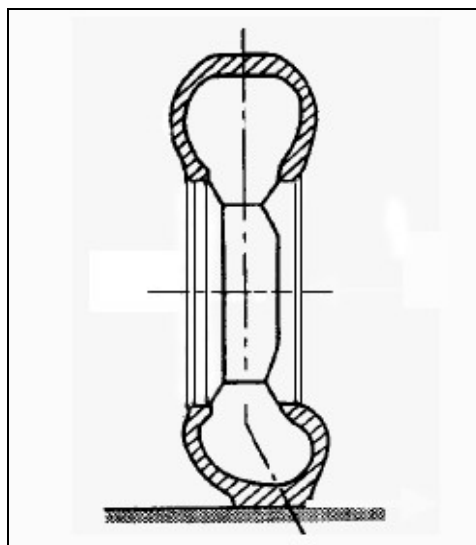
Figure 1.8 Deflected Tire During Cornering

Slip angle is a function of tire steering angle, the longitudinal velocity vector, the lateral velocity vector, and the lateral velocity component due to yaw. On the other hand, cornering stiffnes depends on the tire construction. As stated earlier in this chapter, radial tires have better cornering stiffnes values. Also, tires called low profile, the ones with low aspect ratio have better cornering abilities than the others.

It should be noted that the cornering ability of tires as presented in various sets of plots involving the slip angle, normal tire load and the cornering force are strongly affected by the construction of the tire. For example, radial cords in the

carcass plies results in soft tires providing good ride comfort. However, such a construction results in severely reduced directional control and stability. Thus, in radial ply tires, it is the presence of the breaker belts with cords (nowadays mostly steel) at around 20-25° to the circumference that makes up for this deficiency. Thus in radial ply tires the ride comfort and directional control and stability are provided by two different aspects of tire construction.
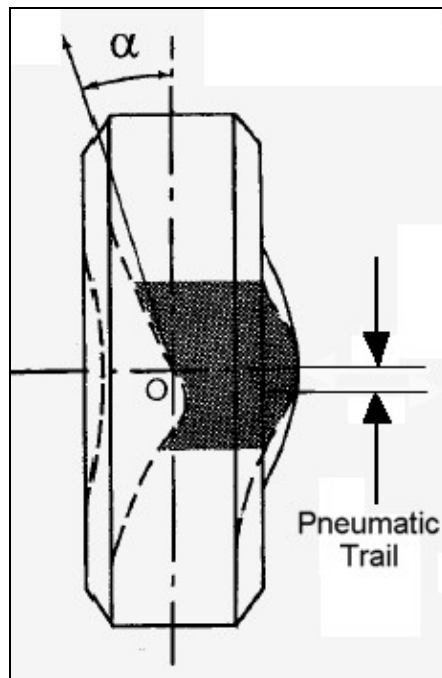
Figure 1.9 Deflected Tire and Contact Patch During Cornering

1.6 Purpose and Scope of the Study

Tire is one of the most important components affecting vehicle dynamics in more than one aspect. In particular, tire's cornering characteristics have a key role in determining directional control and stability, in short vehicle handling. As the characteristics of a tire is a result of its complex construction, consisting of many dissimilar material properties, carcass construction, and breaker belt configuration, its modelling is an extremely difficult process.

Until recently, experimental means were practically the only way to obtain tire cornering force characteristics. However, recently, the use of the Finite Element Analysis (FEA) has opened the possibilities of modeling and simulation of tires, for studying and improving many aspects of tire functions including the cornering behavior.

Studies on the finite element models of the pneumatic tire have appeared just after the appreciation of the Finite Element Method and a great amount of work on tire modeling have been published. However, the FEA of the tire directed towards the cornering force characteristics appeared only at the last few years of the Milennium. One of the pioneering work in this subject is carried out in the Mechanical Engineering Department of the Middle East Technical University, Tönük 1998.

This study is basically a continuation of the work of Tönük. The findings and the recommendations from his study forms the main set of goals for this study. As such, a completely new FE model is recreated by using efficient modeling techniques such that accurate, reliable and short solution times will allow study on tire cornering characteristics for a wide range of vertical loads and slip angles. Further, the study is extended to cover the analysis of the self aligning torque.

CHAPTER 2
LITERATURE SURVEY

There exists a significant number of different tire models in literature; each can be classified according to the methodology used, scope of the study or tire parameter studied.

Three main approaches are used to investigate tire behavior; analytical models, semi-analytical studies and Finite Element Method (FEM).

Tire dynamics studies can also be categorized depending on the scope. The first category is concerned with the lateral forces generated in the contact patch. These models are relevant in the handling analysis of vehicles. The second category deals with the vertical and longitudinal forces generated in the tire, and these are used for ride and performance analysis of vehicles, respectively. The studies in third category are on analyzing noise, vibration and harshness.

Existing work can also be classified as either steady state or transient dynamic response of the tire behavior analyzed. Rolling resistance, cornering force, cornering stiffness, stress and deformations under either steady state or transient conditions, are presented as the results of these studies.

In this chapter, literature survey is limited to the application of the FEM to various aspects of the pneumatic tires. The Finite Element modeling and analysis of the pneumatic tires are examined in detail and their methodology, assumptions, modeling techniques, investigated parameters and results given in

detail. Although the scope of this study is to examine cornering behavior of the tires, some studies with different scopes but using similar modeling techniques are presented in literature survey, thus the literature survey of Finite Element tire models is not limited to cornering behavior tire models. Literature survey on cord-rubber modeling techniques is also performed and summarized.

2.1 Finite Element Tire Models

There are numerous finite element tire models in literature, each using different modeling techniques, assumptions and codes. It is possible to organize the present studies according to different aspects. FEA code, solver type, scope of the work can all be considered as a classification type.

Most of the studies use a commercial FEA code. MARC, ABAQUS, PAM SHOCK, LS DYNA are the most common packages in tire FEA studies. Some authors developed and used their own code.

Implicit FEA codes are used mostly for the static or quasi-static models where number of elements and solution time is not a primary concern. Explicit finite element codes differ from implicit codes in that they don't require the frequent inversion of large stiffness matrices, thus reducing the number of calculations per time step and the storage space required. The compromise arises in that explicit codes need shorter time for each time step but needs more time steps in order to ensure numerical stability and hence accuracy. On the other hand, commercial implicit FEA packages have more choice in element types. Especially composite or layered elements work efficiently which are available in implicit packages.

Another classification may depend on the method used for modeling cord reinforced rubber structure. Some authors used "reinforced concrete" approach,

while most of the current studies in literature use classical laminate (or composite) theory and Halpin-Tsai mixing rules. Some models use continuum elements to model the tread and shell elements to model sidewalls. Besides, some of the models use continuum elements to model all rubber volume and introduce shell elements for cord composite sections.

Almost all studies agree on using hyperelastic material laws such as the Blatz-Ko and Mooney-Rivlin strain energy formulations to represent the highly non-linear behavior of the rubber. On the other hand, for small strains, linear elastic models are used and good correlations obtained with the experimental results of tire vertical and lateral forces. For certain vertical loads and tire inflation pressures, even though the tire geometry undergoes large deformations, local strains are in acceptable limits for linear elastic models; especially if the vertical or cornering stiffness are the main output parameters, which are mostly determined by the reinforcements.

Recent studies on tire finite element models are summarized and given below. Material and structure modeling, scope, and results are given in some detail for each study.

Tönük (1998) constructs a drum type tire testing machine and prepares a tire finite element model to study cornering force characteristics. Marc is used to perform implicit finite element analysis. A 155 R 13 radial tire with one textile body ply and two steel tread plies is used for a case study, and the results are published (Tönük, Ünlüsoy 2001). For rubber structure, both Mooney-Rivlin and linear elastic approximation with large displacement option are used. Because of the stiff reinforcement of the tire structure, strain of the rubber matrix of the tire rarely exceeded 20% strain, and Tönük concluded that linear elastic approximation yields close results with that of Mooney-Rivlin material model. Continuum elements are used to model the rubber matrix, and REBAR elements

used for textile and steel reinforcements. Rebar elements carry only tension and compression in the direction of reinforcement. Bending stiffness of the steel reinforcements is neglected in that way, which is a factor in vertical and lateral stiffness of the tire. A user subroutine is used to place and orient the rebar elements, which is accessed at the beginning of each step of the solution to align position and orientation of the rebar elements. Drum of the test machine is modeled with deformable continuum elements, which are also taken in to consideration during solution. Including a deformable drum increases the number of elements and solution time. More significant than the increasing number of elements, deformable to deformable contact definitions in MARC takes significantly longer solution time when compared with deformable to rigid contact definition. Static deflection test results for the tire are compared with the finite element model to tune model parameters. After the correlation is proved, cornering analysis is performed. Tire structure is fixed in all degrees of freedom at the rim interface, and not rotating. Instead, with an inverse kinematics algorithm, the drum is moved over the tire. The cross section of Tönük's cornering force study is given in Figure 2.1.
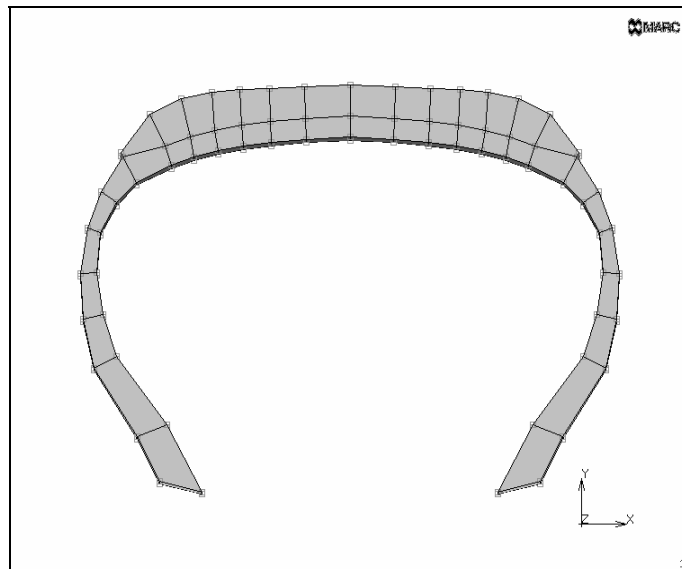
Figure 2.1 Cross Section of Tönük's (1998) Finite Element Model Used for Cornering Force Study.

19

Tire is inflated to 180kPa and for some vertical load-slip angle configurations, test results compared with the finite element model. After half rotation of the tire, cornering force value reached a steady state. Test results are presented in carpet plot from, and finite element model results are placed on the carpet plot obtained from the test.

Further comments of the authors on the limitations and possible improvement of the finite element model are given in Tönük and Ünlüsoy, 2001. The finite element cornering force values are available only up to a slip angle for a tire load and as the tire load increases, the maximum slip angle for which finite element model yields result decreases. Beyond this slip angle, before the cornering force reaches the steady value, the error accumulation starts to be significant. The accumulated error causes the model to become unstable so that cornering force does not settle to a steady state value and cornering force can be obtained for small slip angles. For low tire loads, since the contact patch deformation, which travels around the fixed tire is small, the error accumulation is slow and steady state cornering force values can be obtained. For larger slip angles with low vertical loads, the distance to be rolled by the tire increases, and at some slip angle, the error accumulation dominates the model results before the steady state is reached. With increasing vertical loads, the contact patch deformation increases which causes more rapid increase in accumulated error, hence allowing a shorter distance to be rolled before the accumulated error dominates. Therefore for larger vertical tire loads, the cornering force can only be obtained for small slip angles. The carpet plot showing cornering force characteristics of the 155 R 13 tire and obtained from the tire test setup of the author is given in Figure 2.2. The circles on the lines are finite element estimates. As a final word, Tönük's finite element model show good agreement with the test results for medium slip angles and tire vertical loads.
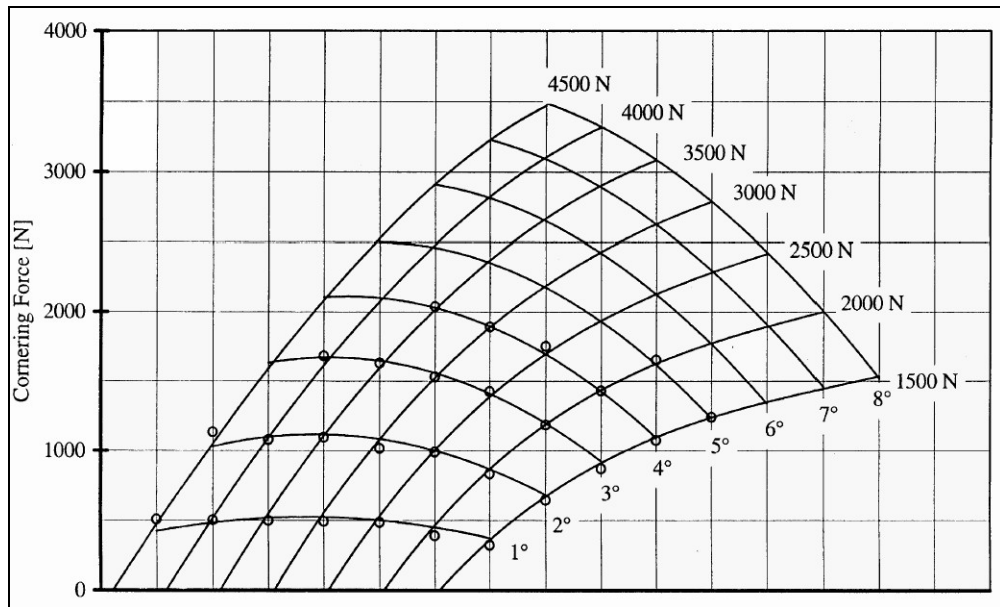
Figure 2.2 Experimental and FEA Carpet Plot Tönük and Ünlüsoy (2001).

Koishi, Kabe, and Shiratori (1998) developed a model using explicit finite element analysis code, PAM-SHOCK. This is an important study from various aspects. They modeled a 175 R 14 S tire. The rubber structure of the tire is modeled with solid elements. Carcass and steel belts are modeled with multi-layered shell elements. This is one of the major contributions of this model. The properties of the rubber materials are represented by the Mooney-Rivlin material model. The properties of the fiber-reinforced rubber composites are represented by an orthotropic material model with linear elastic properties. The cross section of the tire modeled and placement of elements are shown in Figure 2.3. In the tread area, layered shell elements consist of three layers which are the textile reinforce carcass, and the two belts. In the sidewall area these elements consist of a single textile carcass ply. This cross section view of the tire and correlation of the test and FEA results give an important conclusion about the tire cornering force studies. A study of their model shows that the location of the carcass and steel belts are far from the locations they have to be. In case of a stress analysis,

21

this changes all the stress distribution. But, when the scope is stiffness of the tire, such a model gives reliable results.
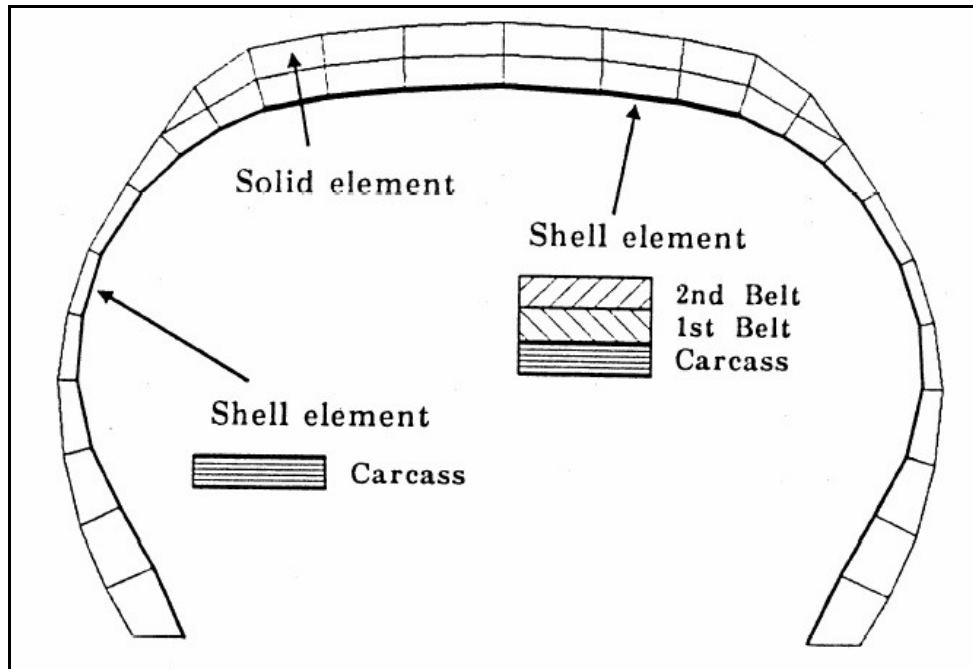
Figure 2.3 Cross section of Koishi (1998) Finite Element Tire Model

Tire is inflated to a pressure of 200 kPa and a vertical load of 3.3 kN is applied on it. The tire is rotating on a flat surface at 10 km/h speed. A flat bed tire test setup is used to obtain experimental data. At this speed, it takes 0.8 seconds to make one complete rotation of the tire. The analysis is performed for 1.2 seconds and tire rotated about 1.5 times. After 0.4 seconds, about 180 degree rotation of the tire, each cornering force values remained same for each slip angle. Time versus cornering force values for each slip angle is shown in Figure 2.4. The results show good agreement with the test results. For 3 degrees slip angle, experimental measurement is 1550 N where finite element result is around 1400 N. The difference is around 10%, which is a very good approximation for a highly nonlinear and complex structure like a tire. Authors examined the effects of the inflation pressure, rubber modulus, and effect of belt angle on cornering

22

force characteristics. They concluded that, cornering force increases linearly as slip angle increases up to 4 degrees, and increasing inflation pressure leads to higher cornering forces. Changing the belt angles from 20 degrees to 0 degree decreased the cornering force by 33%.
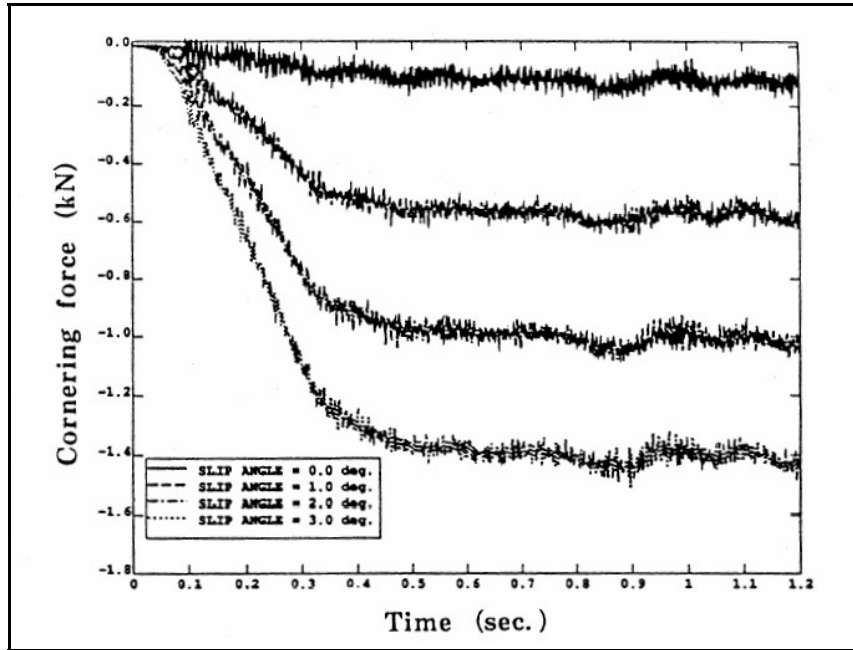
Figure 2.4 Cornering Force versus Time for Koishi et al. (1998) model

Another important conclusion is given on the rubber modulus. Increasing the rubber modulus to twice of the original value, increased the cornering force 21% for 3 degrees slip angle, and less for smaller slip angles.

Kabe and Koishi (2000) investigate cornering force characteristics of a 235/45 R 17 Z tire with two different models, and compare the results, solution times and problems of each technique. They also tested the tire on MTS Flat-Test Tire Test System, which is previously used by Koishi et al (1998)

They used and implicit code (ABAQUS/Standard) and an explicit code (ABAQUS/Explicit). They modeled rubber components by continuum elements and Mooney-Rivlin material model. Fiber reinforcements are modeled with

23

REBAR elements. Tire is inflated to 200 kPa pressure. The model is loaded with 4 kN vertical load and rotated at 10 km/h speed. Slip angles up to 3 degrees examined. For the implicit model, a steady state transport analysis capability is formulated with a moving Lagrangian reference frame model and only contact region area is fine meshed. The rest of the tire is meshed considerably coarse. A total of 4464 elements and 5976 nodes are used. Cornering force value reached a steady state value after half rotation of the tire for 3 degrees slip angle and after almost a complete rotation for 1 degree slip angle.

For the explicit model, a fine mesh is used for the entire structure (11160 elements and 14940 nodes) because the entire tire will come to contact with the road surface as it rotates. The explicit analysis solution time is about 30 times of the implicit one. Buildup of cornering force and self aligning torque with solution time is given in Figure 2.5. Cornering force and self aligning torque curves at different slip angles given by authors are shown in Figure 2.6. Finite element model results are in good agreement with the experiments.
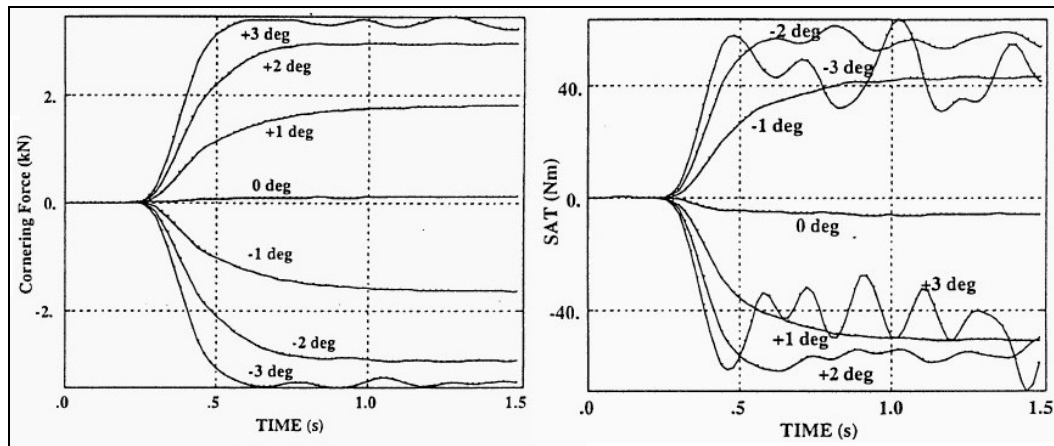
Figure 2.5 Cornering Force and Self Aligning Torque (SAT) Results of Kabe (2000)
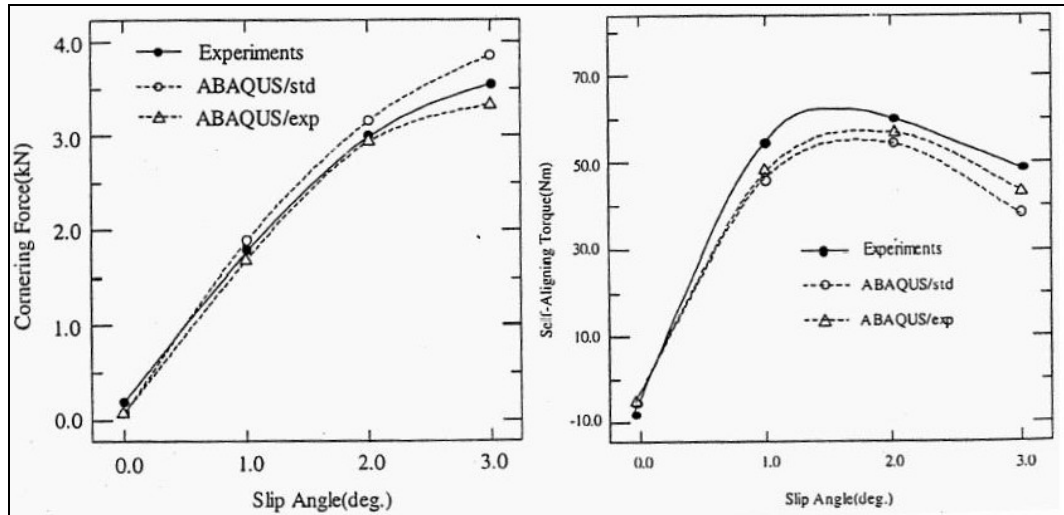
Figure 2.6 Cornering Force and Self Aligning Torque Results of Kabe (2000)

Another important and successful study in literature is published by Pelc (2000). The importance of the study is related with the material model used and verified with the author's own developed finite element code. He verified the orthotropic cord rubber structure model with tests and the finite element model. Then used this model in the finite element modeling of the test tire, and obtained very good correlation. An attempt to improve the pneumatic tire computational model was made in the paper, introducing a more reliable rubber-like material model and modifying the cord-rubber composite parameters. Rubber or other elastomer modeling requires special treatment, due to their physical non-linearity and incompressibility. There are two general approaches to the creation of numerical solutions to the problem: simultaneous approximation of both displacement and stress fields or approximation of displacements only, combined with the use of the appropriate strain energy density function to ensure approximate incompressibility. The first solution is less effective from the numerical perspective (the global stiffness matrix is not positive-definite). It seems to be the most appropriate to apply the other approach, having at disposal the finite element code in the displacement version. Author developed the following equations using Tsai Rule of Mixture.

25

Small strains are assumed in the derivation. Although some authors do not advice to use small strain assumption for the tire finite element studies, using Mooney-Rivlin material model for the rubber matrix which mainly goes under large deformation, and linear orthotropic properties for the steel and textile reinforced parts, gives accurate results. Reinforcement material properties overcome the rubber stiffness and determine the behavior of the section. So, small strain assumption is valid for most conditions. Most of the publications presented in this chapter use the same approach and finite element models showed good agreement with the experiments.

The materials constants for cord-rubber composites are derived by Pelc as:

$$E_1 = E_c v_c + E_r (1 - v_c) \tag{2.1}$$

$$E_2 = E_r \frac{(1 + 2v_c)}{(1 - v_c)} \tag{2.2}$$

$$E_3 = E_2 \tag{2.3}$$

$$G_{12} = G_r \tag{2.4}$$

$$G_{13} = G_{23} = 3G_{12} \tag{2.5}$$

$$v_{12} = v_{13} = 0.5 \tag{2.6}$$

$$v_{23} = 0.98 - v_{21} \tag{2.7}$$

where E_c, E_r are Young modulus of cord and rubber respectively, G_r shear modulus of the rubber, v_c volume fraction of the cord in a ply, subscript 1 denote cord direction and plane (1, 2) indicates the plane of a ply. The other three Poisson ratios are obtained from the reciprocal role- the stiffness matrix should be symmetric. In this way, the layered cord-rubber composite is assumed to be linear orthotropic material. The imposition of the exact incompressibility conditions is impossible, because such a composite would not satisfy the stability requirement given as:

$$1 - v_{12}v_{21} - v_{23}v_{32} - v_{31}v_{13} - 2v_{12}v_{23}v_{31} > 0 \qquad (2.8)$$

The cord rubber model is tested and the results are compared with the finite element model. A truck tire is modeled, and the model validated with inflation analysis, comparing the displacement values obtain in finite element model and experimental measurement.

Most of the studies summarized from the tire dynamics literature were all related with tire stiffness, vertical, lateral or cornering force characteristics of the tire. There some other tire studies, which model the tire in same detail with the other ones, but aiming to perform different analysis.

Bai and Gall (2000), prepared a model using MARC. They studied dynamic characteristics and three dimensional vibration modes and natural frequencies of the tire. Effects of tire pressure, vertical load, deformation, velocity as well as suspension of the car which the tire is mounted are studied as parameters. They published mode shapes of the tire under different loading, inflation pressure and boundary conditions. Boundary conditions vary as the suspension geometry of the car varies. Figure 2.7 shows mode shapes of a tire with different boundary conditions.

27
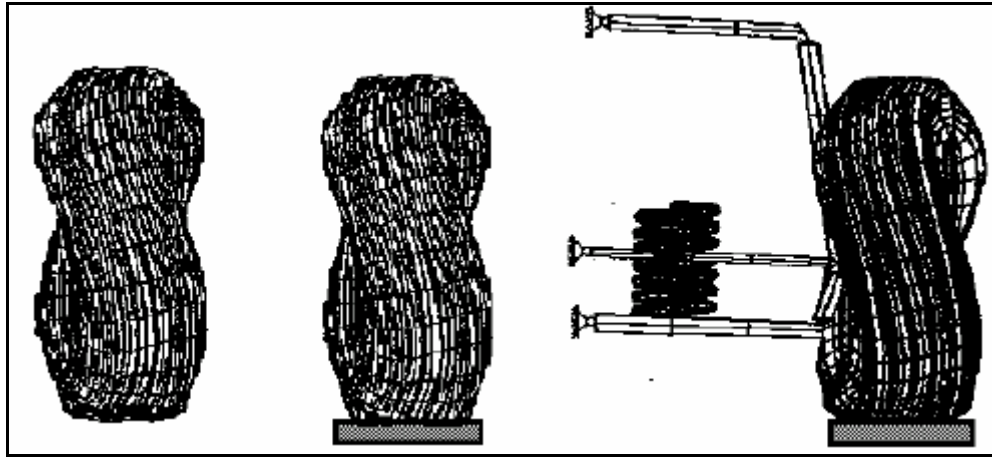
Figure 2.7 Different Mode Shapes from Bai and Gall's Study

Ghoreishy, 2001, used COSMOS FEA program to analyze a 6.45-14 bias tire subjected to inflation and static contact loading. The main purpose of the study was prediction of the deformed shapes and stress components of the tire geometry. A three dimensional finite element model using continuum (solid) elements with Lagrangian formulation is prepared. For cord reinforced rubber parts, linear orthotropic material properties are used. While all other studies in literature are using shell elements for the steel and textile plies, Ghoreishy used continuum (solid) elements. Since he studied the stress distribution in the tire, modeling the geometry precisely is important. Continuum elements with calculated orthotropic material properties gave successive results when compared with the experiments. Textile elastic properties differ in tension and compression and thus different material constants should be used during the analysis of each case. However, owing to the lack of ability of considering of these two effects in the COSMOS/M software, they have not been taken into consideration for the model and effect of neglecting bilinear behavior of textile is investigated in the solution. A smooth tread pattern has been assumed in the model to avoid of excessive computational cost and efforts.
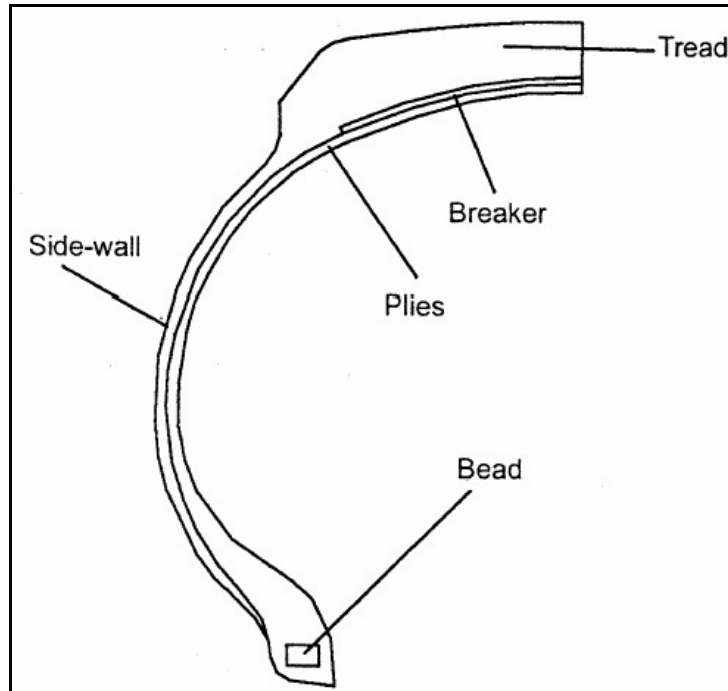
Figure 2.8 Tire Cross Section Modeled By Ghoreishy

This is the only tire finite element model in literature using continuum elements for the entire structure. Figure 2.8 shows the tire cross section modeled. Many authors in the literature expressed analytically the elastic constants of orthotropic laminated layers dependent upon Young Modulus, Poisson's ratios and shear modulus of the cord and rubber according to their volume fractions in composite. Some of the publications on cord rubber modeling are directly used for tire finite element analysis by the authors in later studies. Ghoreishy used Clark's (1983) formulations for orthotropic cord-rubber properties. This study is a good proof of material property derivation and continuum element usage for textile and steel reinforced plies.

Hauke, Hanley and Crolla (2001) prepared a model to investigate tire misuses. They defined the term "misuse simulation" , the tire impacting obstacles up to 140mm height at velocities up to 100 km/h. A 195/65 R 15 tire is modeled with PAMCRASH. Figure 2.9 shows the tire model and the obstacle. Mooney-Rivlin material model is used for rubber matrix of the tire, and for

reinforcements, linear orthotropic material representation is chosen. Again, layered shell elements are used for the reinforced parts of the tire. Orthotropic material properties are calculated with volume fraction based classical laminate theory. The behavior of the air contained within the tire rim assembly is simulated by an Airbag function, which conserves the relationship between the internal pressure and the volume in accordance with the ideal gas law.

Dynamic behavior of the tire is analyzed by loading tire against a surface, at 30 km/h velocity and traversing a 20mm step. The forces at the hub are plotted as a function of time. Change of air pressure in the tire with changing tire volume is rare in tire finite element models.
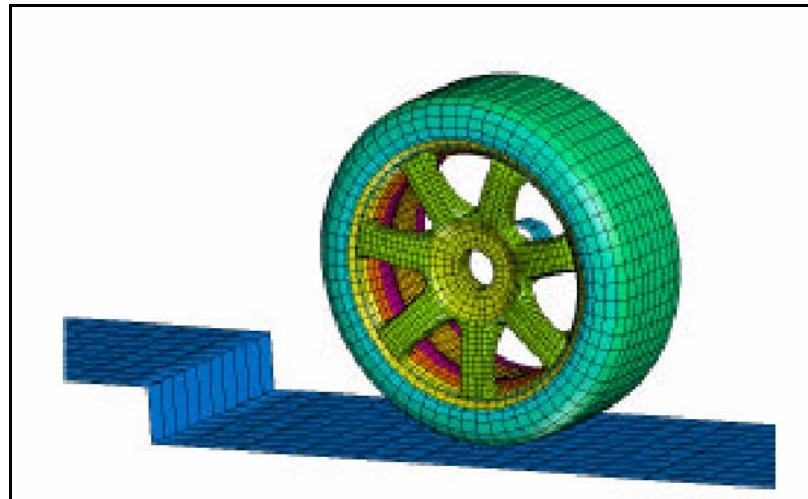
Figure 2.9 Hauke et al. Model for Tire Misuse Study

Darnell (2001) in his PhD thesis, propose a fast and accurate three dimensional tire model and validate for events which occur vehicle durability studies. He uses an implicit code to simulate tire vertical and lateral stiffness. Finite element representation of a tire sidewall for arbitrary, three-dimensional deformations is presented. This element contained no additional degree of freedom and guaranteed that no spurious forces were generated on the rim. A two dimensional large displacement inextensible beam formulation was developed.

This formulation allowed piece-wise constant curvature and pressure loading. It simulates the exact geometry. A Galilean orthotropic contact formulation suitable for analyzing the three dimensional behavior of a tire, where the carcass is composed of linear shell elements developed. Galilean transformation, which is used to solve the rolling contact problem, essentially rotates the computational mesh through the material tire so that the mesh stays relatively steady as the material tire rotates. This convective process occurs in the undeformed state and is axially symmetric. It then is mapped to the deformed state. This is a special case of an Arbitrary Lagrangian Eulerian (ALE) formulation where material tracking is somewhat simpler. This kinematic methodology is often called a moving Lagrangian reference frame. The mesh does not rotate with the tire, but it appears to slide over the step, with the tire passing through the mesh. For the case of steady state rolling motion, a steady state solution can be obtained. This differs from the standard Lagrangian formulations where the computational mesh is constantly deforming. For the steady case, the strain rate at a point is completely determined from the spatial derivative of strain at that point. Further, the strain of the computational mesh represents the strain of the coincident. The interface between the ground and the tire carcass is modeled with an isotropic Coulomb friction model on an orthotropic elastic foundation. This foundation represents the compliance of the tread blocks. Thus, there is a linear elastic response while sticking occurs. The Darnell model looks simple, but it is quite powerful. Figure 2.10 shows a slice from the model.
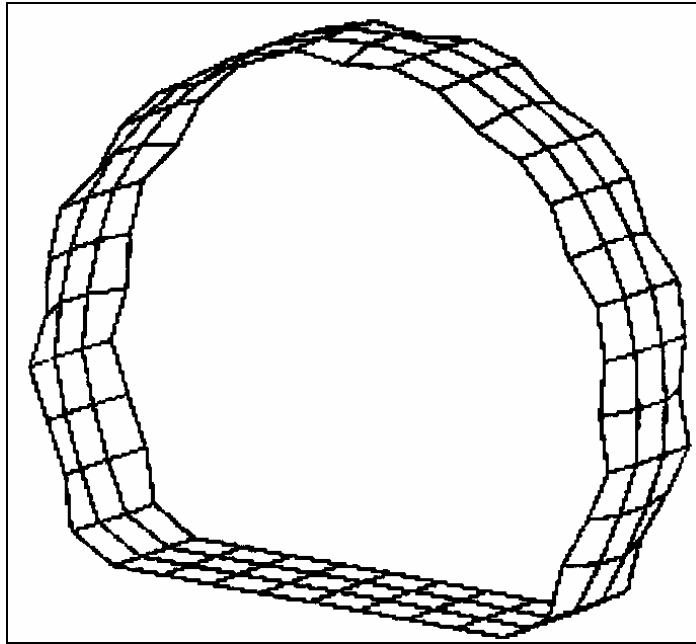
Figure 2.10 A Slice view of Darnell's Tire Finite Element Model

A radial tire (size is not specified) tested on the UMTRI flat bed tire tester. Tire is inflated to 30 psi and pressed onto a flat surface until a vertical load of approximately 800 lbf was reached. The spindle height was then locked, and the test bed was moved laterally at approximately 0.05 in/sec, until the tire was observed to slide. The test bed motion was then reversed, and the test bed was moved until the tire slid in the opposite direction. In the model, the coefficient of friction between the tire and the test bed was adjusted so that slip occurred at the same force level as was measured in the experiments. The lateral response is observed to be soft. The model was run 0.047 m laterally and then 0.047 m back. The step size was 1mm. Then, on a Smithers flat bed tire tester, slip angle tests are performed to measure force and moment build up versus rolling distance for 1degree, 3 degrees and 6 degrees slip angles and 500, 1000 and 1500 lbf normal forces. The lateral and vertical contact compliance of the model and the in-plane shear stiffness of the tread elements are adjusted such that the 18 measured force and moment curves best match the computed response. The tire model was incremented forward in 3 cm steps.

Both the force and moment data are relatively good fits, with deviations typically not more than 20%. The rates at which the aligning moment and force grow are matched well. Figure 2.11 shows rolled distance versus cornering force plot of Darnell's test and FE results for 1 degree slip angle and different vertical loads. Figure 2.12 shows rolled distance versus cornering force plot of Darnell's test and FE results for 6 degrees slip angle and different vertical loads

When Figures 2.11 and 2.12 examined, it can be concluded that, as the slip angle increases, time or tire rotation required for cornering force to reach steady state decreases. On the other hand, for same slip angle, as the vertical load increases, time or rotation required for cornering force to reach steady state increases.
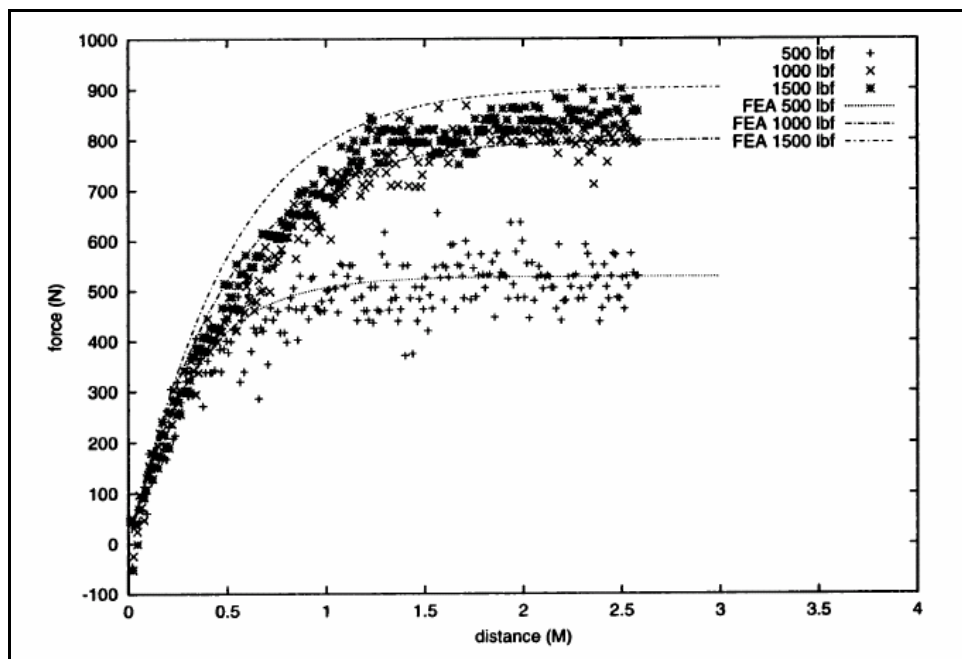
Figure 2.11 Darnell's Rolled Distance versus Cornering Force Plot for 1 Degree Slip Angle, Experimental and FE Data

33
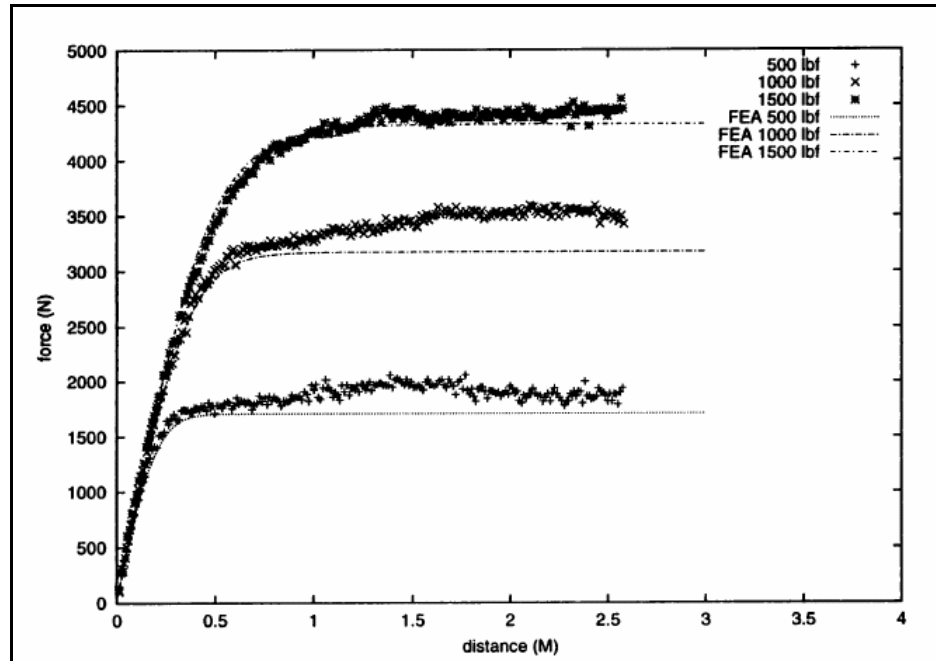
Figure 2.12 Darnell's Rolled Distance versus Cornering Force Plot for 6 Degrees
Slip Angle, Experimental and FE Data

Olatunbosun and Burke (2002) use MSC/NASTRAN to study dynamic
motion of a rolling tire going over a bump. Their study is meant for simulation of
the vibrations of a tire rather than the cornering behavior. A 195/65 R15 is used
for comparison of test results with the FE model. They found out that, tire
dynamics researchers started to use composite material theory widely in order to
model tire material behavior especially for the elastic constants of cord rubber
geometry. Their model is based on an orthotropic material, although it is
recognized that the tire is made up of composite materials that exhibit anisotropy.
They justify this on the basis that, in the radial tire, the material is symmetrical
about two mutually perpendicular directions in the plane of the material, the
direction of the reinforcing cords and the direction orthogonal to that. The only
exception being in the tread area where the belt plies have steel cords oriented at
an angle to the circumferential direction. It is observed that, the authors who did
not choose to use rebar elements, used orthotropic material properties. The
anisotropic shell element has been chosen for modeling the tire carcass because it

combines the ability to model composite, orthotropic material properties with more computational efficiency than the solid element equivalent. To rotate the tire, motion of the ground plane is forced. Two possible methods of modeling tire rotation are planned initially. The first option was applying a torque to the hub center, which due to the friction present at the tire-ground interface, causes the tire to rotate and move forward. This method simulates the driven wheel of a vehicle but wheel translation in the vertical plane is restrained vehicle. Other option was setting the wheel hub displacement and rotations to zero except the rotation degree of freedom about the wheel spin axis. By translating the ground plane, the tire is caused to rotate by contact friction at the tire/ground interface. A frictional coefficient of 0.8 was assumed. This results in free rotation of the tire, which is the duplication of the physical status of the tire test setup which the authors are using. 10, 20 and 30 km/h ground speed is analyses are performed. Radial and lateral forces on the hub is collected and plotted with respect to time. There is a good agreement between test and FE model results. It can be observed that, for physically rotating tires, the hub forces show small oscillations. Their results can be seen in Figure 2.13.
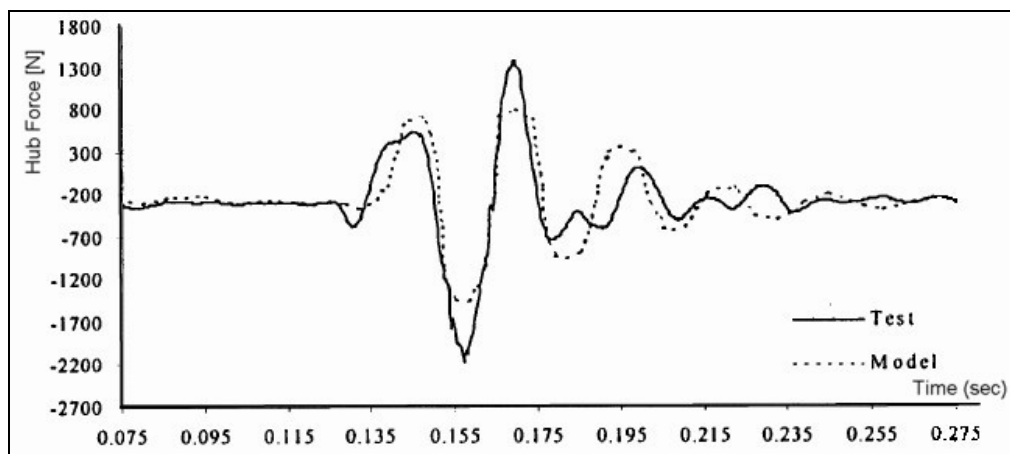
Figure 2.13 Comparison of Test and FEA results for Tire Vertical Force by Olatunbosun and Burke [2002]

They also conclude that, the tire's stiffness reduces once it begins to roll. They discovered by modal tests on the tire that, radial stiffness of the tire was approximately 30% less than the non-rotating one. This is an important conclusion about rotating tire analysis when comparing with the static analyses.

Olatunbosun and Burke use the derivation in their previous publication (Olatunbosun Burke 1997) to calculate orthotropic material properties for cord-rubber structure. In this publication, they reviewed different techniques used to define material properties and presented an alternative experimental/analytical technique. The new technique is applied in the development of a MSC/NASTRAN finite element tire model and the validity of the approach is assessed by examining displacement results under inflation pressure loading. It is shown that the model compares well with experimental measurements for a range of inflation pressures, indicating the usefulness of the technique. Authors stated that, cord plies give direction related stiffness, therefore resulting in anisotropic material characteristics. In order to overcome the problem of modeling tire material behavior, researchers have had to turn to composite theory and analysis. Perhaps the most well known set of equations relating the five engineering constants, four of which are independent, used to characterize an orthotropic ply were those developed during the 1960's known as the Halpin-Tsai equations. These equations are often used for calculating the elastic constants of rigid and compliant filamentary composites but can also be applied to a calendered ply of cord and rubber. Gough developed expressions specifically for the elastic constants of a calendered ply of cord and rubber. In this theory, the rubber matrix is assumed to be incompressible and twisted cord is treated as a unidirectional load-carrying member with no transverse properties. The results obtained for the elastic constants of the ply are independent of the shear modulus and Poisson's ratio of the cord. Closely examining the construction of a radial tire reveals that the cords, running parallel in radial and circumferential directions, clearly define

material symmetry axes. The composite can then be assumed to be orthotropic in nature. Their derivation is given and explained as follows:

When a test sample with length L is stretched and amount of ΔL in the cord direction, the strain in this direction is given by;

$$\varepsilon_1 = \frac{\Delta L}{L} \qquad\qquad (2.9)$$

where ε_1 applies for both the cord and the rubber, and a similar expression can be derived for ε_2, υ_{12} can be obtained from the ratio of these strains, as shown in equation

$$\nu_{12} = -\frac{\varepsilon_2}{\varepsilon_1} \qquad\qquad (2.10)$$

It was noted by Akasaka (1972) that due to the cord modulus being several orders of magnitude greater than the rubber modulus, and the volumetric proportion of the cord being small compared to the overall composite, the major Poisson's ratio is approximately equal to that of the rubber. Further to this, Akasaka also discovered that for cord/rubber composites, the shear modulus is also approximately equal to that of the rubber. However, this does require the rubber shear modulus to be known. Zienkiewicz (1977) proposed an approximation involving only the Young's modulus and Poisson's ratio in the principal material directions, in the form;

$$\frac{1}{G_{12}} \approx \frac{1+\nu_{12}}{E_1} + \frac{1+\nu_{21}}{E_2} \qquad\qquad (2.11)$$

Consideration of the relationship;

$$v_{21} = v_{12} \frac{E_2}{E_1} \tag{2.12}$$

allows equation (2.24) to be re-written in terms of the major Poisson's ratio

$$\frac{1}{G_{12}} \approx \frac{1 + v_{12}}{E_1} + \frac{1 + v_{12}(E_2/E_1)}{E_2} \tag{2.13}$$

Olatunbosun and Burke used their material property derivation in dynamic cornering analysis with success.

Chang (2002), in his Ph. D. thesis builds a finite element model of a passenger car radial-ply tire, P185/70/RI4, and tested on a drum type test machine to investigate tire transient dynamic responses. FEA tire model developed in his research adopted four different types of elements (solid, membrane, shell, and beam) incorporating over 18,000 nodes and 24 different material definitions, to describe the whole tire's construction in extreme detail. Full FEA tire/drum models and the virtual tire rotating test machine were built. The tire thus modeled will then be used to detect in-plane free vibration modes transmissibility and predict standing waves phenomena, of a rotating tire under various inflation pressures, loading conditions and obstacle effects. The tire in-plane free vibration modes transmissibility was successfully detected using the virtual tire/drum rotating test machine created with PAM-SHOCK. The results of the simulations showed excellent agreement, quantitatively and qualitatively, with previous research standing waves phenomenon was also successfully simulated, predicted, and visualized for the first time. The simulations bypassed the practical difficulties of measuring actual tires, and are superior to the oversimplified analytical derivations. Different tire inflation pressures, loading conditions, and obstacle effects on the formation of standing waves were investigated. Six important simulation strategy and tire-model parameters used in this research were tested, verified, and shown to be in excellent agreement with

the experimental results from this research, the previous empirical data, and theoretical/analytical derivations of other investigators.

It has been proved with all of studies in the literature that Mooney-Rivlin material formulation provides reasonably accurate results efficiently and successfully. Most tire industry applications use this material in their FEA tire models and thereby obtain acceptable results. Only two types of hyperelastic materials were available in PAM-SHOCK so far Mooney-Rivlin and Han-Smith formulations. The Mooney-Rivlin type only needs two parameters as the input data, but the Hart-Smith type needs four parameters; use of the latter type would unduly complicate the numerical procedures, and no research has ever shown that the Hart-Smith type often better results than the Mooney-Rivlin. The rule of thumb in FEA analysis states that using more and simpler elements will often get better results than using fewer and more complicated elements. In nonlinear crash analysis, experience shows that higher-order elements also give excellent results, but the computing time they require is longer by orders of magnitude. Therefore, only the simplest finite elements are used in the PAM-SHOCK programs because it is believed that fine meshes of simple elements give better results in highly distorting structures than coarse meshes with higher-order elements. The main reason is that the displacement and shape functions of complex elements we not detailed enough to model sharp deformations across an element. Experience with PAMSHOCK and other codes have confirmed this rule of thumb.

Layered Membrane elements, which are very popular in current tire finite element modes, are used by Chang to model the carcass and layered shell elements to model breaker belts in the tire structure. One of the significant advantages of layered elements is specifying different material properties and different directions for each layer. Another advantage is the capability of modeling thick structures, up to a certain value which classical membrane

elements fail, to model the thickness because of thickness-element surface area ratio.

Solid elements at tread and bead area, layered membrane elements at sidewalls and inner surfaces of tread and bead area can be seen in Figure 2.14. Membrane elements are numbered for better understanding the locations.
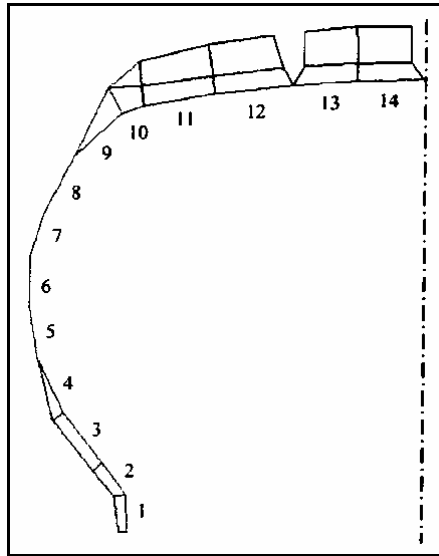
Figure 2.14 Cross Section of Chang's Finite Element Model.

When the cross section in Figure 2.18 is examined, the idea of "approximate modeling the tire geometry for stiffness analysis" can be emphasized. Location of steel and textile belts in FE model is much different than the real tire geometry. This approximation of the geometry, of course, changes the stress distribution in the tire; but if the scope is tire stiffness modeling, the results are acceptable.

To verify the traction friction coefficient versus rolling resistance coefficient, the drum type tire test setup is used and the results are introduced in to the finite element model. First an inflation analysis performed with finite element model and the results are compared with the test. A fixed vertical load of

4500 N is applied the tire, and tire is inflated to 138, 207 and 276 kPa pressures. Deflection of the tire axis is measured. Then, vertical load versus static deflection curves are studied for 2250, 4500 and 9000 N loads.

As the result of the study, tire standing waves phenomenon was predicted and visualized. Three new approaches were developed to verify the tire standing waves phenomenon; they are from the point of view of the vehicle's vibration receptions from the tire axle, from the point of view of the tire energy loss, and from the point of view of the contact interface between the tire and the test drum. These three viewpoints will reveal the influence and information of the dynamic response of the vehicle operating as a unity, the tire itself, and the contact surfaces when the standing waves phenomenon occurs. The tire in-plane free vibration modes transmissibility at 84 Hz vertically and 45 Hz longitudinally were detected. The simulation results show excellent agreement with more than ten previous analytical and experimental studies

Rao, Kumar, Bohara and Mouli (2002), published a study on tire cornering behavior using explicit finite element code supplied by ABAQUS. A 145/70 R 12 tire is modeled with IDEAS mesh generator and exported to the finite element solver. Yeoh incompressible/nearly incompressible three term material model is used to represent the constitutive behavior of rubber parts, as this material model represents the behavior of rubber. Viscoelastic effects of rubber are ignored and stated that, at low and medium speeds, the effect is minor. Reduced integration formulation is chosen for solid elements to reduce computational time. Like most of other studies, tread pattern is not included in the model, as the effect of it on the cornering behavior is minor. Reinforcements are modeled by using REBAR elements. Road is modeled with a rigid surface. Rim is modeled with another rigid surface and total contact between the rim and the tire is assumed. That means the slip between the tire and the rim is restricted.

The model contains 2520 REBAR elements and 6240 solid elements. The analysis performed in two steps. First inflation and loading of the tire is simulated, and then cornering behavior of the tire is simulated for different slip angles.

Tire is inflated to a pressure 180 kPa, and surface representing the road surface is pressed on it. Displacement of the road is used to control the normal load on the tire. For 2200, 3000, 3700 and 5400 N loads, tire is tested. For cornering simulation, rim center node is allowed to rotate freely about the rotation axis. Road is displaced in the longitudinal direction at the rated speed. Tire is rotated due to friction between the tire and the road. Friction coefficient between the tire and the road is used as 1.0. Direction of motion for the road is adjusted to obtain different slip angles. Slip angles up to 20 degrees is tested. Authors observe that, for 0 degree slip angle, cornering force did not remain zero. This is called "ply steer effect" of the rotating tires in the literature, and observed in other studies too. Ply Steer Effect is published by Pottinger (1976) as an effect of radial tires. They presented cornering force for different slip angles and vertical loads. The velocity of the tire for the study is not specified in the publication. A view of loaded tire finite element model is shown in Figure 2.15.
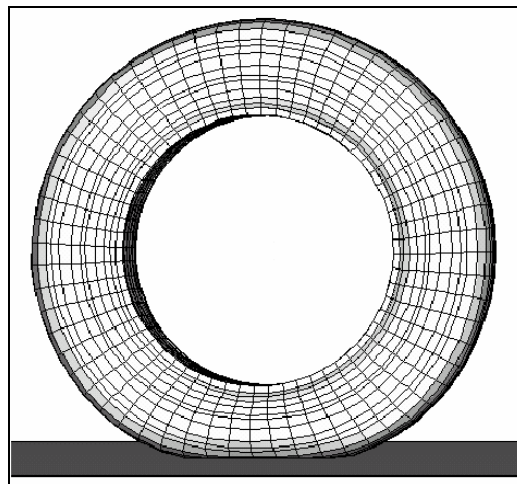
Figure 2.15 Tire Model Prepared by Rao, Kumar et al.

Cornering force for each slip angle, as a function of rotation time is also given in the publication. Figure 2.16 shows the time versus cornering force plots for 3 and 5 degrees slip angles. Cornering force values are plotted in kN.
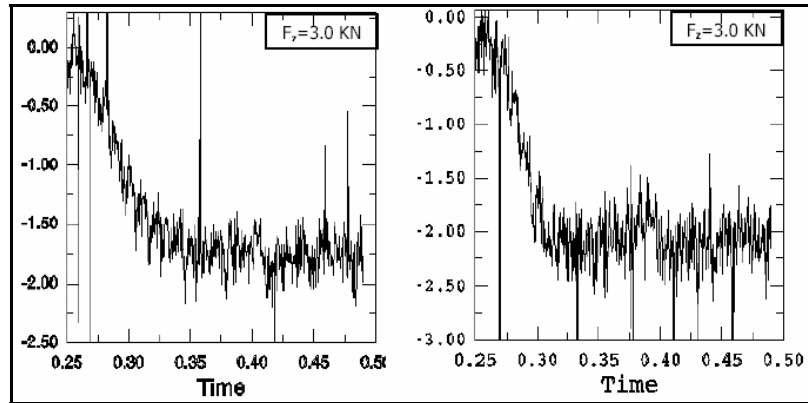
Figure 2.16 Time versus Cornering Force Plots for 3 and 5 Degrees Slip Angles, by Rao et al 2002

Authors also provided Self Aligning Torque versus rotation time plots of the tire for 0, 3, 5 and 20 degrees slip angles. Figure 2.17 shows change of Self Aligning Torque with tire rotation time for 0 and 3 degrees slip angles. Figure 2.18 shows change of Self Aligning Torque for 5 and 20 degrees slip angles.
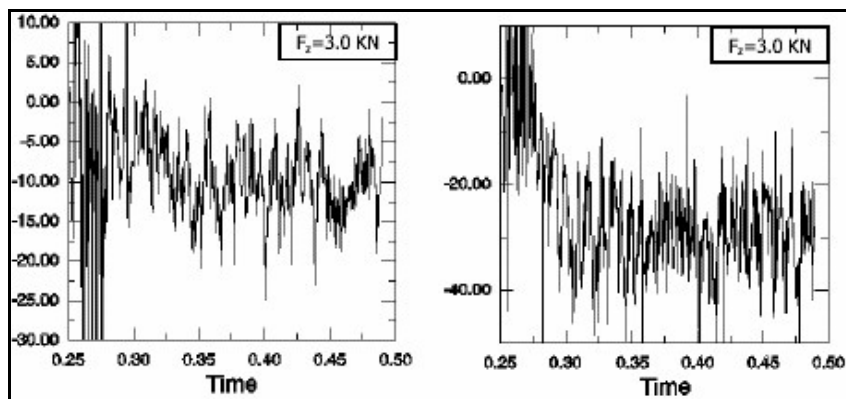
Figure 2.17 Change of Self Aligning Torque with Time for 0 and 3 Degrees Slip Angles, by Rao et al 2002
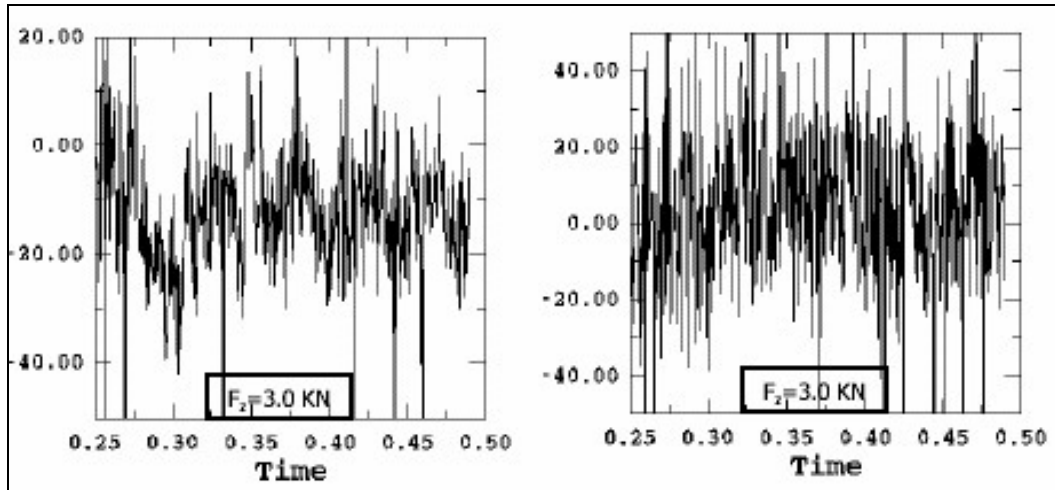
Figure 2.18 Change of Self Aligning Torque with Time for 5 and 20 Degrees Slip Angles, by Rao et al 2002

Figure 2.19 shows the change of cornering force with the changing slip angle for different vertical loads.
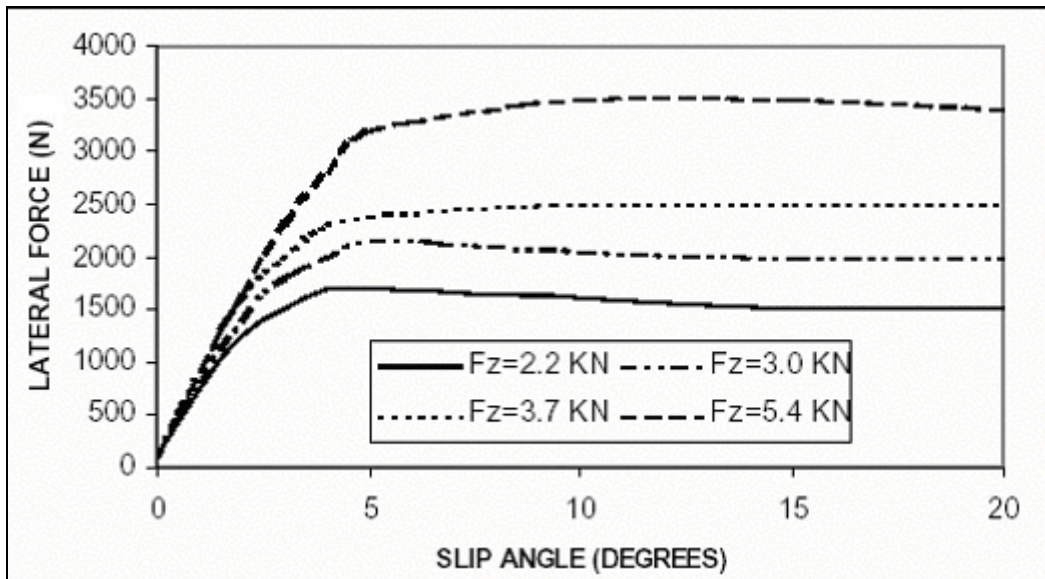
Figure 2.19 Variation of Cornering Force with Changing Slip Angles, by Rao et al 2002
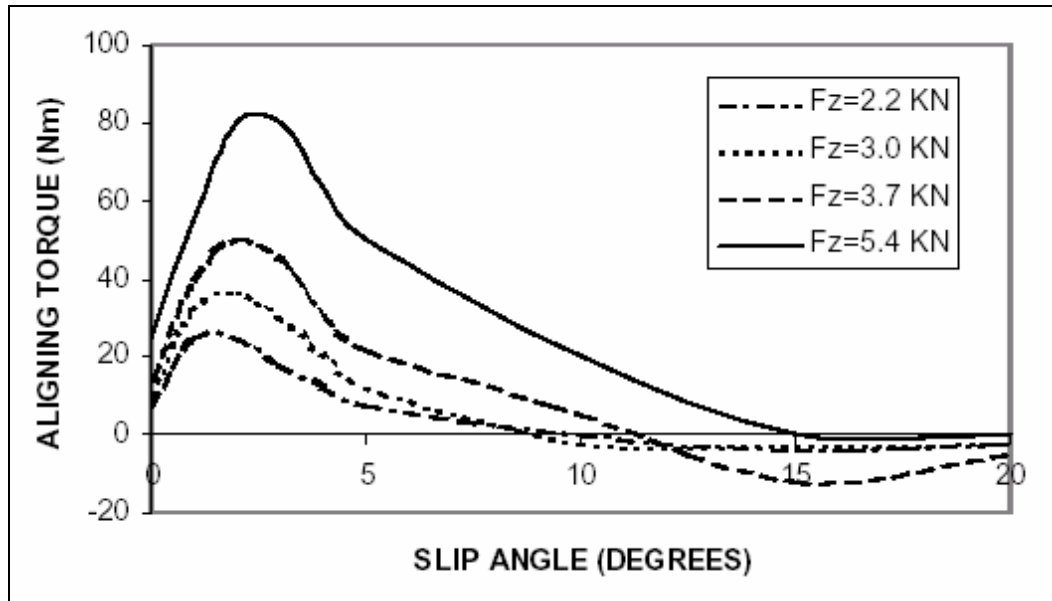
Figure 2.20 Variation of Self Aligning Torque with Changing Slip Angles,
Published by Rao et al 2002

Variations of self aligning torque with respect to slip angle at different vertical forces are presented by authors, given in Figure 2.20. It is observed that the sign of aligning torque changes at around 10 degrees slip angle. Authors concluded that, this change of sign indicates the complete loss of control over the cornering system at very high slip angle cornering.

Rao et al improved the study more and published further data (2003). They performed braking simulation, compared cornering force characteristics for bald and grooved tire (a simplified tread pattern is added to the model) and added camber angle to the simulations as improvements. They added a plot showing a comparison for cornering force, between experimental data and finite element model for 4 degrees slip angle for various vertical loads. Figure 2.21 shows the comparison plot. With the increasing vertical force, difference between the experimental results and the finite element model results increases. The difference is around 25% for 3700N vertical load.
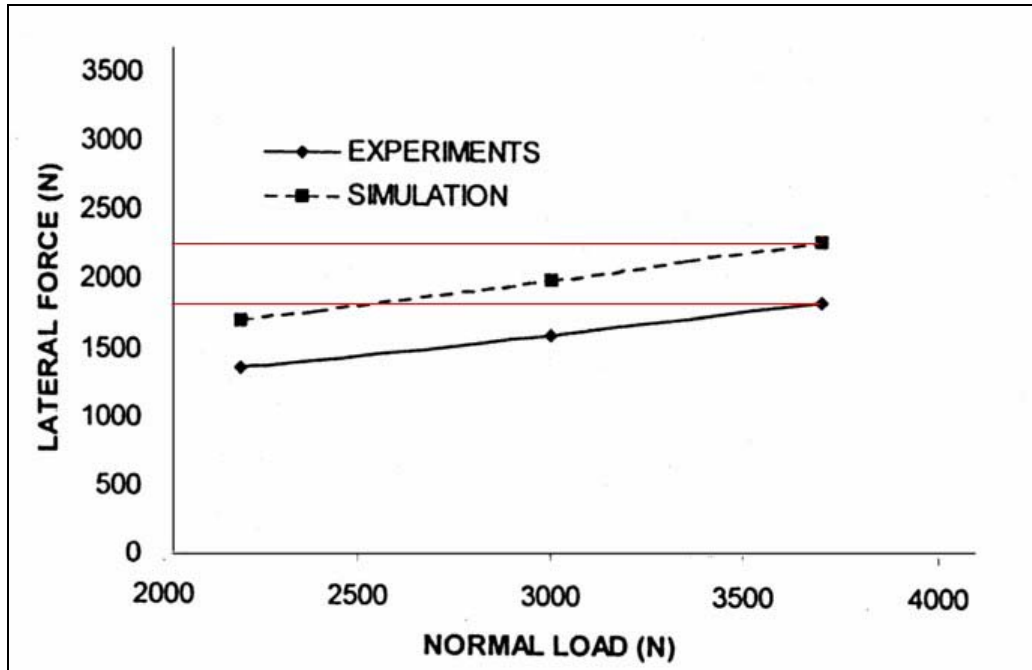
Figure 2.21 Comparison of Cornering Force for 4 Degrees Slip Angle, by Rao et al. 2003

Authors concluded that, the results can be improved by using full integration elements, adding viscoelastic effects, and modeling actual tread pattern, all of which demands serious computational power. But, without them, tire model shows good agreement with the experimental results.

2.2 Summary and Conclusions on Finite Element Tire Models in Literature

Some significant and recent publications directly or indirectly relevant to this study, have been examined in detail and are summarized in this chapter. Key points from the studies are given below.

- Most of the models in literature use Mooney-Rivlin material model for the rubber matrix. Some of the authors, in the hope of decreasing computational effort, compared the results from this material model with results from linear material models, and concluded that they got close

46

results for tire stiffness, in general. However, the convergence problems increase with the use of such linear models.

- Some of the researchers used rebar elements in modeling the carcass and steel belt plies. Other authors modeled the carcass and steel belts with layered shell or membrane elements. Orthotropic material properties are used with success. Only one publication uses continuum (solid) elements for cord reinforced rubber layers, which studied stress and strain distribution on tire structure. This study also gave precise results. Authors calculated unidirectional cord-rubber properties and set the zero degree reinforcement material constants to layered elements. Layer's orientations are set to obtain steel belts configuration.

- Tire geometry is simplified and tread pattern is ignored for all cornering or vertical force studies. Some authors concluded that, tread pattern has minor effect on general stiffness of the tire. Also, textile and steel cords are mostly placed the locations in finite element model different than the real tire. Tire models still showed good agreement with the experimental results.

- In all studies, cornering force values settled to a steady value after half rotation of the tire. The necessary angle to reach steady state cornering force value depends on the tire speed, slip angle and vertical loads. For low slip angles, up to 4 degrees, saturation of cornering force to a steady value takes almost more than one complete rotation of the tire.

- Cornering force data published by the authors have deviations reaching 15 to 25 percent compared with the experimental results. Due to complexity, lack of accurate data and high nonlinearity of the tire structure, this amount of error is concluded as reasonable. Academic

researchers all stated that, obtaining material properties from the manufacturers for the tested tires is very difficult as tire companies keep the material properties as commercial secrets.

- All models require solution times which will give a complete set of cornering force characteristics in at least a month of study even with the fast developments in the computer hardware and software. It is obvious that the priority of development in tire simulation models will be the reduction of solution times rather than accuracy. Thus the models should be clear of all time consuming elements while retaining the essential characteristics of the actual construction.

CHAPTER 3
THEORY OF MATERIAL LAW

In this chapter, basics of material laws, material models and composite theory are discussed.

3.1 Constitutive Relations for Linear Elastic Materials

Robert Hook in 1676 stated that, "The power of any springy body is the same proportion with the extension". This statement announced the birth of elasticity theory. In mathematical terms, Hooke's statement can be expressed as

$$F = k\,u \qquad\qquad (3.1)$$

where F is the applied force (not the power, as Hook mistakenly suggested), u is the deformation of the elastic body subjected to the force F, and k is the spring constant.

The generalized Hooke's law, relating stresses to strains can be written as

$$\sigma_i = C_{ij}\varepsilon_j \qquad\qquad i, j = 1,\ldots,6 \qquad\qquad (3.2)$$

where σ_i are the stress components, C_{ij} is the stiffness matrix, and ε_j are the strain components. The contracted notation is defined in comparison to the usual tensor notation for three-dimensional stresses and strains for situations in which the

stress and strain tensors are symmetric. The strains in contracted notation are defined as

$$\varepsilon_1 = \frac{\partial u}{\partial x} \qquad\qquad \varepsilon_2 = \frac{\partial v}{\partial y} \qquad\qquad \varepsilon_3 = \frac{\partial w}{\partial z}$$

$$\varepsilon_4 = \frac{\partial v}{\partial z} + \frac{\partial w}{\partial y} \qquad \varepsilon_5 = \frac{\partial w}{\partial x} + \frac{\partial u}{\partial z} \qquad \varepsilon_6 = \frac{\partial u}{\partial y} + \frac{\partial v}{\partial x}$$

(3.3)

where u, v and w are displacements in x, y, and z directions respectively.

The stiffness matrix, C_{ij} has 36 constants in Equation 3.2. However, less than 36 of the constants can be shown to be actually independent for elastic materials when the strain energy is considered. Elastic materials for which an elastic potential or strain energy density function exists have incremental work per unit volume of

$$dW = \sigma_i d\varepsilon_i \tag{3.4}$$

When the stresses σ_j act through strains $d\varepsilon_i$. Because of the stress-strain relations, Equation (3.2), the incremental work becomes

$$dW = C_{ij}\varepsilon_j d\varepsilon_i \tag{3.5}$$

Integrating (3.5), the work per unit volume becomes

$$W = \frac{1}{2} C_{ij}\varepsilon_i \varepsilon_j \tag{3.6}$$

Hooke's law, Equation 3.2, can be derived from Equation 3.6:

$$\frac{\partial W}{\partial \varepsilon_i} = C_{ij}\varepsilon_j \qquad (3.7)$$

$$\frac{\partial^2 W}{\partial \varepsilon_i \partial \varepsilon_j} = C_{ij} \qquad (3.8)$$

Similarly

$$\frac{\partial^2 W}{\partial \varepsilon_j \partial \varepsilon_i} = C_{ji} \qquad (3.9)$$

Order of differentiation of W is immaterial, then,

$$C_{ij} = C_{ji} \qquad (3.10)$$

Thus, the stiffness matrix is symmetric so only 21 of the constants are independent. In a similar manner, it can be shown that:

$$W = \frac{1}{2} S_{ij}\sigma_i\sigma_j \qquad (3.11)$$

where S_{ij} is the compliance matrix defined by the inverse of the stress-strain relations, the strain-stress relations:

$$\varepsilon_i = S_{ij}\sigma_j \qquad i,j=1,\ldots,6 \qquad (3.12)$$

Reasoning similar to that in the preceding statement leads to the conclusion that

$$S_{ij} = S_{ji} \qquad\qquad\qquad (3.13)$$

The compliance matrix is symmetric and hence has only 21 independent constants. The stiffness and compliance components will be referred to as elastic constants. With the foregoing reduction from 36 to 21 independent constants, the stress-strain relations are

$$
\begin{Bmatrix} \sigma_1 \\ \sigma_2 \\ \sigma_3 \\ \sigma_4 \\ \sigma_5 \\ \sigma_6 \end{Bmatrix}
=
\begin{bmatrix}
C_{11} & C_{12} & C_{13} & C_{14} & C_{15} & C_{16} \\
C_{21} & C_{22} & C_{23} & C_{24} & C_{25} & C_{26} \\
C_{31} & C_{32} & C_{33} & C_{34} & C_{35} & C_{36} \\
C_{41} & C_{42} & C_{43} & C_{44} & C_{45} & C_{46} \\
C_{51} & C_{52} & C_{53} & C_{54} & C_{55} & C_{56} \\
C_{61} & C_{62} & C_{63} & C_{64} & C_{65} & C_{66}
\end{bmatrix}
\begin{Bmatrix} \varepsilon_1 \\ \varepsilon_2 \\ \varepsilon_3 \\ \varepsilon_4 \\ \varepsilon_5 \\ \varepsilon_6 \end{Bmatrix}
\qquad (3.14)
$$

Equation 3.14 is the most general expression within the framework of linear elasticity. The relations in Equation (3.14) are referred to as characterizing anisotropic materials since there are no planes of symmetry for the material properties. An alternative name for such an anisotropic material is a triclinic material. If there is one plane of material property symmetry, the stress-strain relations reduce to:

$$
\begin{Bmatrix} \sigma_1 \\ \sigma_2 \\ \sigma_3 \\ \sigma_4 \\ \sigma_5 \\ \sigma_6 \end{Bmatrix}
=
\begin{bmatrix}
C_{11} & C_{12} & C_{13} & 0 & 0 & C_{16} \\
C_{12} & C_{22} & C_{23} & 0 & 0 & C_{26} \\
C_{13} & C_{23} & C_{33} & 0 & 0 & C_{36} \\
0 & 0 & 0 & C_{44} & C_{45} & 0 \\
0 & 0 & 0 & C_{45} & C_{55} & 0 \\
C_{16} & C_{26} & C_{36} & 0 & 0 & C_{66}
\end{bmatrix}
\begin{Bmatrix} \varepsilon_1 \\ \varepsilon_2 \\ \varepsilon_3 \\ \varepsilon_4 \\ \varepsilon_5 \\ \varepsilon_6 \end{Bmatrix}
\qquad (3.15)
$$

Where the plane of symmetry is $z=0$. Such a material is termed monoclinic. There are 13 independent constants for monoclinic materials. If there

are two orthogonal planes of material property symmetry for a material, symmetry will exist relative to a third mutually orthogonal plane. The stress-strain relations in coordinates aligned with principal material directions are

$$
\begin{Bmatrix} \sigma_1 \\ \sigma_2 \\ \sigma_3 \\ \sigma_4 \\ \sigma_5 \\ \sigma_6 \end{Bmatrix} = \begin{bmatrix} C_{11} & C_{12} & C_{13} & 0 & 0 & 0 \\ C_{12} & C_{22} & C_{11} & 0 & 0 & 0 \\ C_{13} & C_{23} & C_{33} & 0 & 0 & 0 \\ 0 & 0 & 0 & C_{44} & 0 & 0 \\ 0 & 0 & 0 & 0 & C_{55} & 0 \\ 0 & 0 & 0 & 0 & 0 & C_{66} \end{bmatrix} \begin{Bmatrix} \varepsilon_1 \\ \varepsilon_2 \\ \varepsilon_3 \\ \varepsilon_4 \\ \varepsilon_5 \\ \varepsilon_6 \end{Bmatrix} \tag{3.16}
$$

The material represented with Equation 3.16 is called orthotropic material. There is no interaction between normal stresses σ_1, σ_2, σ_3 and shearing strains υ_{23}, υ_{31}, υ_{12}, such as occurs in anisotropic materials. Similarly there is no interaction between shearing stresses and normal strains as wall as none between shearing stresses and shearing strains in different planes. There are only nine independent constants in the stiffness matrix. If at every point of a material, there is one plane in which the mechanical properties are equal in all directions, than the material is termed transversely isotropic. For example, if the 1-2 plane is the special plane of isotropy, then the 1 and 2 subscripts on the stiffnesses are interchangeable. The stress-strain relations then have only five independent constants and are

$$
\begin{Bmatrix} \sigma_1 \\ \sigma_2 \\ \sigma_3 \\ \sigma_4 \\ \sigma_5 \\ \sigma_6 \end{Bmatrix} = \begin{bmatrix} C_{11} & C_{12} & C_{13} & 0 & 0 & 0 \\ C_{12} & C_{22} & C_{11} & 0 & 0 & 0 \\ C_{13} & C_{23} & C_{33} & 0 & 0 & 0 \\ 0 & 0 & 0 & C_{44} & 0 & 0 \\ 0 & 0 & 0 & 0 & C_{55} & 0 \\ 0 & 0 & 0 & 0 & 0 & \dfrac{(C_{11} - C_{12})}{2} \end{bmatrix} \begin{Bmatrix} \varepsilon_1 \\ \varepsilon_2 \\ \varepsilon_3 \\ \varepsilon_4 \\ \varepsilon_5 \\ \varepsilon_6 \end{Bmatrix} \tag{3.17}
$$

If there are an infinite number of planes of material symmetry, then the foregoing relations simplify to the isotropic material case with only two independent constants in the stiffness matrix:

$$
\begin{Bmatrix} \sigma_1 \\ \sigma_2 \\ \sigma_3 \\ \sigma_4 \\ \sigma_5 \\ \sigma_6 \end{Bmatrix} = \begin{bmatrix} C_{11} & C_{12} & C_{12} & 0 & 0 & 0 \\ C_{12} & C_{11} & C_{12} & 0 & 0 & 0 \\ C_{12} & C_{12} & C_{11} & 0 & 0 & 0 \\ 0 & 0 & 0 & \dfrac{(C_{11}-C_{12})}{2} & 0 & 0 \\ 0 & 0 & 0 & 0 & \dfrac{(C_{11}-C_{12})}{2} & 0 \\ 0 & 0 & 0 & 0 & 0 & \dfrac{(C_{11}-C_{12})}{2} \end{bmatrix} \begin{Bmatrix} \varepsilon_1 \\ \varepsilon_2 \\ \varepsilon_3 \\ \varepsilon_4 \\ \varepsilon_5 \\ \varepsilon_6 \end{Bmatrix} \quad (3.18)
$$

3.2 Engineering Constants for Linear Elastic Materials

Engineering constants are generalized Young's moduli, Poisson's ratios, and shear moduli for an elastic material. These constants are obtained with simple tests and with their obvious physical interpretation, have direct meaning about the material behavior. With known load or stresses, the components of the compliance matrix, S_{ij} are determined more directly than those of the stiffness matrix, C_{ij}. For an orthotropic material, the compliance matrix components in terms of the engineering constants are:

$$
[S_{ij}] = \begin{bmatrix} \dfrac{1}{E_1} & -\dfrac{v_{21}}{E_2} & -\dfrac{v_{31}}{E_3} & 0 & 0 & 0 \\[2ex] -\dfrac{v_{12}}{E_1} & \dfrac{1}{E_2} & -\dfrac{v_{32}}{E_3} & 0 & 0 & 0 \\[2ex] -\dfrac{v_{13}}{E_1} & -\dfrac{v_{23}}{E_2} & \dfrac{1}{E_3} & 0 & 0 & 0 \\[2ex] 0 & 0 & 0 & \dfrac{1}{G_{23}} & 0 & 0 \\[2ex] 0 & 0 & 0 & 0 & \dfrac{1}{G_{31}} & 0 \\[2ex] 0 & 0 & 0 & 0 & 0 & \dfrac{1}{G_{12}} \end{bmatrix}
\qquad (3.19)
$$

Where

E_1, E_2, E_3 = Young's moduli in 1, 2 and 3 directions, respectively.

υ_{ij} = Poisson's ratio for transverse strain in the j-direction when stressed in the i-direction , that is

$$
v_{ij} = -\frac{\varepsilon_j}{\varepsilon_i} \qquad (3.20)
$$

For $\sigma_i = \sigma$ and all other stresses are zero.

G_{23}, G_{31}, G_{12} = shear moduli in the 2-3, 3-1 and 1-2 planes, respectively

For an orthotropic material, there are nine independent constants because

$$
S_{ij} = S_{ji} \qquad (3.21)
$$

Since the compliance matrix is the inverse of the stiffness matrix, if the engineering constants are substituted in Equation 3.21:

$$\frac{\nu_{ij}}{E_i} = \frac{\nu_{ji}}{E_j} \qquad i,j = 1,2,3 \tag{3.22}$$

There are three reciprocal relations that must be satisfied for an orthotropic material. Only υ_{12}, υ_{13} and υ_{23} need to be further considered since υ_{21}, υ_{31} and υ_{32} can be expressed in terms of the first-mentioned Poisson's ratios and the Young's Moduli. Since the stiffness and compliance matrices are mutually inverse, it follows by matrix algebra that their components are related as follows for orthotropic materials.

$$C_{11} = \frac{S_{22}S_{33} - S_{23}^2}{S} \qquad\qquad C_{12} = \frac{S_{13}S_{23} - S_{12}S_{33}}{S}$$

$$C_{22} = \frac{S_{33}S_{11} - S_{13}^2}{S} \qquad\qquad C_{13} = \frac{S_{12}S_{23} - S_{13}S_{22}}{S} \tag{3.23}$$

$$C_{33} = \frac{S_{11}S_{22} - S_{12}^2}{S} \qquad\qquad C_{23} = \frac{S_{12}S_{13} - S_{23}S_{11}}{S}$$

$$C_{44} = \frac{1}{S_{44}} \qquad\qquad C_{55} = \frac{1}{S_{55}} \qquad\qquad C_{66} = \frac{1}{S_{66}}$$

where

$$S = S_{11}S_{22}S_{33} - S_{11}S_{23}^2 - S_{22}S_{13}^2 - S_{33}S_{12}^2 + 2S_{12}S_{23}S_{13} \tag{3.24}$$

The stiffness matrix, C_{ij}, for an orthotropic material in terms of the engineering constants is obtained by inversion of the compliance matrix, S_{ij}, in

Equation 3.19 or by substitution in Equations 3.23 and 3.24. The nonzero stiffnesses in Equation 3.16 are:

$$C_{11} = \frac{1 - v_{23}v_{32}}{E_2 E_3}$$

$$C_{12} = \frac{v_{21} + v_{31}v_{23}}{E_2 E_3 \Delta} = \frac{v_{12} + v_{32}v_{13}}{E_1 E_3 \Delta} \qquad (3.25)$$

$$C_{13} = \frac{v_{13} + v_{21}v_{32}}{E_2 E_3 \Delta} = \frac{v_{13} + v_{12}v_{23}}{E_1 E_2 \Delta}$$

$$C_{22} = \frac{1 - v_{23}v_{32}}{E_1 E_3 \Delta}$$

$$C_{23} = \frac{v_{32} + v_{12}v_{31}}{E_1 E_3 \Delta} = \frac{v_{23} + v_{21}v_{13}}{E_1 E_2 \Delta} \qquad (3.25 \text{ cont.})$$

$$C_{33} = \frac{1 - v_{12}v_{21}}{E_1 E_2 \Delta}$$

$$C_{44} = G_{23} \qquad\qquad C_{55} = G_{31} \qquad\qquad C_{66} = G_{12}$$

where

$$\Delta = \frac{1 - v_{12}v_{21} - v_{23}v_{32} - v_{31}v_{13} - 2v_{12}v_{32}v_{13}}{E_1 E_2 E_3} \qquad (3.26)$$

For isotropic materials, certain relations between the elastic constants must be satisfied.

$$G = \frac{E}{2(1+v)} \qquad\qquad (3.27)$$

In order that E and G always be positive, a positive normal stress or shear stress times the respective normal strain or shear strain yield positive work,

$$v > -1 \qquad\qquad (3.28)$$

In the same manner, if an isotropic body is subjected to hydrostatic pressure, p, then the volumetric strain, the sum of the three normal or extensional strains is defined by

$$\theta = \varepsilon_x + \varepsilon_y + \varepsilon_z = \frac{p}{E/3(1-2v)} = \frac{p}{K} \qquad\qquad (3.29)$$

Then, the bulk modulus, K is

$$K = \frac{E}{3(1-2v)} \qquad\qquad (3.30)$$

Is positive only if E is positive and

$$v < \frac{1}{2} \qquad\qquad (3.31)$$

If the bulk modulus were negative, a hydrostatic pressure would cause expansion of a cube of isotropic material. Thus, in isotropic materials, Poisson's ratio is restricted to the range

$$-1 < v < \frac{1}{2} \tag{3.32}$$

In order that shear or hydrostatic loading not produce negative strain energy.

For orthotropic materials, the relations between elastic constants are more complex. The product of a stress component and the corresponding strain component represents work done by the stress. The sum of the work done by all stress components must be positive in order to avoid the creation of energy.

$$E_1, E_2, E_3, G_{23}, G_{31}, G_{12} > 0 \tag{3.33}$$

Similarly, under suitable constraints, deformation is possible in which only one extensional strain arises. Again, work is produced by the corresponding stress alone. Thus, since the work done is determined by the diagonal elements of the stiffness matrix, those elements must be positive, that is,

$$C_{11}, C_{22}, C_{33}, C_{44}, C_{55}, C_{66} > 0 \tag{3.34}$$

Using Equation 3.25,

$$(1 - v_{23}v_{32}) > 0$$
$$(1 - v_{13}v_{31}) > 0 \tag{3.35}$$
$$(1 - v_{12}v_{21}) > 0$$
and

$$\Delta = 1 - v_{12}v_{21} - v_{23}v_{32} - v_{31}v_{13} - 2v_{21}v_{32}v_{13} > 0 \tag{3.36}$$

Since all the determinants must be positive for positive definiteness. Also from Equation 3.23, the positive definiteness leads to :

$$|S_{23}| < \sqrt{S_{22}S_{33}}$$
$$|S_{13}| < \sqrt{S_{11}S_{33}} \tag{3.37}$$
$$|S_{12}| < \sqrt{S_{11}S_{22}}$$

By using the condition of symmetry of the compliances,

$$\frac{\nu_{ij}}{E_i} = \frac{\nu_{ji}}{E_j} \qquad i, j = 1,2,3 \tag{3.38}$$

The condition of Equation 3.35 and 3.38 can be written as;

$$|\nu_{21}| < \left(\frac{E_2}{E_1}\right)^{\frac{1}{2}} \qquad |\nu_{12}| < \left(\frac{E_1}{E_2}\right)^{\frac{1}{2}}$$

$$|\nu_{32}| < \left(\frac{E_3}{E_2}\right)^{\frac{1}{2}} \qquad |\nu_{23}| < \left(\frac{E_2}{E_3}\right)^{\frac{1}{2}} \tag{3.39}$$

$$|\nu_{13}| < \left(\frac{E_1}{E_3}\right)^{\frac{1}{2}} \qquad |\nu_{31}| < \left(\frac{E_3}{E_1}\right)^{\frac{1}{2}}$$

and Equation 3.36 can be expressed as

$$\nu_{12}\nu_{32}\nu_{13} < \frac{1 - \nu_{21}^2\left(\frac{E_1}{E_2}\right) - \nu_{32}^2\left(\frac{E_2}{E_3}\right) - \nu_{13}^2\left(\frac{E_3}{E_1}\right)}{2} < \frac{1}{2} \tag{3.40}$$

The preceding restrictions on engineering constants for orthotropic materials are used to examine experimental or derived data to see if they are

physically consistent within the frame work of the mathematical elasticity model. Those restrictions can also be used to solve the differential equations of a physical problem which the solution depends on the constants.

3.3 Basics of Composite Materials

Composite materials have different elastic behavior. Some composite materials have very simple forms of in-homogeneity. For example, laminated safety glass has three layers each of which is homogeneous and isotropic; thus, the in-homogeneity of the composite is a step function in the direction perpendicular to the plane of the glass. Fiber reinforced composites mainly shows transversely isotropic or orthotropic material behavior depending on the fiber construction. Figure 3.1 shows a fiber reinforced composite structure. The reinforcements are all in 0 degrees to Z direction, and material constants in XY plane shows isotropy. This composition is transversely isotropic.
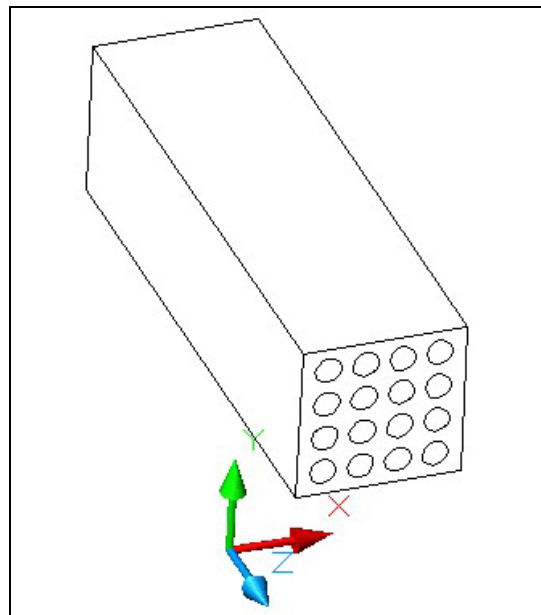
Figure 3.1 Unidirectional Fibers

Laminated composites consist of layers of at least two different materials that are bonded together. Lamination is used to combine the best aspects of the constituent layers in order to achieve a more useful material. Laminated fiber-reinforced composites are a hybrid class of composites involving both fibrous composites and lamination techniques. Layers of fiber-reinforced material are built up with the fiber directions of each layer typically oriented in different directions to give different strength and stiffness in the various directions. Thus, the strength and stiffness of the laminated fiber-reinforced composite can be tailored to the specific design requirements of the structural element being built.

A lamina is an arrangement of unidirectional fibers or woven fibers in a matrix. The fibers are the principal reinforcing or load-carrying agent. They are typically strong and stiff. The matrix can be elastomer, ceramic, or metallic. The function of the matrix is to support and protect the fibers and to provide a means of distributing load among and transmitting load between the fibers. Fibers generally exhibit linear elastic behavior, although reinforcing steel bars in concrete are more nearly elastic-perfectly plastic. Commonly, resinous matrix materials are Viscoelastic, if not viscoplastic. Fiber-reinforced composites are usually treated as linear elastic materials since the fibers provide the majority of the strength and stiffness. Refinement of that approximation requires consideration of some form of plasticity, viscoelasticity, or both (visco plasticity). Very little work has been done to implement those idealizations of composite material behavior in structural applications. (Tsai, 1988)

A laminate is a stack of laminae with various orientations of principal material directions in the laminae. Generally the fiber orientation of the layers are not symmetric about the middle surface of the laminate. The layers of a laminate are usually bound together by the same matrix material that is used in the laminae. Laminates can be composed of plates of different materials or layers of fiber-reinforced laminae. A major purpose of lamination is to tailor the

directional dependence of strength and stiffness of a material to match the loading environment of the structural element. Laminates are uniquely suited to this objective since the principal material directions of each layer can be oriented according to need.

3.4 Classical Laminate Theory

Although the laminate is made up of multiple laminae, it is assumed that the individual laminae are perfectly bonded together so as to behave as a unitary, nonhomogeneous, anisotropic plate. Interfacial slip is not allowed and the interfacial bonds are not allowed to deform in shear, which means that displacements across lamina interfaces are assumed to be continuous. These assumptions mean that the deformation hypothesis from the classical homogeneous plate theory can be used for the laminated plate the laminate force-deformation equations resulting from this deformation hypothesis are now derived following the procedure outlined by Whitney. Although Whitney has presented a general analysis including the equations of motion, only the static analysis will be considered. The basic assumptions relevant to the present static analysis are

1 The plate consists of orthotropic laminae bonded together, with the principal material axes of the orthotropic laminae oriented along arbitrary directions with respect to the xy axes.

2 The thickness of the plate, t, is much smaller than the lengths along the plate edges.

3 The displacements u, v and w are small compared with the plate thickness.

4 The in-plane strains $\in_x$, $\in_y$ and γ_{xy} are small compared with unity.

5 Transverse shear strains γ_{xz} and γ_{yz} are negligible.

6 Tangential displacements u and v are linear functions of the z coordinate.

7 The transverse normal strain $\in_z$ is negligible.

8 Each ply obeys Hooke's law.

9 The plate thickness t is constant.

Assumption 5 is a result of the assumed state of plane stress in each ply, whereas assumptions 5 and 6 together define the Kirchhoff deformation hypothesis that normals to the middle surface remain straight and normal during deformation. According to assumptions 6 and 7, the displacements can be expressed as

$$u = u^0(x,y) + zF_1(x,y)$$
$$v = v^0(x,y) + zF_2(x,y) \tag{3.55}$$

Where u^0 and v^0 are the tangential displacements of the middle surface along the x and y directions, respectively. Due to assumption 7, the transverse displacement at the middle surface, $w^0(x,y)$, is the same as the transverse displacement of any point having the same x and y coordinates, so

$$w^0(x,y) = w(x,y) \ . \tag{3.56}$$

In order to account for possible warping of the cross section of the laminate and resulting transverse shear deformations, it is necessary to use a so-called higher order laminations theory. One such theory, which is based on the assumption that the displacements are nonlinear, functions of the z coordinate as follows:

$$u = u^0(x,y) + z\psi_x(x,y) + z^2\zeta_x(x,y) + z^3\phi_x(x,y)$$

$$v = v^0(x,y) + z\psi_y(x,y) + z^2\zeta_y(x,y) + z^3\phi_y(x,y) \qquad (3.57)$$

$$w = w^0(x,y) + z\psi_z(x,y) + z^2\zeta_2(x,y)$$

Substituting Equations (3.55) in the strain displacement equations for the transverse shear strains and using assumption 5,

$$\gamma_{xz} = \frac{\partial u}{\partial z} + \frac{\partial w}{\partial x} = F_1(x,y) + \frac{\partial w}{\partial x} = 0$$

$$\qquad (3.58)$$

$$\gamma_{yz} = \frac{\partial v}{\partial z} + \frac{\partial w}{\partial y} = F_2(x,y) + \frac{\partial w}{\partial y} = 0$$

$$F_1(x,y) = -\frac{\partial w}{\partial x} \qquad\qquad F_2(x,y) = -\frac{\partial w}{\partial y} \qquad (3.59)$$

Substituting Equations (3.55) and (3.59) in the strain displacement relations for the in plane strains,

$$\in_x = \frac{\partial u}{\partial x} = \in_x^0 + z\kappa_x$$

$$\in_y = \frac{\partial v}{\partial x} = \in_y^o + z\kappa_y \qquad (3.60)$$

$$\gamma_{xy} = \frac{\partial u}{\partial y} + \frac{\partial v}{\partial x} = \gamma_{xy}^0 + z\kappa_{xy}$$

where the strains on the middle surface are

$$\epsilon_x^0 = \frac{\partial u^0}{\partial x} \qquad \epsilon_y^0 = \frac{\partial v^0}{\partial y} \qquad \gamma_{xy}^0 = \frac{\partial u^0}{\partial y} + \frac{\partial v^0}{\partial x} \tag{3.61}$$

and the curvatures of the middle surface are

$$\kappa_x = -\frac{\partial^2 w}{\partial x^2} \qquad \kappa_y = -\frac{\partial^2 w}{\partial y^2} \qquad \kappa_{xy} = -2\frac{\partial^2 w}{\partial x \partial y} \tag{3.62}$$

κ_x is a bending curvature associated with bending of the middle surface in the xz plane and κ_y is a bending curvature associated with bending of the middle surface in the yz plane, κ_{xy} is a twisting curvature associated with out-of-plane twisting of the middle surface, which lies in the xy plane before deformation.

Since Equations (3.60) give the strains at any distance z from the middle surface, the stresses along arbitrary xy axes in the kth lamina of a laminate may be found by substituting Equations (3.60) into the lamina stress-strain relationships as follows:

$$\begin{Bmatrix} \sigma_x \\ \sigma_y \\ \tau_{xy} \end{Bmatrix}_k = \begin{bmatrix} \overline{Q}_{11} & \overline{Q}_{12} & \overline{Q}_{16} \\ \overline{Q}_{12} & \overline{Q}_{22} & \overline{Q}_{26} \\ \overline{Q}_{16} & \overline{Q}_{26} & \overline{Q}_{66} \end{bmatrix}_k = \begin{Bmatrix} \epsilon_x^0 + z\kappa_x \\ \epsilon_y^0 + z\kappa_y \\ \epsilon_{xy}^0 + z\kappa_{xy} \end{Bmatrix} \tag{3.63}$$

where the subscript k refers to the kth lamina.

The force per unit length, N$_x$, is given by

66

$$N_x = \int_{-t/2}^{t/2} \sigma_x dz = \sum_{k=1}^{N} \left\{ \int_{z_{k-1}}^{z_k} (\sigma_x)_k \, dz \right\} \tag{3.64}$$

and the moment per unit length, M_x, is given by

$$M_x = \int_{-t/2}^{t/2} \sigma_x z dz = \sum_{k=1}^{N} \left\{ \int_{z_{k-1}}^{z_k} (\sigma_x)_k \, z dz \right\} \tag{3.65}$$

where

t= laminate thickness

$(\sigma_x)_k$ = stress in the kth lamina

z_{k-1}= distance from middle surface to inner surface of the kth lamina

z_k= corresponding distance from middle surface to outer surface of the kth lamina

Substituting the lamina stress-strain relationships from Equations. (3.62) to Equations. (3.64) and (3.65), respectively,

$$N_x = \sum_{k=1}^{N} \int_{z_{k-1}}^{z_k} \left\{ (\bar{Q}_{11})_k (\in_x^0 + z\kappa_x) + (\bar{Q}_{12})_k (\in_y^o + z\kappa_y) + (\bar{Q}_{16})_k (\gamma_{xy}^o + z\kappa_{xy}) \right\} dz \tag{3.66}$$

and

$$M_x = \sum_{k=1}^{N} \int_{z_{k-1}}^{z_k} \left\{ (\bar{Q}_{11})_k (\in_x^0 + z\kappa_x) + (\bar{Q}_{12})_k (\in_y^0 + z\kappa_y) + (\bar{Q}_{16})_k (\gamma_{xy}^0 + z\kappa_{xy}) \right\} z dz \tag{3.67}$$

Combining terms and rearranging Equations. (3.65) and (3.66),

$$N_x = A_{11} \in_x^0 + A_{12} \in_y^0 + A_{16}\gamma_{xy}^0 + B_{11}\kappa_x + B_{12}\kappa_y + B_{16}\kappa_{xy} \tag{3.68}$$

and

$$M_x = B_{11} \, \epsilon_x^0 + B_{12} \, \epsilon_y^0 + B_{16}\gamma_{xy}^0 + D_{11}\kappa_x + D_{12}\kappa_y + D_{16}\kappa_{xy} \qquad (3.69)$$

where the laminate extensional stiffnesses are given by

$$A_{ij} \int_{-t/2}^{t/2} (\bar{Q}_{ij})_k \, dz = \sum_{k=1}^{N} (\bar{Q}_{ij})_k (z_k - z_{k-1}) \qquad (3.70)$$

The laminate coupling stiffnesses are given by

$$B_{ij} = \int_{-t/2}^{t/2} (\bar{Q}_{ij})_k \, z\,dz = \frac{1}{2}\sum_{k=1}^{N} (\bar{Q}_{ij})_k (z_k^2 - z_{k-1}^2) \qquad (3.71)$$

and the laminate bending stiffnesses are given by

$$D_{ij} = \int_{-t/2}^{t/2} (\bar{Q}_{ij})_k \, z^2\,dz = \frac{1}{3}\sum_{k=1}^{N} (\bar{Q}_{ij})_k (z_k^3 - z_{k-1}^3) \qquad (3.72)$$

where the subscripts i,j=1, 2, or 6. The other stress resultants can be written in similar form, and the complete set of equations can be expressed in matrix form as

$$\begin{Bmatrix} N_x \\ N_y \\ N_{xy} \\ M_x \\ M_y \\ M_{xy} \end{Bmatrix} = \begin{bmatrix} A_{11} & A_{12} & A_{16} & B_{11} & B_{12} & B_{16} \\ A_{12} & A_{22} & A_{26} & B_{12} & B_{22} & B_{1126} \\ A_{16} & A_{26} & A_{66} & B_{16} & B_{26} & B_{66} \\ B_{11} & B_{12} & B_{16} & D_{11} & D_{12} & D_{16} \\ B_{12} & B_{22} & B_{26} & D_{12} & D_{22} & D_{26} \\ B_{16} & B_{26} & B_{66} & D_{16} & D_{26} & D_{66} \end{bmatrix} = \begin{Bmatrix} \epsilon_x^0 \\ \epsilon_y^0 \\ \gamma_{xy}^0 \\ \kappa_x \\ \kappa_y \\ \kappa_{xy} \end{Bmatrix} \qquad (3.73)$$

or in partitioned form as

$$\left\{ \begin{array}{c} N \\ \cdots \\ M \end{array} \right\} = \left[\begin{array}{ccc} A & \vdots & B \\ \cdots & \vdots & \cdots \\ B & \vdots & D \end{array} \right] \left\{ \begin{array}{c} \in^0 \\ \kappa \end{array} \right\} \qquad (3.73)$$

3.5 Cord Reinforced Composites

Tsai (1998) gives the Rule-of-Mixture relation for fiber-reinforced matrix as:

$$E_x = v_f E_f + v_m E_m \qquad (3.74)$$

where v_f is the volume fraction of the fiber, v_m is the volume fraction of the matrix, E_f is the Young's modulus of the fiber and E_m is the Young's modulus of the matrix. For unidirectional fiber reinforced composites, the main concern is mostly the stiffness of the structure in fiber direction, E_x. Since the fiber stiffness is many times the matrix stiffness, the second term in Equation 3.74 is often being ignored.

Pelc (2001) derived and used the following equations for cord rubber composites,

$$E_1 = E_c v_c + E_r (1 - v_c) \qquad (3.75)$$

$$E_2 = E_r \frac{(1 + 2v_c)}{(1 - v_c)} \qquad (3.76)$$

$$E_3 = E_2 \qquad (3.77)$$

69

$$G_{12} = G_r \qquad\qquad (3.78)$$

$$G_{13} = G_{23} = 3G_{12} \qquad\qquad (3.79)$$

$$\nu_{12} = \nu_{13} = 0.5 \qquad\qquad (3.80)$$

$$\nu_{23} = 0.98 - \nu_{21} \qquad\qquad (3.81)$$

where c denotes cord and r denotes rubber. For multilayer structures like steel belts of the tire, each layer's property can be calculated by selecting reinforcement direction as the principal direction. Then, this data can be used either separately or combined.
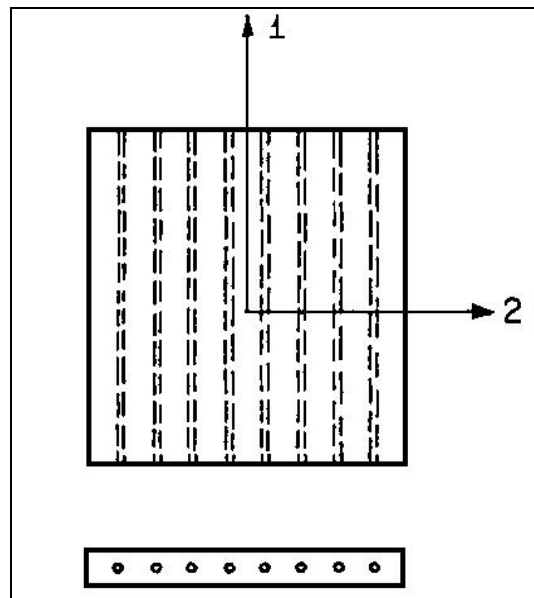
Figure 3.2 Unidirectional Ply Configuration

Halpin-Tsai equations take the form for the cord-rubber construction shown in Figure 3.2,

$$E_1 = E_c v_c + E_r(1 - v_c)$$

$$E_2 = \frac{E_r(1 + 2v_c)}{1 - v_c}$$

$$G_{12} = \frac{G_r\left[G_c + G_r + (G_c - G_r)v_c\right]}{G_c + G_r - (G_c - G_r)v_c}$$

$$v_{12} = v_c v_c + v_r(1 - v_c)$$

$$v_{21} = \frac{v_{12}E_2}{E_1}$$

(3.87)

where, E_c, E_r = Young's modulus of cord and rubber, respectively;

G_c, G_r = Shear moduli of cord and rubber, respectively;

v_c, v_r = Poisson's ratio of cord and rubber, respectively; and

v_c = Volume fraction of cord

The relation for E_1 and v_{12} are obtained from the law of mixtures. E_2 and G_{12} are semiempirical. In order to employ the Halpin-Tsai equations, it is necessary to know cord properties G_c and v_c which are often difficult to obtain experimentally.

Tangorra (1971) developed a set of expressions specifically tailored to the properties of cord reinforced rubber in the form

$$E_1 = E_c v_c + E_r(1 - v_c)$$

$$E_2 = \frac{4E_r(1 - v_c)\left[E_c v_c + E_r(1 - v_c)\right]}{3E_c v_c + 4E_r(1 - v_c)}$$

$$G_{12} = G_r(1 - v_c)$$

(3.88)

$$v_{12} = 0.5$$

$$\nu_{21} = \frac{\nu_{12}E_2}{E_1}$$

The incompressibility of the rubber matrix has been used, and the cord has been treated as a load carrying member with properties only in its lengthwise direction. This eliminates the need for detailed cord stiffness data.

The following set of equations was developed by Akasaka and Hirano (1972) (as approximations to the Gough-Tangorra equations by noting that, for usual cord-rubber composites, the very high cord stiffness results in the cord providing essentially all of the E_1 stiffness, while in the transverse direction the rubber modulus is so low that it dominates E_2. These types of approximations lead to expressions

$$E_1 = E_c \nu_c$$
$$E_2 = \frac{4E_r}{3}$$
$$G_{12} = G_r \qquad\qquad (3.89)$$
$$\nu_{12} = 0.5$$
$$\nu_{21} = 0$$

Once the elastic constants of a single sheet are known, they may be used to generate the elastic constants of another type of construction often used for tires, and common in other products as well, whereby a series of laminate are bonded together in pairs to form an equi-angular, or bias, construction Any numbers of pairs of plies may be used, provided that they are bonded together with the same angle $\pm\alpha$. Such a construction is sometimes termed specially orthotropic.

By summing the properties of one, or more, pairs of such plies, the elastic constants, E_y, G_{xy} and ν_{xy} can be obtained in terms of E_1, E_2, G_{12}, ν_{12} and ν_{21}. As a specific example of this, the Gough-Tangorra Equations (3.88) may be used in such a formulation to directly express E_y, G_{xy} ν_{xy} and in terms of E_y, G_r, ν_c, etc. Such formulations are given below:

$$\frac{E_y}{G_r} = \frac{E_c}{G_r} \nu_c \cos^4 \alpha + 4(1 - \nu_c) - \frac{\left[\frac{E_c}{G_r} \nu_c \sin^2 \alpha \cos^2 \alpha + 2(1 - \nu_c) \right]^2}{\frac{E_c}{G_r} \nu_c \sin^4 \alpha + 4(1 - \nu_c)} \qquad (3.90)$$

$$\frac{G_{xy}}{G_r} = 1 + \nu_c \left[\frac{E_c}{G_r} \sin^2 \alpha \cos^2 \alpha - 1 \right] \qquad (3.91)$$

$$\nu_{yx} = \frac{\frac{E_c}{G_r} \nu_c \sin^2 \alpha \cos^2 \alpha + 2(1 - \nu_c)}{\frac{E_c}{G_r} \nu_c \sin^4 \alpha + 4(1 - \nu_c)} \qquad (3.92)$$

The theory proposed by Clark (1983) is intended to provide an alternate approach to the Halpin-Tsai equations by using energy methods to formulate expressions for E_y, G_{xy} and ν_{yx} directly, without requiring detailed cord properties such as G_c and ν_c, but in a form more accurate than the Gough-Tangorra equations.

When more than one ply is considered, the simple equations become more complex. Typically, steel cords in tread plies are in bias configuration as shown in Figure 3.3.
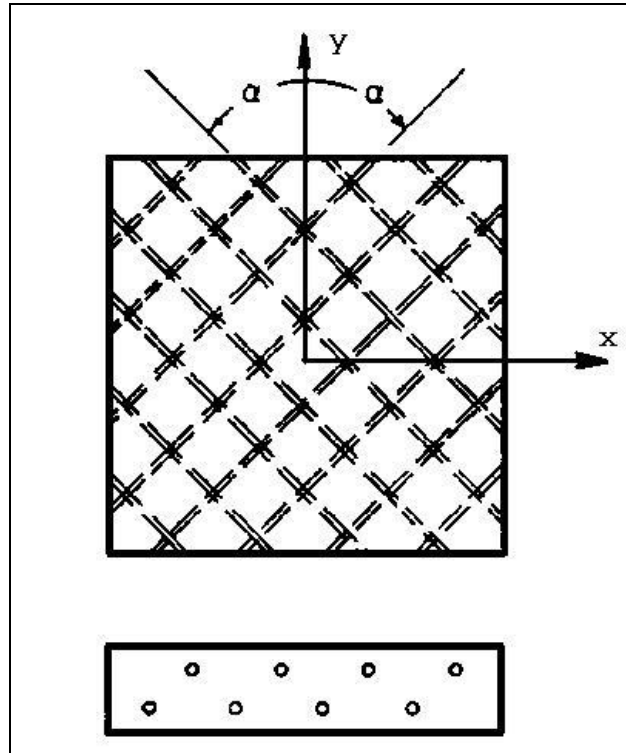
Figure 3.3 Bias Reinforcement Configuration
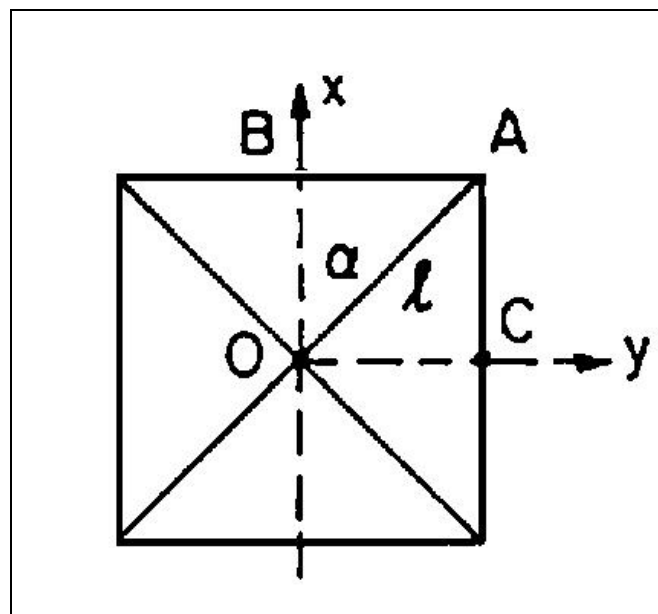
Figure 3.4 Bias Configuration Parameters for Clark's Derivation

74

Considering an element with extensible cords in bias configuration as it is in Figure 3.4 and where the cord OA does not change angle but simply changes length as it is in Figure 3.5.

Let the length from O to A be l. then the length of sides OB and OC are

$$dx = dl \cos \alpha \qquad\qquad dy = dl \sin \alpha$$

$$\varepsilon_x' = \frac{dx}{x} = \frac{dl \cos \alpha}{l \cos \alpha} = \frac{dl}{l} = \varepsilon_c = \text{cord strain}$$

$$\varepsilon_y' = \frac{dy}{y} = \frac{dl \sin \alpha}{l \sin \alpha} = \frac{dl}{l} = \varepsilon_c = \text{cord strain}$$

$$x = l \cos \alpha \qquad\qquad y = l \sin \alpha$$

$$dx = -l \sin \alpha d\alpha \qquad\qquad dy = l \cos \alpha d\alpha$$

and when l=constant, only the angle can change so that

$$\varepsilon_x = \frac{dx}{x} = -\tan \alpha d\alpha \qquad\qquad \varepsilon_y = \frac{dy}{y} = \cot \alpha d\alpha \qquad (3.93)$$
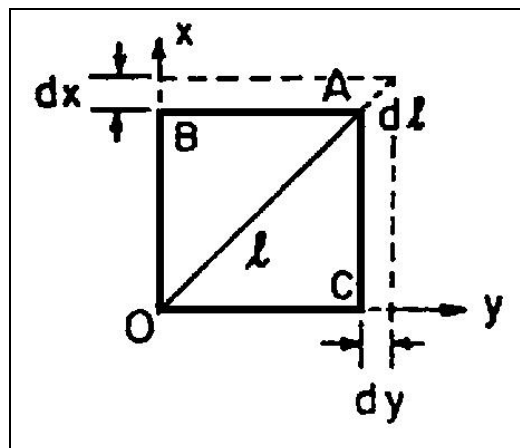
Figure 3.5 Cord Changes in Length Only

75

The total strain in an actual cord-rubber element is a combination of cord rotation and cord strain. Now, the total strain in the element becomes the sum of the two:

$$\varepsilon_x = -\tan\alpha \, d\alpha + \varepsilon_c, \qquad\qquad \varepsilon_y = \cot\alpha \, d\alpha + \varepsilon_c,$$

$$\varepsilon_x - \varepsilon_c = -\tan\alpha \, d\alpha, \qquad\qquad \varepsilon_y - \varepsilon_c = \cot\alpha \, d\alpha, \qquad (3.94)$$

$$\frac{\varepsilon_x - \varepsilon_c}{\varepsilon_y - \varepsilon_c} = -\tan^2\alpha,$$

$$\varepsilon_x - \varepsilon_c = -\varepsilon_y \tan^2\alpha + \varepsilon_c \tan^2\alpha,$$

$$\varepsilon_x = \varepsilon_c\left(1 + \tan^2\alpha\right) - \varepsilon_y \tan^2\alpha. \qquad (3.95)$$

Assuming that a value of ε_y is specified and constructing Mohr's circle for strain as shown in Figure 3.6. The offset d and the radius R are given by

$$d = \frac{\varepsilon_y + \varepsilon_x}{2} = \frac{\varepsilon_y\left(1 - \tan^2\alpha\right) + \varepsilon_c\left(1 + \tan^2\alpha\right)}{2}, \qquad (3.96)$$
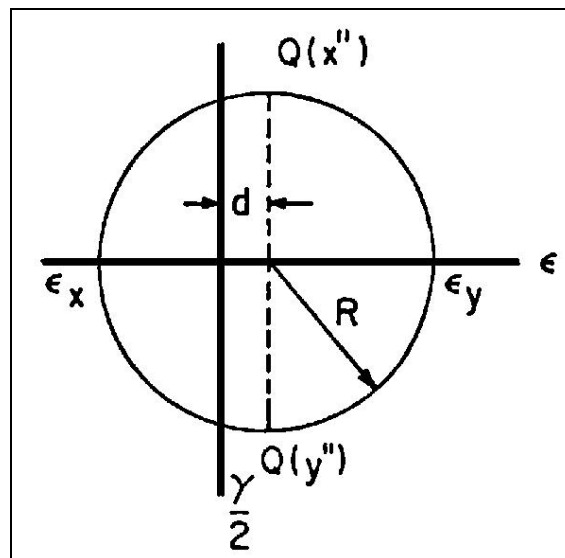
Figure 3.6 Mohr's Circle

$$R = \frac{\varepsilon_y - \varepsilon_x}{2} = \frac{\varepsilon_y\left(1 - \tan^2\alpha\right) - \varepsilon_c\left(1 + \tan^2\alpha\right)}{2} = \frac{(\varepsilon_y - \varepsilon_c)}{2}\left(1 + \tan^2\alpha\right) (3.97)$$

Taking the state of strain of the element of Figure 3.4 to be represented by point Q of Figure 3.6:

$$\varepsilon_x^{''} = \varepsilon_y^{''} = d = \frac{\varepsilon_y\left(1 + \tan^2\alpha\right) + \varepsilon_c\left(1 + \tan^2\alpha\right)}{2}, \qquad (3.98)$$

where $x^{''}$ and $y^{''}$ are now at $45°$ to the x and y directions due to rotation of point Q from the original ε_y direction and γ is diameter of the Mohr's Circle, then

$$R = \frac{\gamma}{2} = \frac{(\varepsilon_y - \varepsilon_c)}{2}\left(1 + \tan^2\alpha\right). \qquad (3.99)$$

The total strain energy in the element of unit volume is now given by the strain energy stored in the cord. Only the tensile elongation of the cord is considered in computing its strain energy. Let V=strain energy,

$$V = \left\{\frac{1}{2}\sigma_x\varepsilon_x + \frac{1}{2}\sigma_y\varepsilon_y + \frac{1}{2}\gamma_{xy}\tau_{xy}\right\}\left(1 - v_c\right)^{-1} + \left\{\frac{1}{2}\sigma_c\varepsilon_c\right\}v_c, \qquad (3.100)$$

$$\{\text{Rubber}\} \qquad\qquad \{\text{Cord}\}$$

where v_c is the volume fraction of cord. For the isotropic rubber, with equal extensional strains in the two directions $x^{''}$ and $y^{''}$, the stresses must be equal:

$$\varepsilon_x^{''} = \varepsilon_y^{''} = \varepsilon = 0.5\frac{\sigma}{E}$$

$$\sigma = 2E_r\varepsilon = 6G_r\varepsilon \qquad (3.101)$$

Since $E_r = 3G_r$.

Also $\tau = G_r\gamma$., then the strain energy becomes:

$$V = \left\{ \frac{1}{2}.6G_r\varepsilon^2 + \frac{1}{2}.6G_r\varepsilon^2 + \frac{1}{2}.6G_r\gamma^2 \right\}\left(1 - v_c\right)^{-1} + \frac{1}{2}E_c\varepsilon_c v_c \quad (3.102)$$

Since cord is in uniaxial tension, where $\sigma_c + E_c\varepsilon_c$. Substituting Equation (3.98) for ε and Equation (3.99) for $\frac{\gamma}{2}$. The Equation 3.102 becomes

$$2V = \left[\begin{array}{l} 12G_r\left\{ \dfrac{\varepsilon_y^2\left(1-\tan^2\alpha\right)^2 + 2\varepsilon_y\varepsilon_c\left(1-\tan^4\alpha\right) + \varepsilon_c^2\left(1+\tan^2\alpha\right)^2}{4} \right\} \\ + G_r\left\{ \left(\varepsilon_y - \varepsilon_c\right)^2\left(1+\tan^2\alpha\right)^2 \right\} \end{array} \right]\left(1-v_c\right)^{-1} + \varepsilon_c^2 E_c v_c$$

$$(3.103)$$

Defining a variable $\lambda = \dfrac{\varepsilon_c}{\varepsilon_y}$, equation (3.93) becomes

$$2V = \left[\left[\begin{array}{l} 12G_r\left\{ \dfrac{\left(1-\tan^2\alpha\right)^2 + 2\lambda\left(1-\tan^4\alpha\right) + \lambda^2\left(1+\tan^2\alpha\right)^2}{4} \right\} \\ + G_r\left\{ 2\left(1-\lambda\right)^2\left(1+\tan^2\alpha\right)^2 \right\} \end{array} \right]\left(1-v_c\right)^{-1} + \lambda^2 E_c v_c \right]\varepsilon_y^2$$

$$(3.104)$$

For a given strain ε_y, the strain energy V must be minimized with respect to the variable λ, which represents the amount of cord extension associated with a given level of strain ε_y. Set $\dfrac{\partial V}{\partial \lambda} = 0$.

$$\left(\frac{2}{\varepsilon_y 2}\right)\frac{\partial V}{\partial \lambda} = \left[\begin{array}{c} 3G_r\left\{2\left(1-\tan^4\alpha\right)2\lambda\left(1+\tan^2\alpha\right)^2\right\} \\ -G_r\left\{2\left(1-\lambda\right)\left(1+\tan^2\alpha\right)^2\right\} \end{array}\right]\left(1-v_c\right)^{-1} + 2\lambda v_c E_c = 0$$

(3.105)

Solving for λ,

$$\lambda = \frac{\left[2G_r\left(1+\tan^2\alpha\right)^2 - 6G_r\left(1-\tan^4\alpha\right)\right]\left(1-v_c\right)^{-1}}{\left[8G_r\left(1+\tan^2\alpha\right)^2\left(1-v_c\right)^{-1} + 2v_c E_c\right]}$$

(3.106)

or

$$\lambda = \frac{\left(\tan^2\alpha+1\right)\left(2\tan^2\alpha-1\right)\left(1-v_c\right)^{-1}}{2\left(\tan^2\alpha+1\right)^2\left(1-v_c\right)^{-1} + \left(\dfrac{v_c E_c}{2G}\right)}.$$

(3.107)

The quantity

$$\frac{v_c E_c\left(1-v_c\right)}{2G_r} = \phi$$

(3.108)

is a stiffening parameter indicating the degree of stiffening imposed by the cord structure. Using Equation 3.108, λ becomes

$$\lambda = \frac{\left(\tan^2 \alpha + 1\right)\left(2\tan^2 \alpha - 1\right)}{2\left(\tan^2 \alpha + 1\right)^2 + \phi}$$

(3.109)

Equation 3.105 gives a minimum for $\dfrac{\partial V}{\partial \lambda}$. Having the value of λ available allows Poisson's ratio to be calculated since from Equation (3.95), for a given ε_y,

$$\varepsilon_x = \left\{\lambda\left(1+\tan^2 \alpha\right) - \tan^2 \alpha\right\}\varepsilon_y$$

$$v_{xy} = -\frac{\varepsilon_x}{\varepsilon_y} = -\lambda\left(1+\tan^2 \alpha\right) + \tan^2 \alpha = \tan^2 \alpha - \lambda\left(1+\tan^2 \alpha\right)$$

(3.110)

$$= \left(1+\tan^2 \alpha\right)\left(1-\lambda\right) - 1$$

Also, the strain energy function V becomes from Equation (3.104)

$$V = V\left(\alpha, \lambda, \varepsilon_y\right)$$

$$\frac{\partial V}{\partial \varepsilon_y} = E_y \varepsilon_y,$$

and

$$E_y = \left[\begin{array}{l} 3G_r\left\{\left(1-\tan^2 \alpha\right)^2 + 2\lambda\left(1-\tan^4 \alpha\right) + \lambda^2\left(1+\tan^2 \alpha\right)^2\right\} \\ + G_r\left(1-\lambda\right)^2\left(1+\tan^2 \alpha\right)^2 \end{array}\right]\left(1-v_c\right)^{-1} + \lambda^2 E_c v_c,$$

or

$$\frac{E_y\left(1-v_c\right)}{2G_r} = \left[\begin{array}{l} \dfrac{3}{2}\left\{\left(1-\tan^2 \alpha\right)^2 2\lambda\left(1-\tan^4 \alpha\right) + \lambda^2\left(1+\tan^2 \alpha\right)^2\right\} \\ + \dfrac{1}{2}\left(1-\lambda\right)^2\left(1+\tan^2 \alpha\right)^2 \end{array}\right] + \lambda^2 \phi.$$

(3.111)

This may also written as

$$\frac{E_y\left(1-v_c\right)}{G_r} = 4\left[\begin{array}{l}\left(1+\lambda+\lambda^2\right)-\left(1+\lambda-2\lambda^2\right)\tan^2\alpha \\ +\left(1-2\lambda+\lambda^2\right)\tan^4\alpha\end{array}\right]+2\lambda^{2\phi.}$$

(3.112)

When the same element considered in shear, there is no angle change which will give pure shear without cord extension. The Mohr's circle for pure shear is centered on the origin as shown in Figures 3.7 and 3.8.
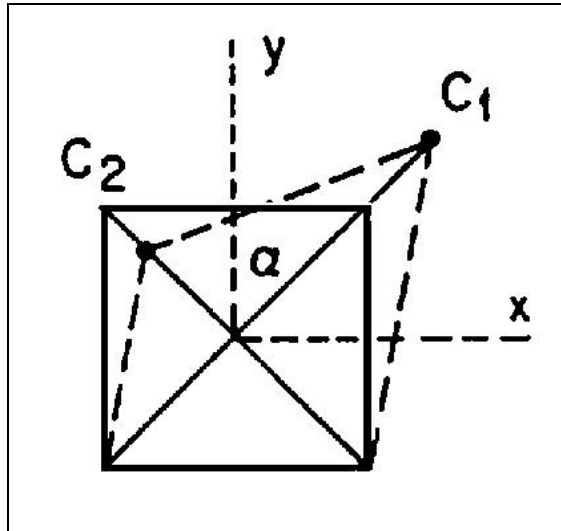
Figure 3.7 Pure Shear Configuration
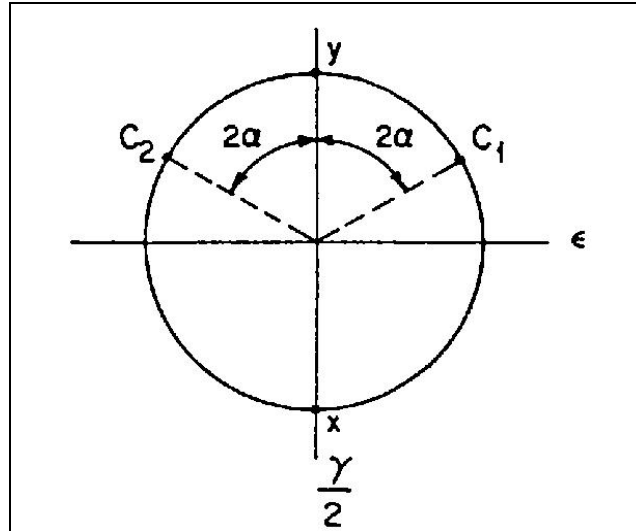
Figure 3.8 Mohr's Circle

The cord strains are

$$\varepsilon_{c_1} = \frac{\gamma}{2}\sin 2\alpha$$

(3.113)

$$\varepsilon_{c_2} = -\frac{\gamma}{2}\sin 2\alpha$$

The strain energy stored is

$$V = \frac{1}{2}\gamma_{xy}\tau_{xy}\left(1 - v_c\right)^{-1} + \frac{1}{2}\sigma_c\varepsilon_c v_c = \frac{1}{2}G_r\gamma^2\left(1 - v_c\right)^{-1} + \frac{1}{2}E_c\varepsilon_c^2 v_c$$

$$= \frac{1}{2}G_r\gamma^2\left(1 - v_c\right)^{-1} + \frac{1}{2}E_c\left(\frac{\gamma^2}{4}\right)v_c\sin^2 2\alpha.$$

$$V = G_r\left(1 - v_c\right)^{-1}\left[\frac{1}{2}\gamma^2 + \frac{1}{2}\frac{\gamma^2}{2}\phi\sin^2 2\alpha\right]$$

(3.114)

82

$$\frac{\partial V}{\partial \gamma} = G_{xy}\gamma$$

$$G_{xy} = G_r \left(1 - v_c\right)^{-1} \left[1 + \frac{\phi}{2}\sin^2 2\alpha\right].$$
(3.115)

For the case where cords are not pre-stressed by some loading mechanism other than shear, the presence of shear stresses causes one set of cords go into compression while the other set goes into tension. In the extreme case, where a textile cord buckles completely under compressive loads, the contribution of the buckled cord to strain energy is zero. This reduces the cord contribution to the shear modulus by a factor of two, so that

$$G_{xy} = G_r \left(1 - v_c\right)^{-1} \left[1 + \frac{\phi^2}{4}\sin^2 2\alpha\right].$$
(3.116)

This may be considered as a lower bound on shear modulus in a bias construction.

Alternatively, to combine the properties of individual plies in to bias configuration, compliance or stiffness matrix combination method can be used. Longitudinal and transverse properties of the ply are again calculated by Halpin-Tsai rule.

Let subscripts L and T denote the longitudinal and the transverse properties of a single ply respectively. The compliance matrix in the fiber coordinate system can be written as :

$$S_0 = \begin{bmatrix} \dfrac{1}{E_L} & -\dfrac{v_{LT}}{E_L} & -\dfrac{v_{LT}}{E_L} & 0 & 0 & 0 \\[2mm] -\dfrac{v_{LT}}{E_L} & \dfrac{1}{E_T} & -\dfrac{v_{TT}}{E_T} & 0 & 0 & 0 \\[2mm] -\dfrac{v_{LT}}{E_L} & -\dfrac{v_{TT}}{E_T} & \dfrac{1}{E_T} & 0 & 0 & 0 \\[2mm] 0 & 0 & 0 & \dfrac{1}{G_{LT}} & 0 & 0 \\[2mm] 0 & 0 & 0 & 0 & \dfrac{1}{G_{LT}} & 0 \\[2mm] 0 & 0 & 0 & 0 & 0 & \dfrac{1}{G_{TT}} \end{bmatrix} \tag{3.117}$$

For a given cord angle θ, transformation matrix can be written as

$$T = \begin{bmatrix} \cos(\theta)^2 & \sin(\theta)^2 & 0 & 2\cos(\theta)\sin(\theta) & 0 & 0 \\ \sin(\theta)^2 & \cos(\theta)^2 & 0 & -2\cos(\theta)\sin(\theta) & 0 & 0 \\ 0 & 0 & 1 & 0 & 0 & 0 \\ -\cos(\theta)\sin(\theta) & \cos(\theta)\sin(\theta) & 0 & \cos(\theta)^2 - \sin(\theta)^2 & 0 & 0 \\ 0 & 0 & 0 & 0 & \cos(\theta) & \sin(\theta) \\ 0 & 0 & 0 & 0 & -\sin(\theta) & \cos(\theta) \end{bmatrix}$$

$$\tag{3.118}$$

Because engineering shear strain is two times the tensor shear strain, $\gamma_{ij}(i \neq j) = 2\varepsilon_{ij}(i \neq j)$, a Γ matrix is defined as below to convert tensor shear strains to engineering shear strains :

$$\Gamma = \begin{bmatrix} 1 & 0 & 0 & 0 & 0 & 0 \\ 0 & 1 & 0 & 0 & 0 & 0 \\ 0 & 0 & 1 & 0 & 0 & 0 \\ 0 & 0 & 0 & 2 & 0 & 0 \\ 0 & 0 & 0 & 0 & 2 & 0 \\ 0 & 0 & 0 & 0 & 0 & 2 \end{bmatrix} \tag{3.119}$$

Transformation matrix T can be written for positive and negative θ as T_1 and T_2. S can be written for each ply as

$$S_1 = \Gamma T_1^{-1} \Gamma^{-1} S_0 T_1 \qquad (3.120)$$

$$S_2 = \Gamma T_2^{-1} \Gamma^{-1} S_0 T_2 \qquad (3.121)$$

For a lower bound estimation of elastic properties, the compliances are combined.

$$S_{tot} = 0.5 \left(S_1 + S_2 \right) \qquad (3.122a)$$

Or, for an upper bound estimation of compliances, stiffness matrix can be combined

$$S_{tot} = \left[0.5 \left(S_1^{-1} + S_2^{-1} \right) \right]^{-1} \qquad (3.122b)$$

Elastic properties can be calculated from the compliance as

$$E_1 = \frac{1}{S_{tot_{0,0}}} \qquad (3.123)$$

$$E_2 = \frac{1}{S_{tot_{1,1}}} \qquad (3.124)$$

$$E_3 = \frac{1}{S_{tot_{2,2}}} \qquad (3.125)$$

$$v_{12} = \frac{\left(-S_{tot} \right)_{0,1}}{S_{tot_{0,0}}} \qquad (3.125)$$

$$v_{13} = \frac{\left(-S_{tot} \right)_{0,2}}{S_{tot_{0,0}}} \qquad (3.126)$$

$$v_{23} = \frac{\left(-S_{tot} \right)_{1,2}}{S_{tot_{1,1}}} \qquad (3.127)$$

$$G_{12} = \frac{1}{S_{tot_{3,3}}} \tag{3.128}$$

$$G_{13} = \frac{1}{S_{tot_{4,4}}} \tag{3.129}$$

$$G_{23} = \frac{1}{S_{tot_{5,5}}} \tag{3.130}$$

3.6 Constitutive Laws for Elastomer

Rubber elasticity can be addressed through two different approaches. The first one is based on statistical models using molecular and structural considerations. Rubber is described as a network of flexible molecular chains that can deform and change conformation when subjected to a stress. The second approach makes no reference to molecular structure and assumes that the material is characterized by a purely mechanical constitutive relation. It is referred to as the continuum theory of rubber elasticity. The continuum theory includes several models; all are based on the strain energy density function W. Two categories of models can be distinguished. In the first category, W is written as a polynomial function of the principal strain invariants I_1, I_2 and I_3 defined by:

$$\begin{aligned}
I_1 &= \lambda_1^2 + \lambda_2^2 + \lambda_3^2 \\
I_2 &= \lambda_1^2 \lambda_2^2 + \lambda_2^2 \lambda_3^2 + \lambda_3^2 \lambda_1^2 \\
I_3 &= \lambda_1^2 \lambda_2^2 \lambda_3^2
\end{aligned} \tag{3.131}$$

where, λ_1, λ_2, λ_3 are the three principal extension ratios along the three mutually perpendicular axes of strain for a pure homogenous strain. The extension ratio is defined as the ratio of the deformed length to the undeformed length.

In the second category, W is assumed to be a separable function of the extension ratios λ_1, λ_2 and λ_3. For both categories, the strain tensor is the

Lagrangian strain tensor ε and σ the stress tensor conjugate to this strain is the second Piola-Kirchhoff stress tensor. It relates to W as follows:

$$\sigma = \frac{\partial W}{\partial \varepsilon}$$

(3.132)

And the constitutive relation tensor D is

$$D = \frac{\partial \sigma}{\partial \varepsilon} = \frac{\partial^2 W}{\partial \varepsilon^2}$$

(3.133)

For isotropic materials, the strain energy density function is a symmetrical function of I_1, I_2 and I_3. Rivlin showed that all possible forms of W could be represented in terms of these three invariants. If the material is incompressible, $I_3 = 1$, and W is a function of only I_1 and I_2.

Oden proposed the following form of W:

$$W = \sum_{i=0}^{\infty} \sum_{j=0}^{\infty} C_{ij} (I_1 - 3)^i (I_2 - 3)^j$$

(3.134)

where, C_{ij} are material constants.

Originally, Mooney proposed the particular form of Equation 3.60 with only linear terms in I_1 and I_2, which is often named as Mooney-Rivlin equation. Two terms Mooney-Rivlin equation is:

$$W = C_{10} (I_1 - 3) + C_{01} (I_2 - 3)$$

(3.135)

87

Gadala proposed a modified generalized Mooney-Rivlin model for compressible materials as

$$W = \sum_{i=0}^{\infty} \sum_{j=0}^{\infty} C_{ij} (I_1' - 3)^i (I_2' - 3)^j \tag{3.136}$$

where I'_1 and I'_2 are modified invariants defined as:

$$\begin{aligned} I_1' &= I_1 - (I_3 - 1) \\ I_2' &= I_2 - 2(I_3 - 1) \end{aligned} \tag{3.137}$$

Another proposed model depending on first and the third invariants:

$$W = \frac{1}{2} \mu \left[(I_1 - 3) + \frac{2}{a} (I_3^{-a/2} - 1) \right] \tag{3.138}$$

$$a = \frac{2\upsilon}{1 - 2\upsilon} \quad \text{and} \quad \mu \text{ is a material constant}$$

Ogden expressed the strain energy density function as:

$$W = \sum_{i=1}^{3} \sum_{j=1}^{m} \frac{c_j}{b_j} (\lambda_i^{b_j} - 1) \tag{3.139}$$

where b_j and c_j are material coefficients and m is adjusted for desired accuracy of the model.

Yeoh proposed a model, which uses only the first invariant:

$$W = C_{10} (I_1 - 3) + C_{20} (I_1 - 3)^2 + C_{30} (I_1 - 3)^3 \tag{3.140}$$

CHAPTER 4
TIRE FINITE ELEMENT MODEL

In this chapter, development stages of tire finite element model are given. Parts of the tire, modeling details of cord reinforced rubber, and settings of MARC program parameters are explained in detail.

Material properties for steel and textile reinforced rubber are analytically derived. Different approaches are used for derivations, and calculated material constants are compared with an FEA model. Classical continuum elements are compared with layered continuum elements and rebar elements. Selected material model is implemented to the tire finite element model.

Tire sections are modeled in different ways for comparison. Marc program parameters are iterated for improving performance, convergence characteristics and solution time. Element size and solution increments are optimized for faster and stable solution.

4.1 Tire Geometry and Properties

A 155 R 13 78 S radial passenger car tire is modeled to verify proposed material and finite element modeling techniques. The tire is the one used by Tönük, 1998. Tönük performed tests on the physical tire and compared the results with finite element model. Tönük and Ünlüsoy (2001) published cornering force characteristics obtained with finite element model and compared with the experimental results. To compare the results of this study with the experiments

and compare the performance of the finite element tire model, the same tire is selected with previously published geometry and material properties by the authors.

Figure 4.1 shows the simplified tire geometry. The red block represents the body ply, which is a rubber matrix reinforced with textile cords. Yellow and cyan blocks represent the steel plies. Reinforcements in steel plies are in 20 and - 20 degrees with the circumferential direction. Orientation and placement of the steel and textile reinforcements are shown in Figures 4.2 and 4.3.
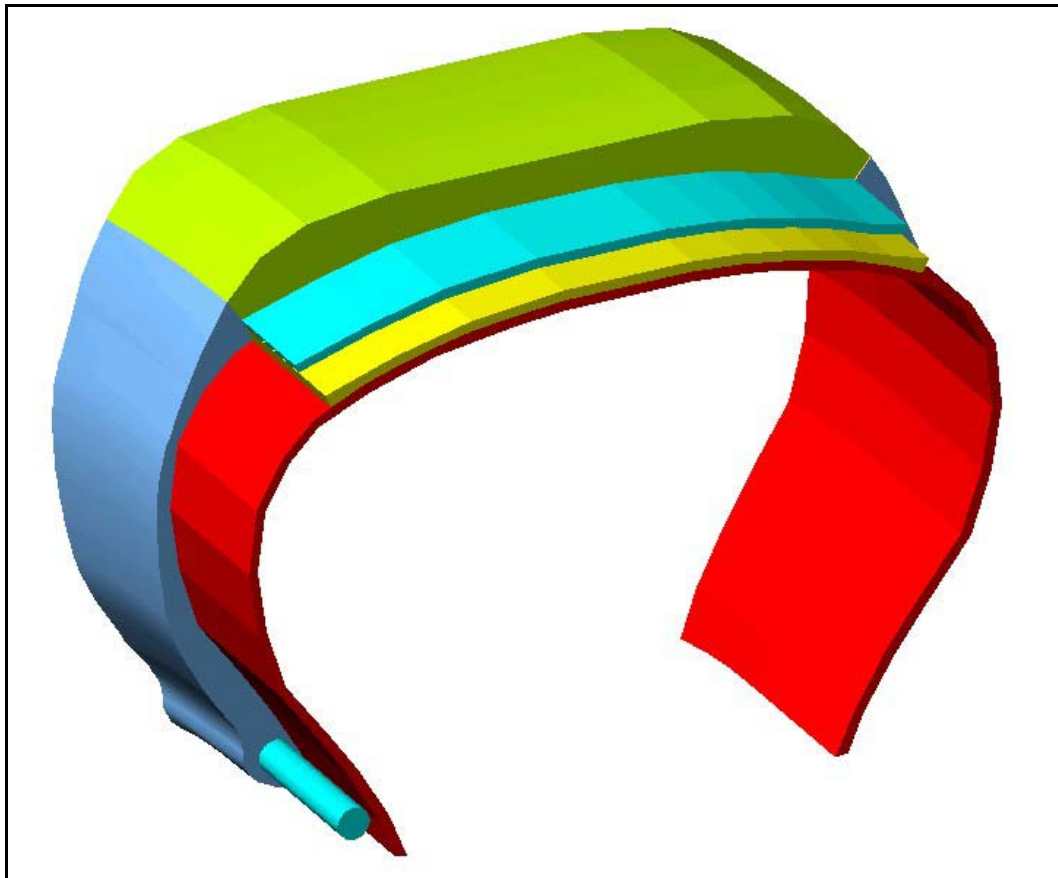

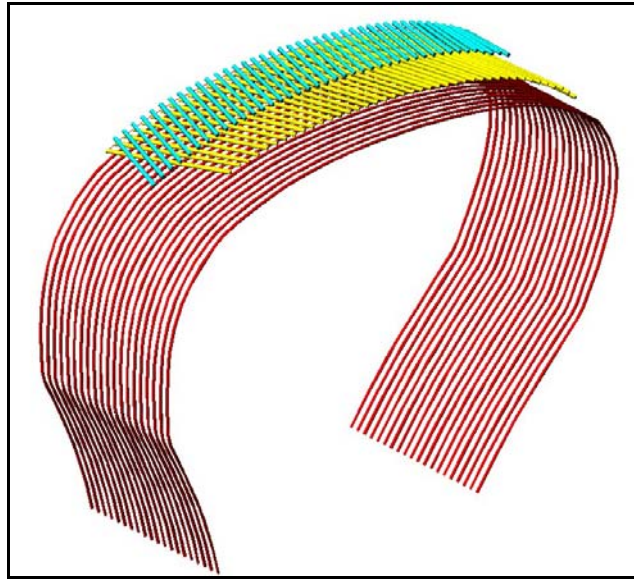Figure 4.1 Simplified Tire Structure for Finite Element Model

Figure 4.2 Orientations and Placement of Reinforcements

The reinforcements shown in Figure 4.2 are embedded in the layers shown in Figure 4.1 with same colors.

Figure 4.3 Placements of Reinforcements
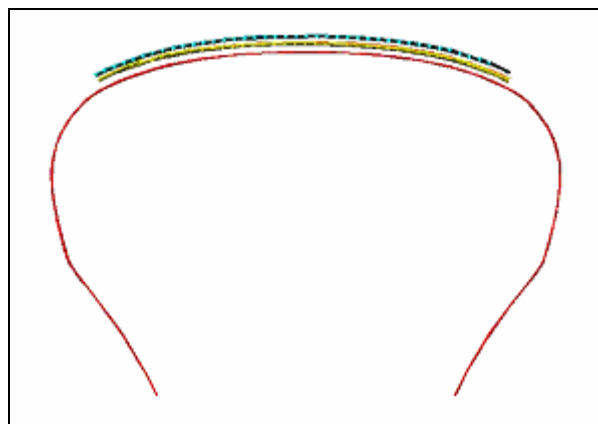
For rubber, two different sets of material properties are used in the study for comparison. Linear elastic properties are used for initial model setup and program parameter adjustments. Mooney-Rivlin material properties used for the cornering characteristics studies. Tables 4.1 and 4.2 (Tönük, 1998) give Mooney-Rivlin material model constants and linear elastic material properties for rubber

respectively. Different material properties are used for different parts of the tire model. Figure 4.4 shows the nomenclature for the tire parts.
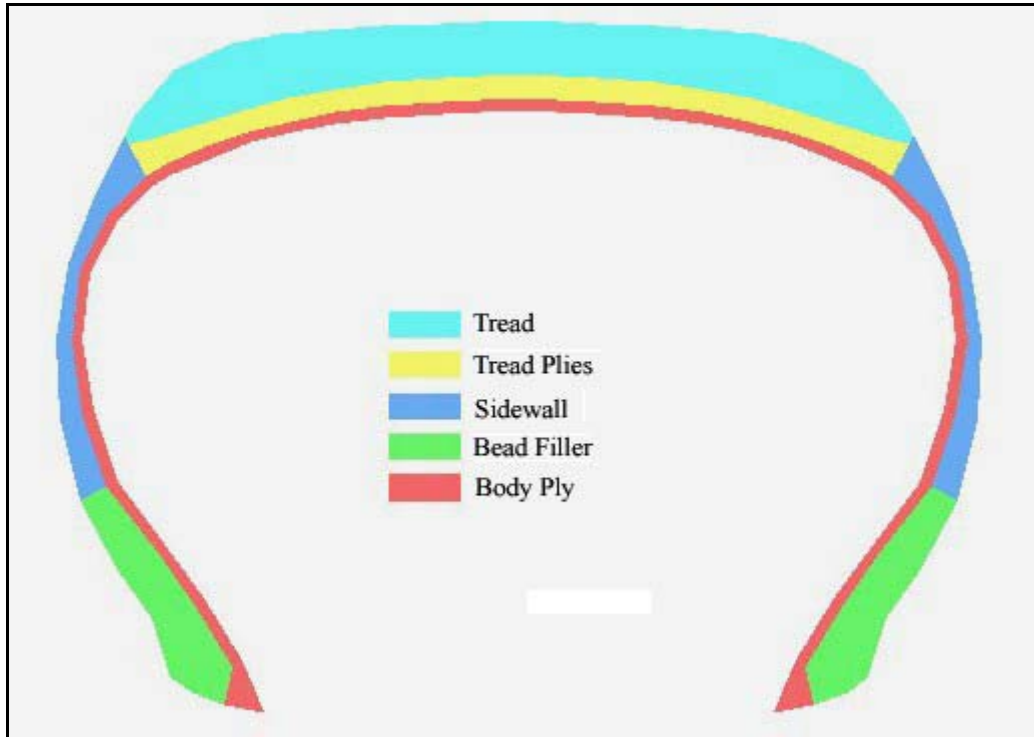
Figure 4.4 Material Classifications for Tire Sections.

Table 4.1 Mooney-Rivlin Material Constants of Rubber (Tönük 1998)

Tire Section	C_{10}	C_{01}
Bead Filler	14.14 MPa	21.26 MPa
Sidewall	171.8 kPa	830.3 kPa
Tread	806.1 kPa	1.805 MPa

For tread plies and body ply, orthotropic linear material properties are used for some of the models. For the model uses three dimensional truss elements for textile cords, body ply matrix is modeled with Mooney Rivlin model.

93

Table 4.2 Linear Elastic Material Properties of Rubber (Tönük 1998)

Tire Section	E [Mpa]	MPa	Density [kg/m^3]
Bead Filler	16.15	0.45	1250
Sidewall	3.74	0.45	1250
Body Ply	3.74	0.45	1250
Tread Plies	3.25	0.45	1250
Tread	4.56	0.45	1250

Material and geometric properties of reinforcing materials are given in Table 4.3 (Tönük 1998). Ply angles are given relative to circumferential direction.

Table 4.3 Properties of Reinforcing Materials (Tönük, 1998)

Properties	Steel Cords	Textile
E (Tension)	200 GPa	3.97 GPa
E (Compression)	100 GPa	198.5 MPa
ν	0.3	0.3
Area of Fiber	0.126 mm^2	0.126 mm^2
Distance btw Fibers	0.33 mm	1.05 mm
Ply Angle	$\pm$20 Deg	90 Deg
Ply Thickness	2 mm	2 mm

4.2 Cord-Rubber Material Properties

Different authors (Tsai, Pelc, Olatunbosun, Chamis, Hashin and Clark) published methods to model cord-rubber composite structures. Pelc (2000) and Olatunbosun (1997) used their derivations in the tire finite element models and obtained successful results. Ghoreishy (2001) used derivations of Clark (1983).

These four different approaches use Tsai Rule of Mixture for elastic constants in reinforcement direction. Authors presented slightly different formulations for elastic modulus in other directions, Poisson's ratios and shear modulus.

Using the material and geometric properties given in Tables 4.2 and 4.3, ply properties for 0 degree reinforcements are calculated.

Unidirectional laminae properties are used to calculate oriented laminate properties. Both stiffness matrix combination and compliance matrix combination methods are applied to 0 degree orthotropic properties to obtain mixed properties for different angles. Unidirectional laminae and ±20 degrees oriented laminate, with the coordinate system used in calculations, are shown in Figure 4.5.
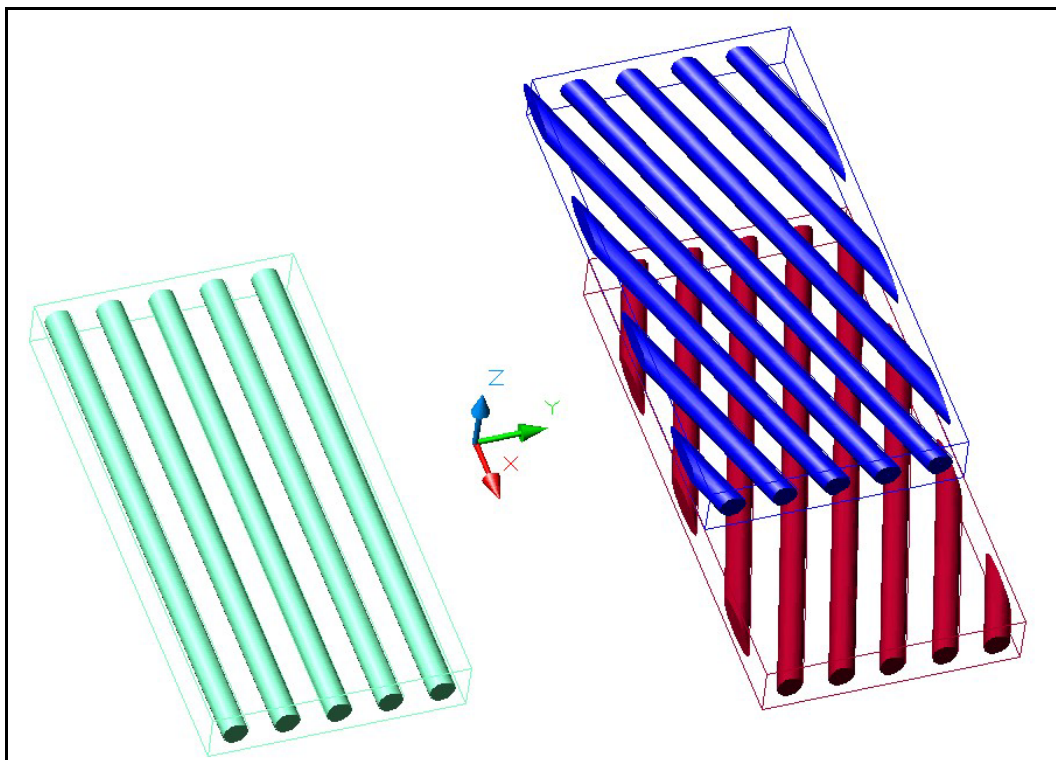

Figure 4.5 Unidirectional Laminae and ±20 Degrees Oriented Laminate

For a better understanding of effect of ply angles, a set of "virtual test specimens" are prepared. Performance of classical continuum and layered continuum elements are tested.

For the first model, classical laminate theory is used to combine the material properties of plies and resultant orthotropic material constants are assigned to the classical continuum elements. For the second model, the calculated cord-rubber mixture properties for zero degree orientation are assigned to each layer and layers are then oriented by setting layered continuum element's properties. In other words, the software automatically calculated combined properties. All specimens gave close results.

4.3 History of the Tire Finite Element Model

After the cord-rubber composite modeling is decided, a finite element model is prepared by LS-DYNA. Figure 4.6 shows the cross section of the tire finite element model.
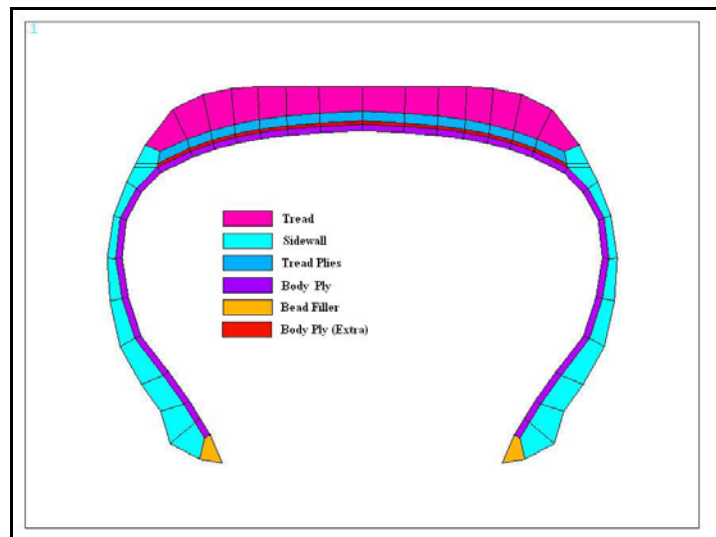

Figure 4.6 Cross Section of Tire Finite Element Model

This cross section is revolved around the center of the tire. 5 Degrees increment is used to obtain proper aspect ratio for extra body ply elements, which are relatively thin. This set of elements are added to the model for parameter study, such as effect of extra tread ply or body ply on tire stiffness. Figure 4.7 shows three dimensional tire finite element model. Some of the elements are removed for better display. For body ply and tread plies, layered continuum elements are used. Unidirectional material properties are assigned to the layered elements, and "Real Constants" for the elements are set to obtain cord orientation.
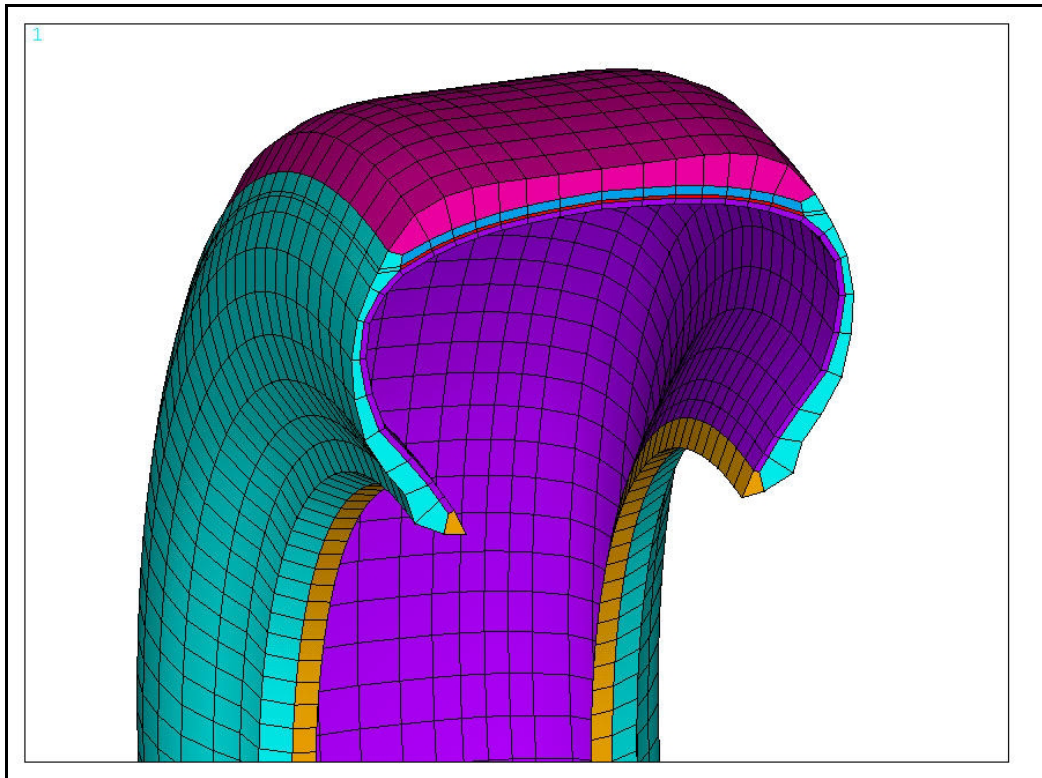

Figure 4.7 Tire Finite Element Model with Layered Continuum Elements

Another model, with the same geometry is created to compare the layered continuum elements and layered shell elements. Material properties are calculated for layered continuum and shell elements.

97

For shell representation of body ply and tread plies, the layered continuum elements of the previous model are converted to regular continuum elements with rubber material properties.

For rubber parts of the both models, linear elastic material properties are used. Figure 4.8 shows the finite element model with layered shell elements.
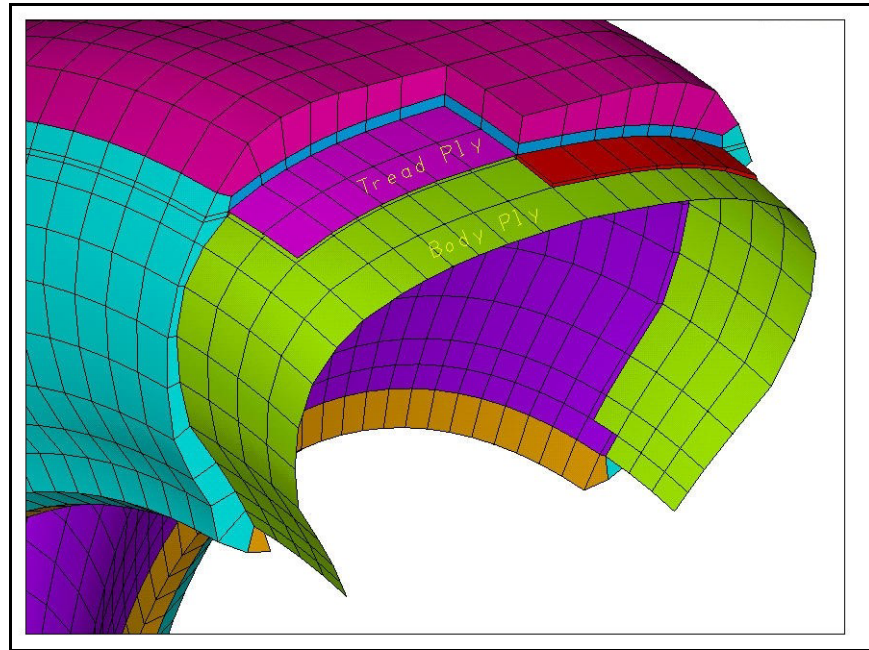

Figure 4.8 Tire Finite Element Model with Layered Shell Elements

Shell elements have 6 degrees of freedom, and continuum elements have 3 degrees of freedom at each node. Elements having different number of degrees of freedom at the nodes are inconsistent. When they are used together, the nodal forces corresponding to displacement degrees of freedom are transmitted to the continuum elements. However, the nodal moments corresponding to the rotational degrees of freedom are not transmitted to the continuum elements. This causes higher stress outputs at the nodes, which different type of elements share.

Tire is fixed in all degrees of freedom at the rim interface. 180 KPa pressure is applied to the tire inner surface. A flat rigid plate is modeled, and

inflated tire is pressed on to it. The rigid plate is given a total of 30 mm translation and reactions at the corners are collected. Figures 4.11 and 4.12 shows deflected tire (the model with layered shell elements).
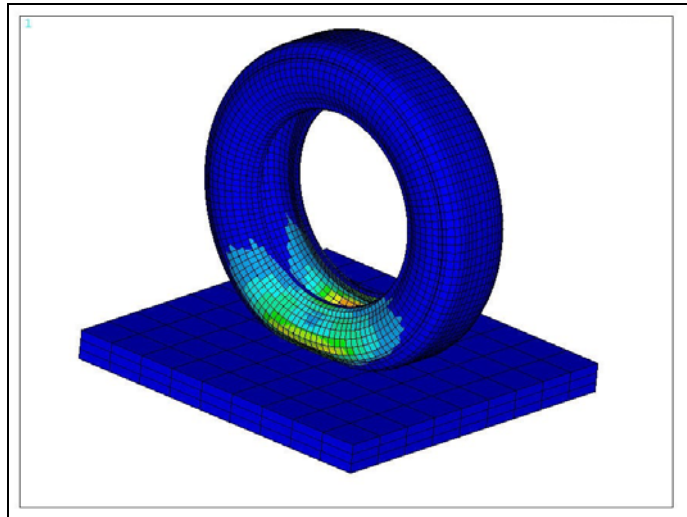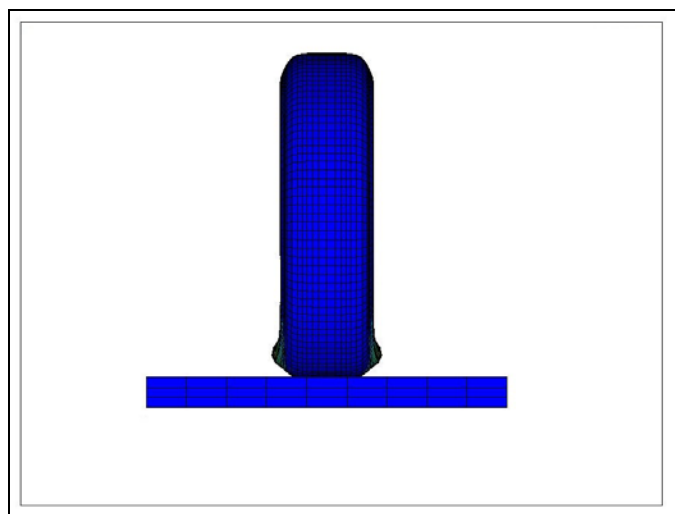

Figure 4.9 30 mm Deflected Tire

Figure 4.10 Front View of the 30 mm Deflected Tire

Figure 4.11 shows the total vertical reaction force versus plate vertical translation characteristics of the finite element model. Results of layered shell model are slightly higher than the continuum element model. As the deflection

increases, the difference also increases due to higher bending stiffness of the shell elements.
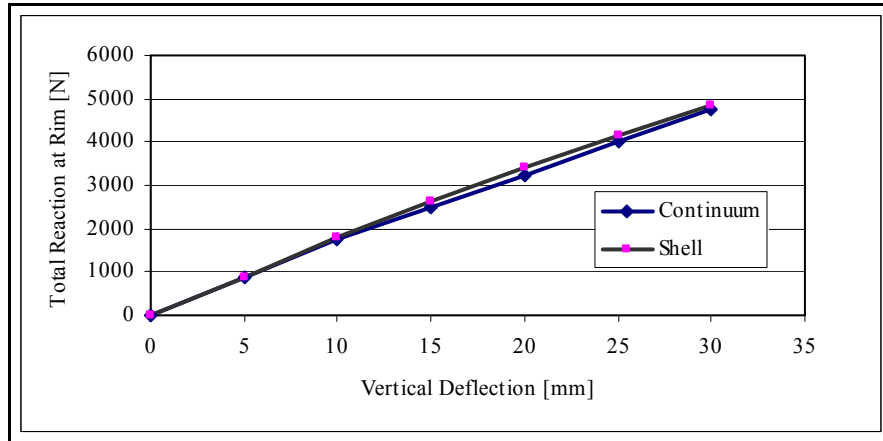
Figure 4.11 Deflection Vertical Force Characteristics of the Tire on a Flat Surface Obtained with Explicit Solver

Vertical stiffness of the tire is used as a benchmark for the tire finite element models for most of the studies mentioned in Chapter 2. Some of the authors in the literature performed only inflation and vertical stiffness analysis. Figure 4.12 shows change of vertical stiffness with changing deflection. It is observed that the vertical stiffness of the tire is affected by the use of shell elements.

Figure 4.12 Change of Vertical Stiffness with Changing Vertical Deflection

This model is used for verification of material properties and element selection. Also, comparison of performance of layered shell elements and layered continuum elements. From the results, it can be observed that, shell elements result in stiffer models. The model with laye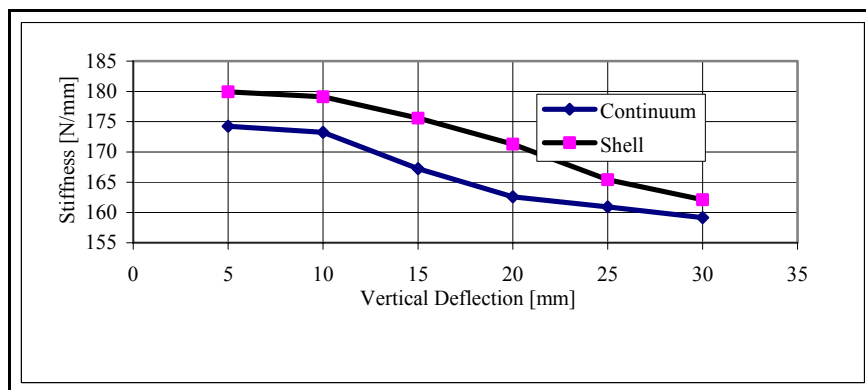red continuum elements is solved in 3 hours on a Pentium III 800 MHz Processor, 256 MB of Ram equipped machine. On the other hand, the model with layered shell elements is solved on the same machine in 11 hours. This is due to more degrees of freedom of the shell elements, and using the shell elements with combination of continuum elements.

4.4 Tire Finite Element Model for Cornering Analysis

To study complete tire cornering force characteristics, MARC is used to build a new model. The same tire, 155 R 13 78 S with material properties given in Tables 4.1, 4.2 and 4.3 is modeled. Tire cross section is prepared with a previously prepared tire preprocessor, Korkmaz 2000.

4.4.1   Material Properties for Cornering Analysis Model

As stated earlier, two different sets of material properties are used for rubber. Elements are grouped into sets as Body Ply, Tread Plies, Tread, Sidewall and Bead Filler. For the first model, linear elastic properties are used for all parts of the tire. Material properties given in Table 4.2 with the corresponding names are given to the element sets. For the second model, Mooney Rivlin material properties are used with the constants given in Table 4. Figure 4.13 shows the element sets with different material properties.
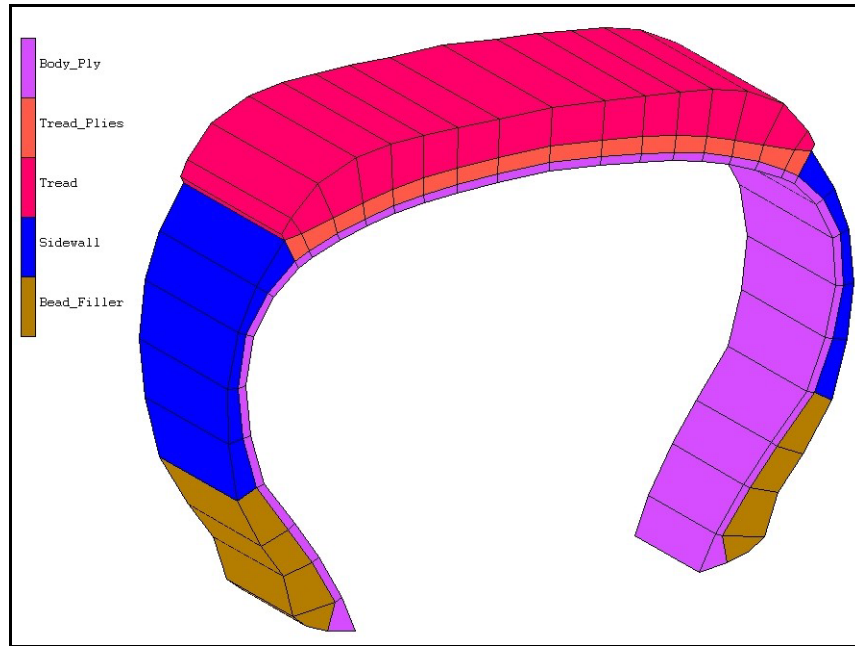
101

Figure 4.13 Classifications of Elements on 10 Degrees Tire Sector

Details and formulations about the element types chosen are given later in this chapter.

4.4.2   Cord Rubber Modeling For Cornering Analysis Model

For tread plies, unidirectional elastic properties of steel-rubber structure are calculated as explained in Section 4.2. Two different element types are examined for the initial studies. For the first model, layered continuum composite elements are used. Zero degree steel-rubber mixture properties are set to each layer, and layer orientations are set to 20 and -20 degrees.

For the second model, reduced integration classical continuum elements are used. Material properties which combine +20 and -20 degrees oriented steel cords are assigned to the elements.

Layered continuum elements have four integration points for each layer, and require longer solution time than the classical continuum elements.

Performances of both element types are compared for solution time point of view and results.

For Body Ply elements, which the rubber is reinforced with textile, classical continuum elements are used for both of the models.

4.4.3   Orientation of Element Coordinate Systems

Orthotropic material properties for cord reinforced rubber parts, for Tread Plies and Body Ply, are defined relative to global coordinate system. Material constants are given relative to global X, Y and the Z axes. Each element's edges make certain angles with the global axes. A user subroutine is developed to orient material properties for each element's own coordinate system and set correct orientation for elements.

First, elements of the tire cross section are grouped into subsets, depending on their angles with the vertical axis, and given a name. Then, using each element's integration point's coordinate, element's orientation is calculated and orientation of the coordinate system is set. In Figure 4.14, orientation of the global coordinate system, and orientations of some of the body ply elements are shown. Figure 4.15 shows coordinate system for some of the tread plies elements. The planar sections shown in Figures 4.14 and 4.15 are cross sections taken at the elements center. Coordinate system icons are shown for some of the elements for better understanding and clarity of the picture.

As the number of elements with oriented coordinate system increases, solution time increases considerably.
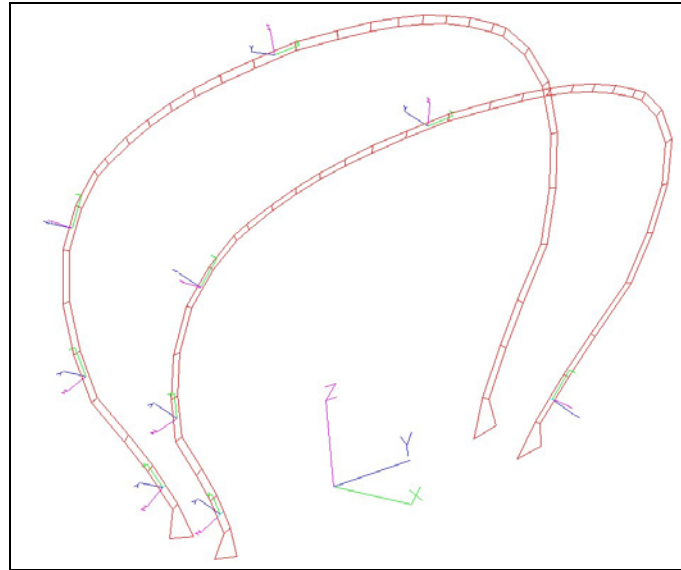
Figure 4.14 Orientation of Coordinate System For Some of the Body Ply
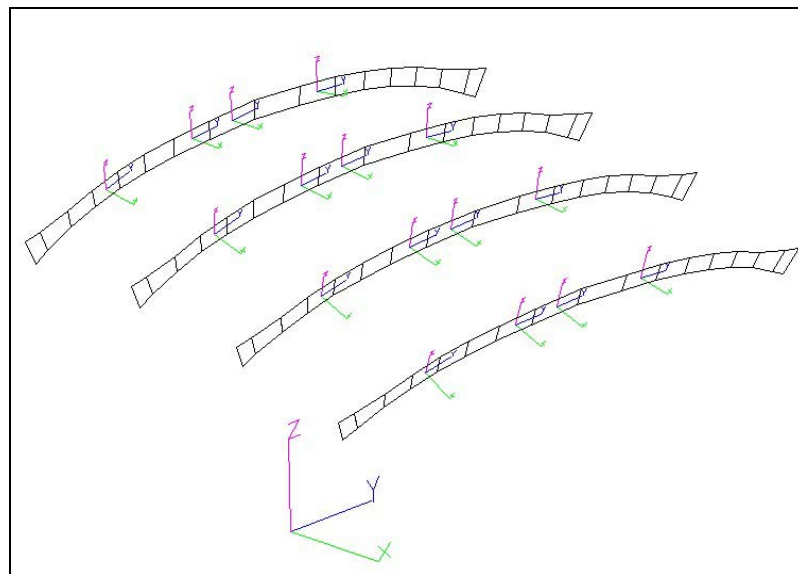Elements.

Figure 4.15 Orientation of Coordinate System for Some of the Tread Plies
Elements.

4.4.4   Tire Rim Assembly and the Drum

Two different tire models are prepared using different mesh densities. For
the fine meshed one, half of the tire is divided into 5 degrees increment sectors,
the other half is divided in to 10 degrees increment sectors. For a coarser model,

30 degrees increment, the portion first comes into contact with the drum, is divided in to 5 degrees sectors, the rest of the tire is divided in to 10 degrees sectors. The fine meshed model has 6590 nodes and 4536 elements. The coarse meshed model has 5126 nodes and 3526 elements.

The rim, which the tire is mounted, is modeled as a rigid body. A rigid body in Marc is an analytical entity and is not included in the solution like deformable elements. When a rigid body is represented as an analytical surface, the normal is recalculated at every iteration based upon the current position. This leads to a more accurate solution.

Tire is mounted on the rim as seen in Figure 4.16. Glue option, which glues the bodies in contact up to a specified separation force, is used for the contact of tire and the rim. Bead bundle in the tire structure is removed and not modeled. When the bead element is glued to the rigid rim, it cannot expand as the tire inflates, and this compensates neglecting of the bead bundle.
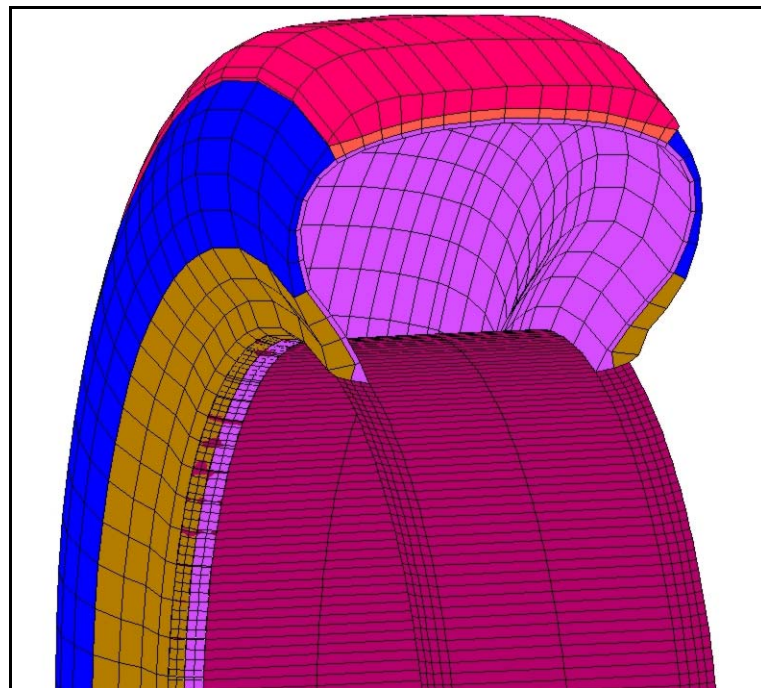

Figure 4.16 Tire Mounted on the Rigid Rim

Displacement of the tire is fixed at the bead area by gluing to the rigid rim. Motion of the rim is controlled by two nodes at the rotation center. One of the nodes controls the translational degrees of freedom; the other is to control the rotational degrees of freedom.

For the first studies, the control node of the rim is fixed in two horizontal degrees of freedom, and set free in vertical motion. The vertical load, which is a parameter of the cornering force study, is applied to this node. In this way, the tire-rim assembly is pressed on to the drum. Small fluctuations on the vertical loads due to tire rotation changed the vertical position of the tire. This also increased solution time due to more difficult convergence of the contact problem. This method is changed, and tire center is fixed in all degrees of translational freedom. The drum is given an initial displacement, and vertical force is adjusted by adjusting the vertical deflection of the tire.

For the initial studies, slip angle is adjusted by rotating the tire in vertical axes. Later, instead of rotating the tire mesh, the drum is rotated to obtain desired slip angle.

The drum is also modeled as a rigid body as the rim is modeled. After the tire is inflated to the rated pressure, drum is pressed on to the tire. When getting the desired vertical deflection, drum starts to rotate. The friction force between the drum and the tire rotates the tire-rim system.

Figure 4.17 shows the fine meshed tire mounted on to the rim, with boundary conditions of the rim control nodes. The single arrows represent the translational degrees of freedom and double arrows represent the rotational degrees of freedom. There are two nodes at the center, since they are at the same location; they look like a single node in the figure. The translational degrees of

106

freedom arrows are on one of the nodes, and rotational degrees of freedom arrows are on the other node.

During the inflation and drum vertical movement load cases, all rotational degrees of freedom at the rim center are fixed. Rotation about the tire axis is set free after the pressing of drum is completed.

In Figure 4.18, fine meshed and coarse meshed tires are shown. The fine meshed tire gives smoother numerical results while the results of coarse meshed tire fluctuate. Comparison between different mesh densities are given in the next chapter. Tire rim and drum system is shown in Figure 4.19.
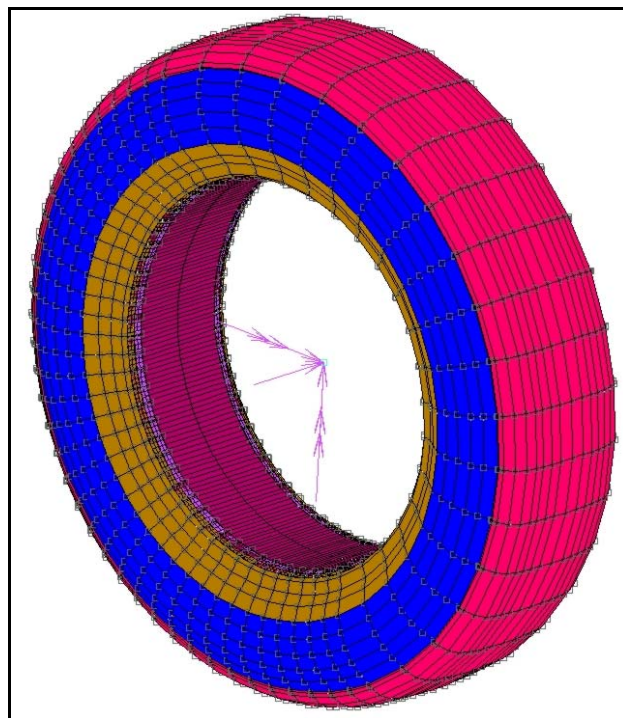

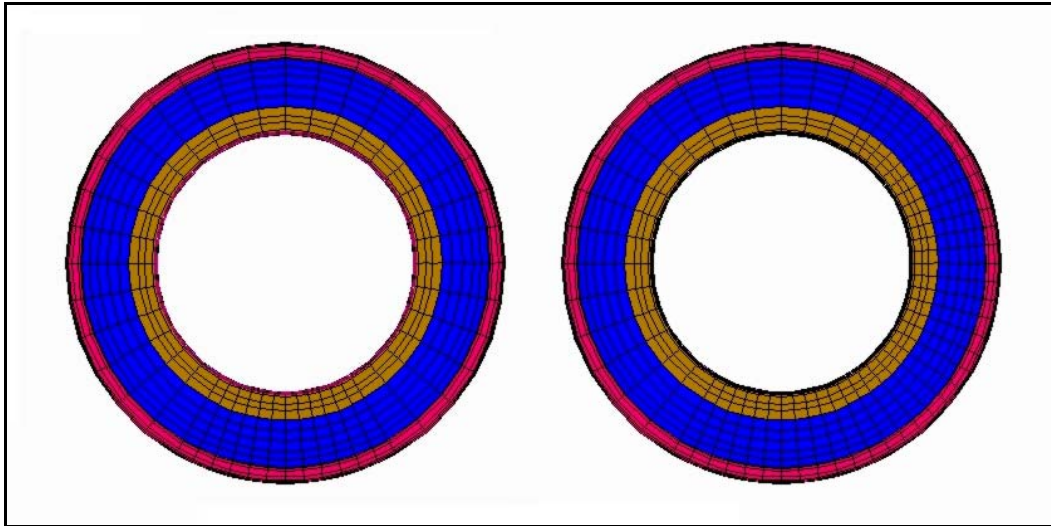Figure 4.17 Boundary Conditions Applied to Tire Center
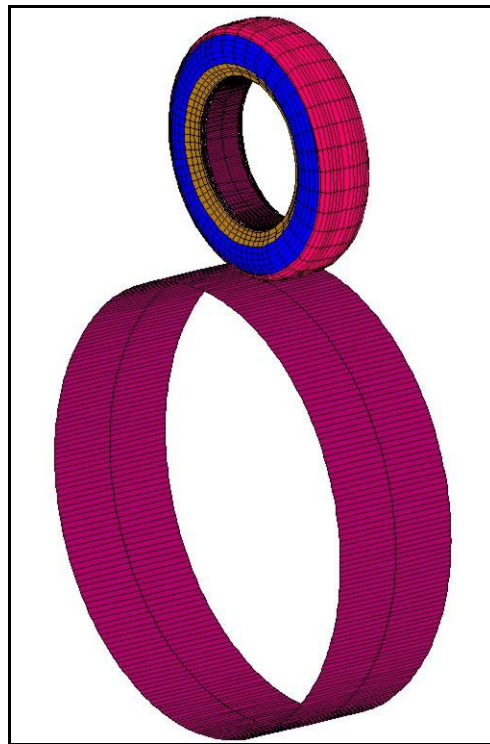
Figure 4.18 Coarse and Fine Meshed Tire Models

Figure 4.19 Tire-Rim Assembly And The Drum.

4.4.5   Friction Models and Parameters for Cornering Analysis

Coulomb and Stick-Slip friction models are both examined to model friction between the tire and the drum. Although the Stick-Slip friction model simulates the real behavior of the tire rotating on the drum, almost no difference is observed when compared with the results of Coulomb friction model. Tönük (1998) stated that, the changes in the results between two friction models are minor. Stick Slip friction model increased the solution time and for the study, Coulomb friction model is used. Marc offers a special option using Coulomb model, Coulomb for Rolling, for rolling bodies in contact with rigid surfaces, is selected as the friction model option.

Coulomb model is defined as (MARC, 2000 A)

$$\sigma_{fr} \leq -\mu\sigma_{n} \cdot t \tag{4.1}$$

where

σ_{n} is the normal stress

σ_{fr} is the tangential (friction) stress

μ is the friction coefficient

t is the unit tangential vector in the direction of the relative velocity

t is defined as

$$t = \frac{v_{r}}{|v_{r}|} \tag{4.2}$$

v_{r} is the relative sliding velocity and given to the program as input.

For a given normal stress, the friction stress has a step function behavior based on the value of relative sliding velocity. To avoid the numerical difficulties based on the discontinuity of σ_{fr}, MARC uses the modified Coulomb friction model which is defined as:

$$\sigma_{fr} \leq -\mu\sigma_n \frac{2}{\pi} \arctan\left(\frac{v_r}{C}\right) \cdot t \qquad (4.3)$$

C is the value of the relative velocity when sliding occurs. A large value of C results in a reduced value of the effective friction. A small value of C results in convergence problems. Figure 4.20 shows the effect of C graphically.
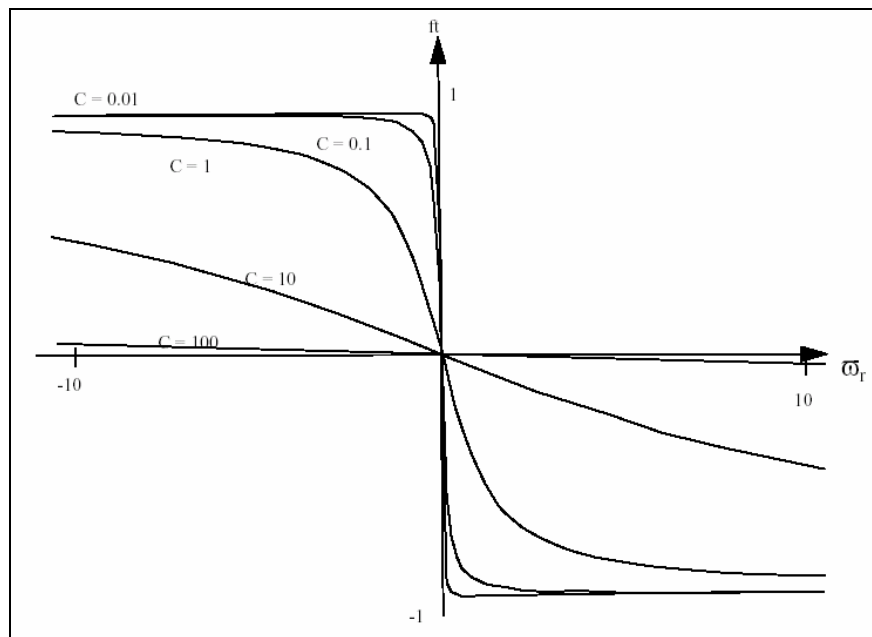

Figure 4.20 Effect of Relative Sliding Velocity Parameter on Stick Slip Approximation (Marc 2000a)

Different values are selected for relative sliding velocity, and 0.01 is used with success.

4.5 Summary of Tire Models in Literature and a New Approach

The tire finite element models in literature are summarized in Chapter 2. For rubber parts of the tire, most authors used continuum elements. For tread plies and body plies different approaches are used. The tire models are constructed depending on the aim of the study. Authors who studied stress distribution on the tire geometry used different techniques than the authors who studied tire cornering force characteristics or tire ride comfort characteristics.

Comparison of layered continuum elements and classical continuum elements from solution time point of view is given in the next chapter.

For cornering force studies, authors either used rebar elements, or layered shell elements for breaker plies. For body plies, rebar elements, layered shell and layered membrane elements are used.

Tire is an axisymmetric structure. For element with direction dependent material properties, it is necessary to set material properties for each individual element. Figures 4.14 and 4.15 show coordinate system for some selected elements.

Using rebar elements for breaker plies, which do not have bending capability, neglects the bending stiffness of steel cords. With shell elements or continuum elements with orthotropic material properties it is possible to introduce bending stiffness for the steel cords. Rebar, shell and continuum elements are used to model steel reinforced rubber for different studies as given in Chapter 2.

For body plies, textile reinforcement does not carry compression and bending. Rebar elements, if elastic modulus can be set different for tension and compression, models the behavior of textile cords as it is in reality. Shell

elements, which have additional rotational degrees of freedom, introduce slight and acceptable error, because the orthotropic material properties reduce bending stiffness of the element to a value close to rubber. Material exhibits mixture properties for tension and rubber like properties for bending. All alternative approaches used by different researchers give results with reasonable accuracy.

As the tire rotates, element's orientation changes, and should be updated for directions of the reinforcements. This introduces additional computational time for solution. For the increment that will be solved, the deformation of the element is not known. Positions and orientations of the elements are considered same with the previous solved increment. Besides the elements deformation, the rigid body motion of the rotating elements also introduces an error. At each increment, this error increases. As the deformation increases with increasing load or slip angle, the error accumulation also increases and causes instability for the model. Tönük and Ünlüsoy (2001) concluded for rebar elements that, for larger slip angles, amount of error dominates the model results before the steady state cornering value is reached. Rao et al (2003) stated that, their model with rebar elements has convergence problems at higher slip angles.

Membrane elements, which are reduced forms of shell elements, do not carry bending; they have only translational degrees of freedom at their nodes. Orthotropic material properties can be assigned to the element to obtain directional material properties. Again, elements coordinate system should be oriented. Membrane elements are very unstable in nature (Marc 2000B). Membrane elements have no hourglass control. Koishi et al. (1998) tested the performance of membrane and shell elements. They conclude that, shell elements cause numerical instability as the tire rotates.

Shell or layered shell elements are widely used by researchers. Using layered elements avoids calculating combined properties of plies each have

different directions for tread plies. On the other hand, layered elements introduce additional computational time. Shell elements have six degrees of freedom and using with continuum elements which have three degrees of freedom either increases solution time or causes some error. Again, for shells, orientation of each element should be set and updated as the tire rotates and deforms.

In view of the above detailed considerations, to be able to reduce the computational effort considerably while avoiding error accumulation at the same time, a new modeling strategy is developed and proposed. For body plies, there is only one reinforcement in radial direction. Thus, instead of orienting the element's coordinate system, an element, which acts like a textile fiber carrying tension without bending stiffness, can reduce the solution time considerably and decrease error accumulation. Although the error accumulation is not a problem for the model with all continuum elements, decreasing solution time gives flexibility to analyze tire cornering force characteristic for a wide range of slip angle to vertical force combinations. For this purpose, three dimensional truss elements are introduced to the model. The selected element has two nodes and three translational degrees of freedom per node. The element has large strain and large displacement capabilities and has no bending stiffness. It can be used in conjunction with continuum elements. Because the element is placed between two nodes and act in the direction as it is created or rotated, no orientation of coordinate system for each solution increment is necessary. This reduces the computational time drastically, and avoids error accumulation which results instability of solution.

Figure 4.21 shows a rubber block reinforced with textile cords. When this block is modeled with a four-node element, rebar, shell or membrane and truss reinforced representations looks as it is in the figure.

Using the new approach, a new tire model is constructed. The body ply, which is previously modeled with orthotropic linear elastic material properties, is converted to incompressible, Mooney-Rivlin formulation material model. Cords are placed into inner surface of the element. To control the performance and solution time, coarse meshed with 10 degrees increment per sector, and a fine meshed with 5 degrees increment per sector model is prepared. Figure 4.22 shows the reinforcements for the fine mesh. Figure 4.23 shows the partial view of the fine mesh. Coarse mesh model is given in Figure 4.24. Fine mesh model includes 8496 elements and 8784 nodes. Coarse mesh model includes 4248 elements and 4392 nodes.
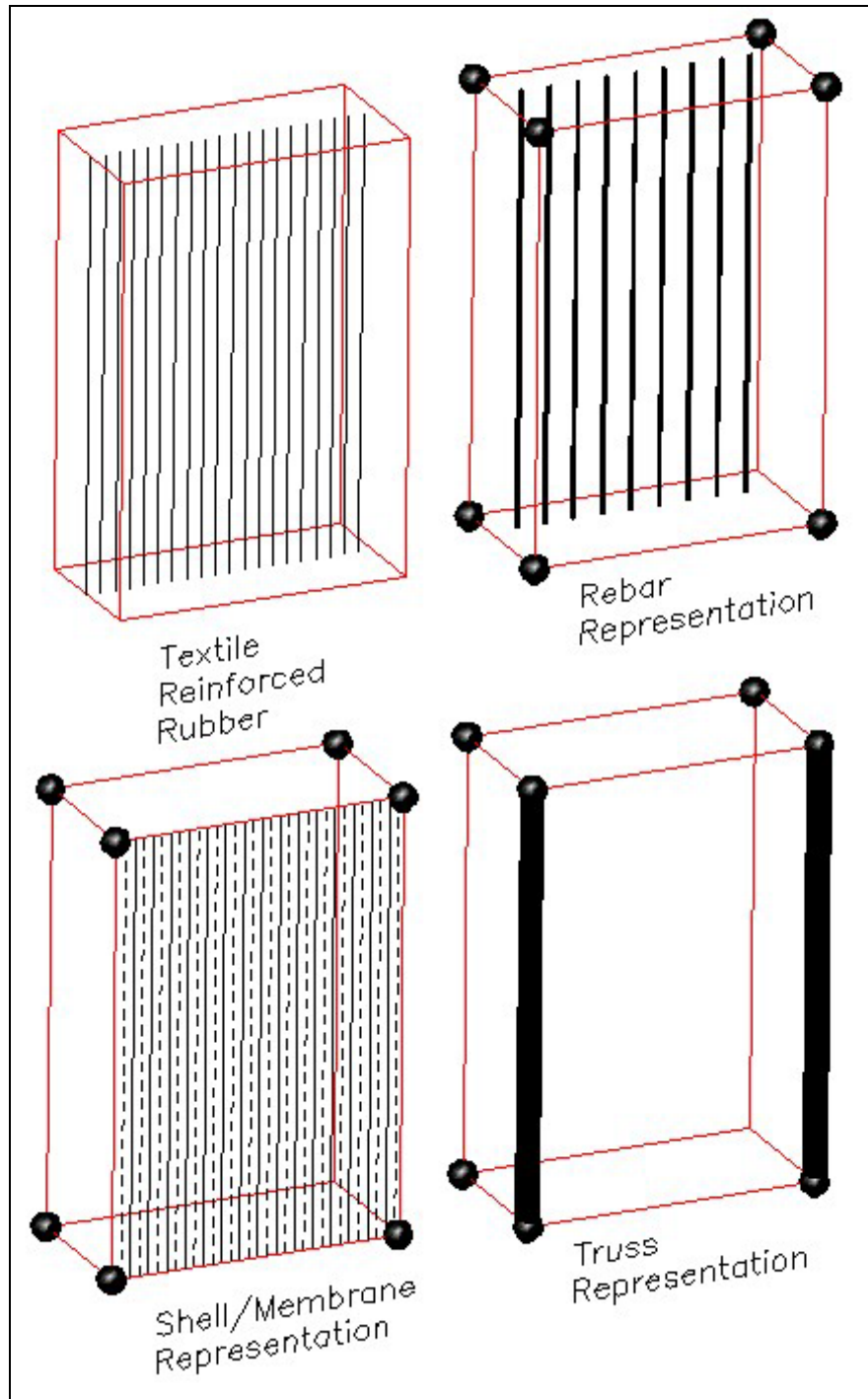
Figure 4.21 Textile Reinforced Rubber Block and Rebar, Shell/Membrane, Truss
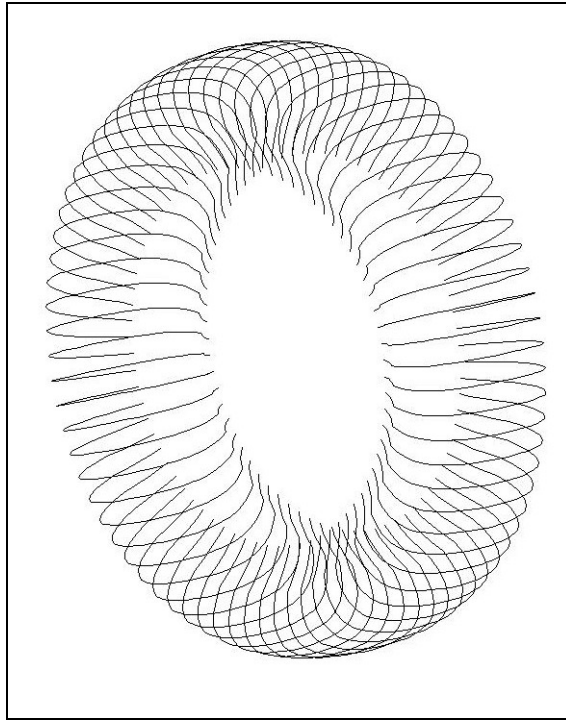Representations.

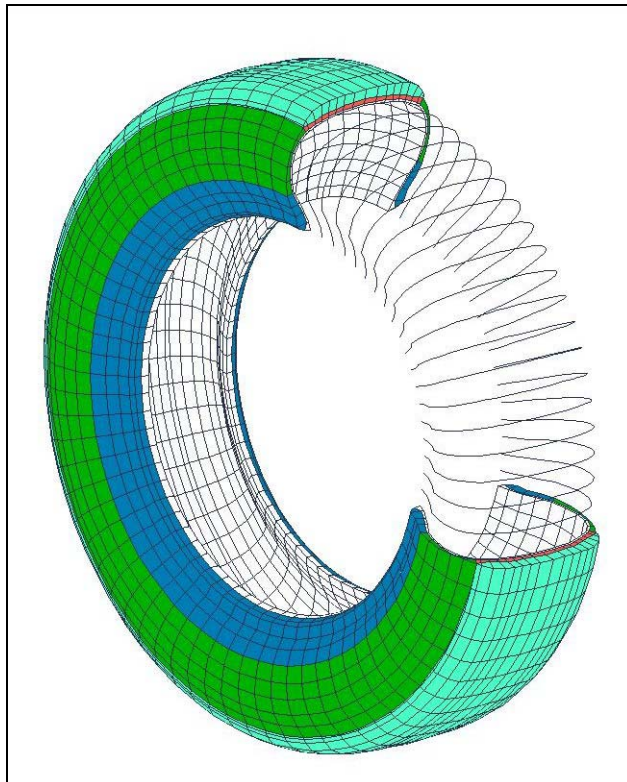Figure 4.22 Truss Elements used for Textile Cords in Fine Mesh Model

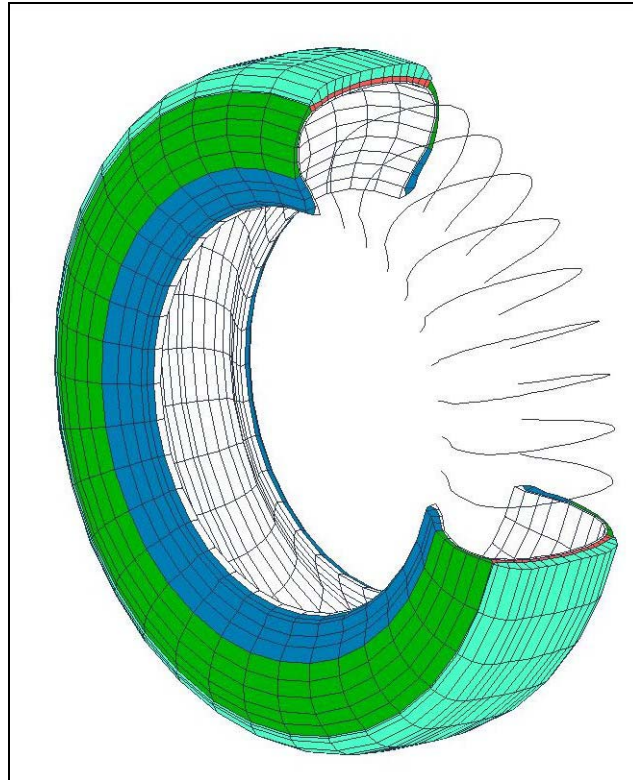Figure 4.23 Partial View of Fine Mesh Model

116

Figure 4.24 Partial View of Coarse Mesh Model

Coarse mesh model is solved for different vertical load and slip angle combinations. The same load cases are also solved with fine meshed model. Solution time for half rotation of the tire dropped to 3 hours for coarse meshed model on a P4 2.6 GHz processor, 1GB Ram personal computer. For fine meshed model, on the same computer, half rotation is solved in 12 hours. This time is less than the solution time of coarse meshed continuum model which is 14 hours.

Textile, by nature, does not carry compression. MARC does not have an option to specify different elastic modulus for tension and compression. The only way is using a subroutine to control the stress state of the elements after each solution increment and changing material elastic constant accordingly. But, the same problem as explained before is faced in this situation. Element's status can be obtained for the last solved increment and new properties for the next increment can be given accordingly. The first increment which textile goes in to

compression cannot use elastic modulus which is chosen for compression case because the increment used to decide on material properties of that particular elements experience tension in the previous increment. As the tire inflates, textile goes into tension and for moderate loads even at road contact, remains in tension. Stress state of textile elements is closely observed during solution and neglecting the bilinear behavior of textile is examined.

4.6 Summary of Element Types Selected For Tire Model

Mainly two different tire models are prepared as stated earlier. One of the models uses linear elastic material law for both rubber and cord reinforced rubber parts of the tire. The other model uses Mooney Rivlin material model for rubber parts and linear elastic material model for cord reinforced parts.

For linear elastic model, 8-noded isoparametric hexahedral elements are used. The selected element type uses reduced integration. The stiffness of the element is calculated using a single integration point located at the centroid of the element. For contact analysis, linear elements are preferred over higher order elements by all the authors in the literature. Instead of using higher order elements, linear elements with higher mesh density gives more accurate results and solution converges faster. The selected element type has hourglass control, avoiding numerical instability which is normally associated with reduced integration elements.

For Tread Plies, 8-noded isoparametric composite brick elements are used as well as 8-noded isoparametric hexahedral elements. Composite brick elements use four integration points for each layer. This increases solution time. Figure 4.25 shows the layer representation of a composite brick element. The main advantage of the composite element is assigning the unidirectional properties and

118

simply adjusting number of layers and layer orientations. This avoids calculating combined properties of layers for a single element.
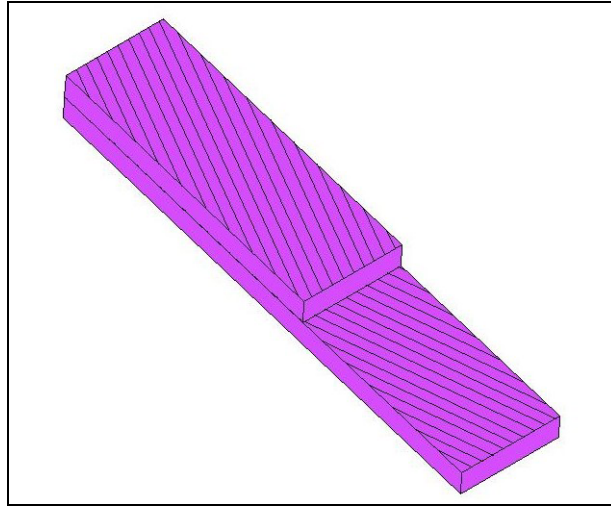

Figure 4.25 Layer Orientations for Composite Continuum Element

For the model, which uses Mooney-Rivlin material formulation to simulate nonlinear incompressible rubber behavior, 8-noded, incompressible, reduced integration brick elements with Herrmann formulation are used. This element has hourglass control too. The element can be used in conjunction with compressible elements in the same model with success.

The truss elements are two node simple linear elements and can be used in conjunction with all element types. They have large displacement capability. These elements have no bending capability.

CHAPTER 5
CORNERING FORCE CHARACTERISTICS WITH THE FINITE ELEMENT MODEL

Different tire models are prepared for the cornering study as explained in Chapter 4. These models are analyzed to obtain the cornering force characteristics. Their performances are compared in different aspects by using the experimental results by Tönük and Ünlüsoy (2001).

The first classification of the tire models depends on rubber material properties. Rubber is modeled with linear elastic material constants and Mooney-Rivlin parameters. Material nonlinearity increased total solution time by around 20 percent. After solution time is reduced with changing solution options such as applying displacement rather than force to load the tire and parameters, linear elastic model is completely left out and the cornering force characteristics presented in this chapter are obtained with Mooney Rivlin material formulation.

The second classification depends on the mesh density. Both the fine and coarse mesh models provided stable and reliable solutions. Without any convergence problem, both of the models can run for high slip angles and vertical load combinations.

The third classification can be done according to element types used for tread plies. Layered continuum elements and reduced integration continuum elements are used to model orthotropic behavior of the steel reinforced rubber. With reduced integration elements, solution time reduces considerably. After

120

some trials, the model with layered continuum elements is left out and reduced integration continuum elements are used.

The tire is tested on a drum and finite element model is run on a cylindrical surface with same dimensions.

Cornering force versus solution increment or rolled distance values plotted in this chapter, are not filtered, and not averaged. Also, solution increment is used as 1 in the plots. So, these plots give an idea about the performance and accuracy of each modeling technique, as well as effect of slip angle and vertical force on solution characteristics.

5.1 Static Vertical Stiffness Analysis

All tire models are first tested for static vertical stiffness. The rim is kept fixed and the drum is pressed on to the tire. Forces on the rim are measured from the node at the center.

For the model with continuum elements, the force deflection characteristic is given in Figure 5.1. For cornering tire models, pressing operation is performed in 5 increments. Figure 5.1 shows vertical force versus rim displacement plot obtained experimentally by Tönük (1998) and tire - drum finite element model.

It is observed that the FEM results indicate a stiffening static tire behavior. This is probably due to the values of Mooney-Rivlin parameters used in the solution.
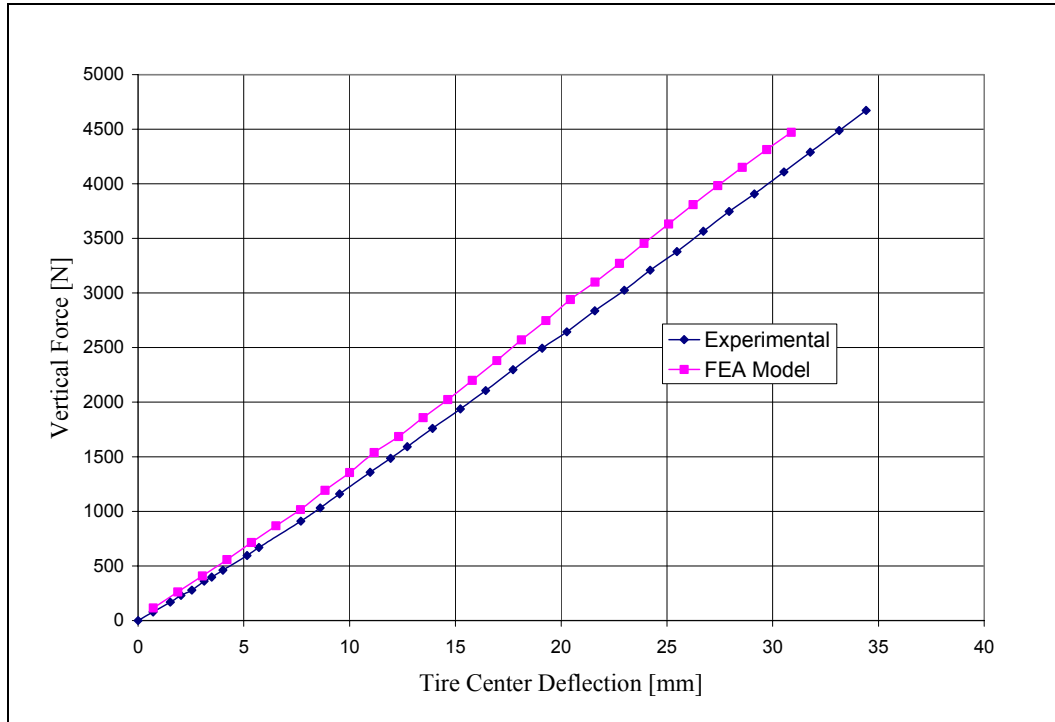
Figure 5.1 Vertical Force versus Rim Displacement on Drum

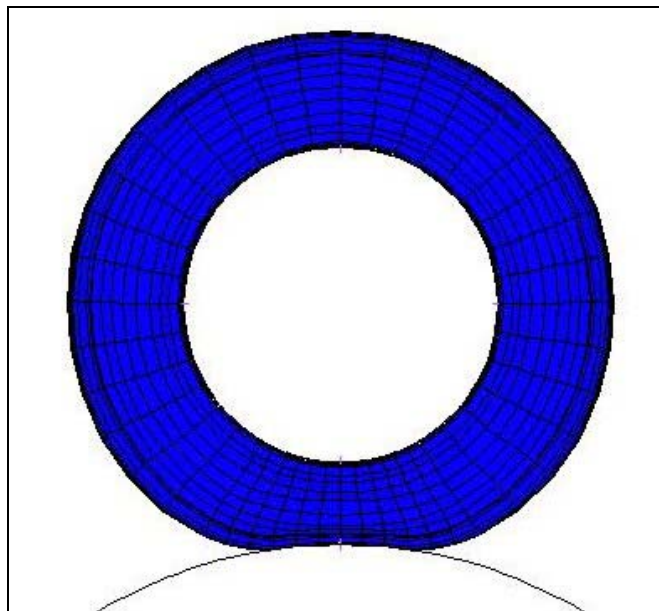The 30 mm deflected tire on drum is shown in Figure 5.2.

Figure 5.2 30 mm Deflected Tire on Drum

5.2 Cornering Force Characteristics on Drum

5.2.1   Model with continuum elements

For cornering analysis, the coarse tire model with Mooney-Rivlin material formulation for rubber matrix is used. Body ply and tread plies are modeled with reduced integration continuum elements.

The tire is inflated in 5 increments to 180kPa pressure. Then, the drum is pressed on to the inflated tire. For low speed cornering characteristics, quasi static approach is chosen for solution speed. Effect of solution increment per rotational position of the tire, convergence criteria, relative force tolerance are optimized by trial and error to obtain fastest possible solution without loosing accuracy and stability of the model.

For 2, 4, 6, 8, 10 degrees slip angles and 2000, 3000, 4000 Newton vertical loads, the model is run. Without any problem, the model converged and half rotation of the tire is completed approximately in 11 hours on a P4 2.6 GHz processor, 1GB ram, 60 GB hard disk equipped computer. This time is around 17 hours for the same configuration with a 512Mb ram machine. For 2 degrees and 4 degrees slip angles, the tire is rotated 360 degrees to obtain a steady state cornering force value
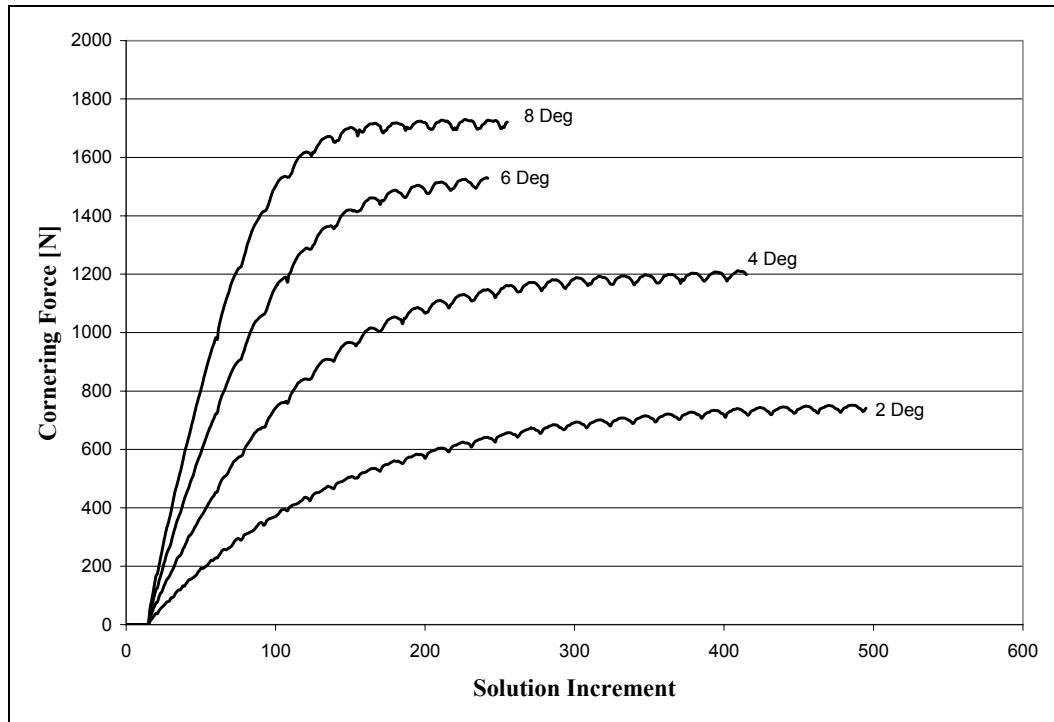
Figure 5.3 Cornering Force versus Solution Increments for 2kN Vertical Load

Figure 5.3 shows increase in cornering force as the tire rotates for 2kN vertical load and 2, 4, 6, and 8 degrees slip angles. 250 solution increments correspond to 180 degrees rotation of the tire. From the plots, it can be concluded that, as the slip angle increases for a certain vertical load, cornering force value saturates to a steady state value faster. For 2 degrees slip angle, the saturation takes almost one complete rotation of the tire. For 6 degrees and above, it is faster and takes only half tire rotation or less.

The same tendency is observed in all vertical load slip angle combinations for buildup of cornering force with tire rotation. As the slip angle increases, the required rotation to reach a steady state value increases.

Deflected shapes of the tire under 3000N vertical force and 0, 2, 4, 6, 8, 10 degrees slip angles are shown in Figure 5.4.
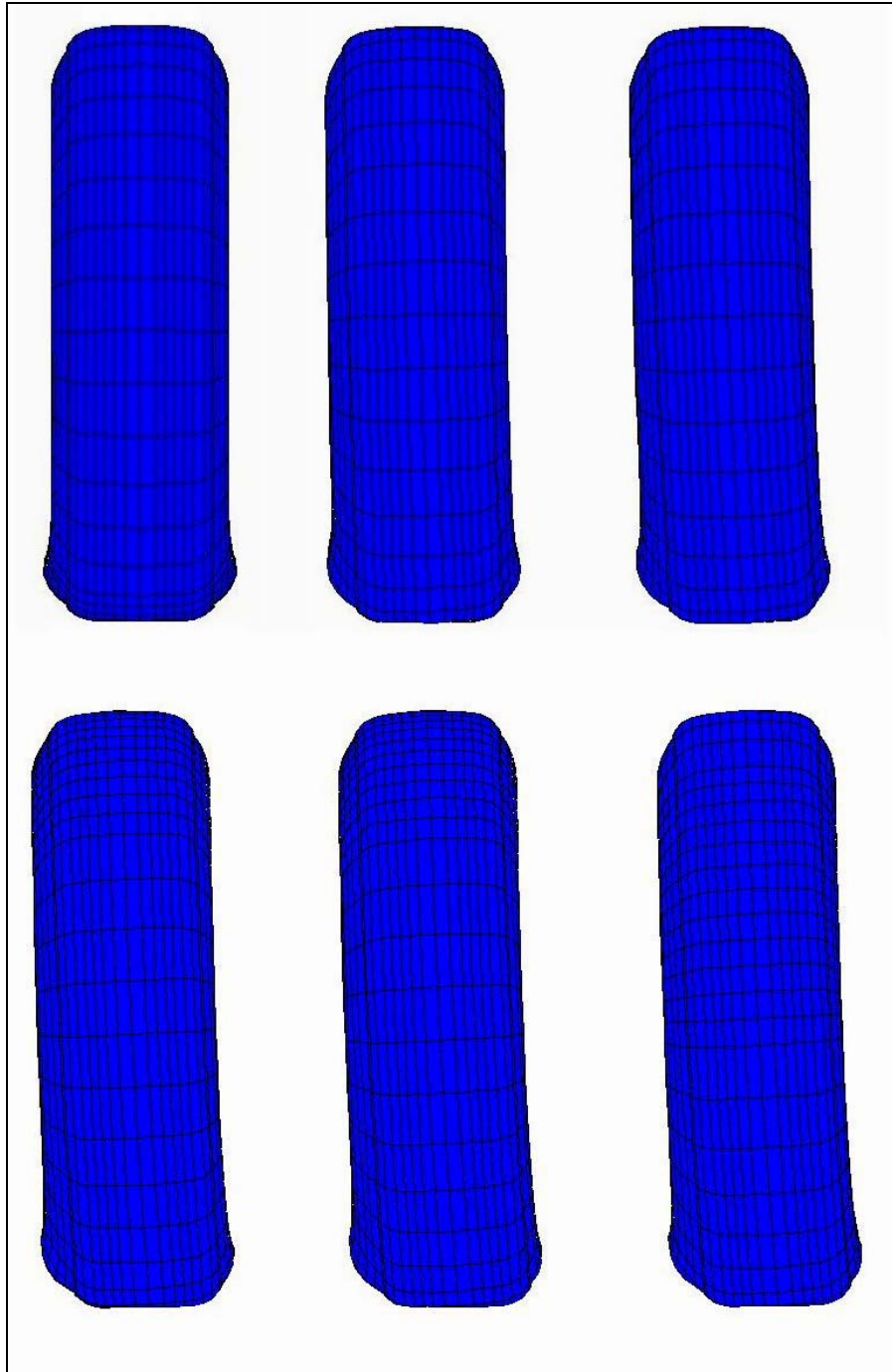
124

Figure 5.4 Steady State Deflected Shapes of the Tire under 3000 N vertical Load
and 0, 2, 4, 6, 8, 10 Degrees Slip Angles

Data from experiments of Tönük (1998) is given in Chapter 2. To compare the finite element model results with the experimental data, two sets are presented in Figure 5.6.
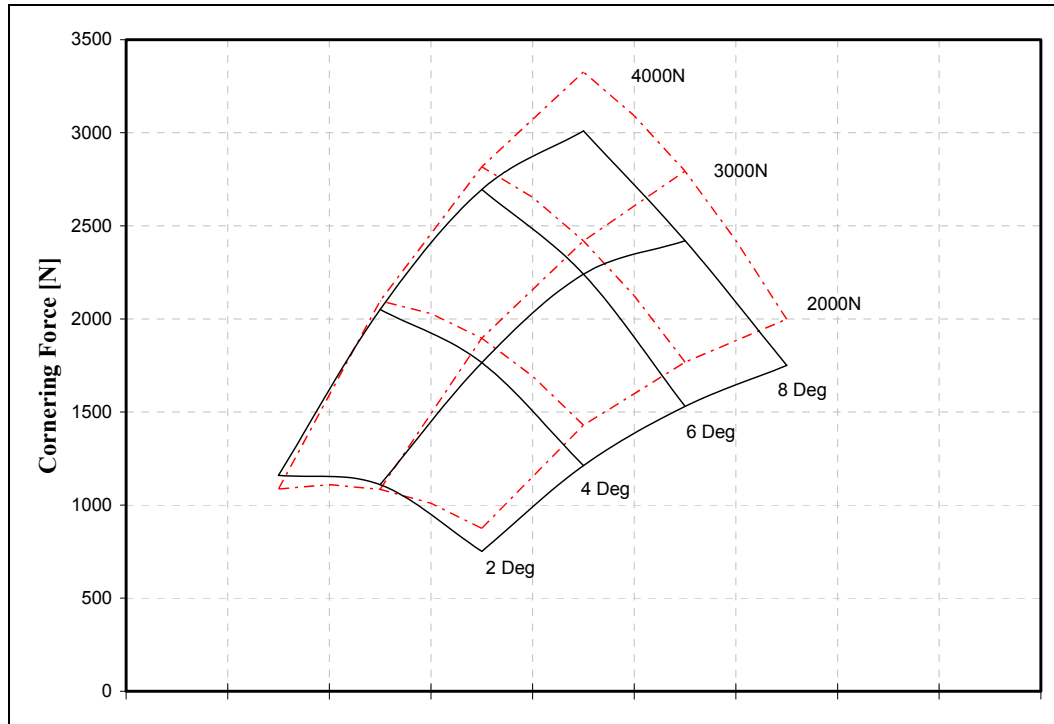

Figure 5.5 Cornering Force Characteristics, 180 kPa. (Red dashed lines are Experimental Data Published by Tönük, 1998)

It is observed that the characteristics from the model tend to saturate earlier and more than the experimental curves particularly at higher slip angles. This is partly due to the fact that at higher slip angles, the normal force tends to drop below the nominal tire load set for the particular test. No control or compensation is attempted in these cases and the nominal tire load value initially intented is used in plotting. Thus the saturation characteristics are sharper in the carpet plot than those of the actual calculations using the model.

126

5.2.1.1 Effect of Traction on Cornering Characteristics

To obtain tire rotation, as explained previously, drum is pushed on to the tire and given an angular velocity. Tire, which is mounted on to the rim, rotates with the traction transmitted by the drum. The node which controls the rim's motion is fixed in all translational degrees of freedom. The other node which controls the rotational degrees of freedom of the rim, is fixed in two axes, and set free in rotation axis of the tire. This is a duplication of the tire test setup, where the tire is rotating with traction transmitted from the drum.

To observe traction free cornering force characteristics, the finite element model is modified. For 3000N vertical force, the rim is assigned an angular velocity, which is calculated according to deflected radius of the tire. Model is run for 4, 6, 8 degrees slip angles. Results are given in Figure 5.6
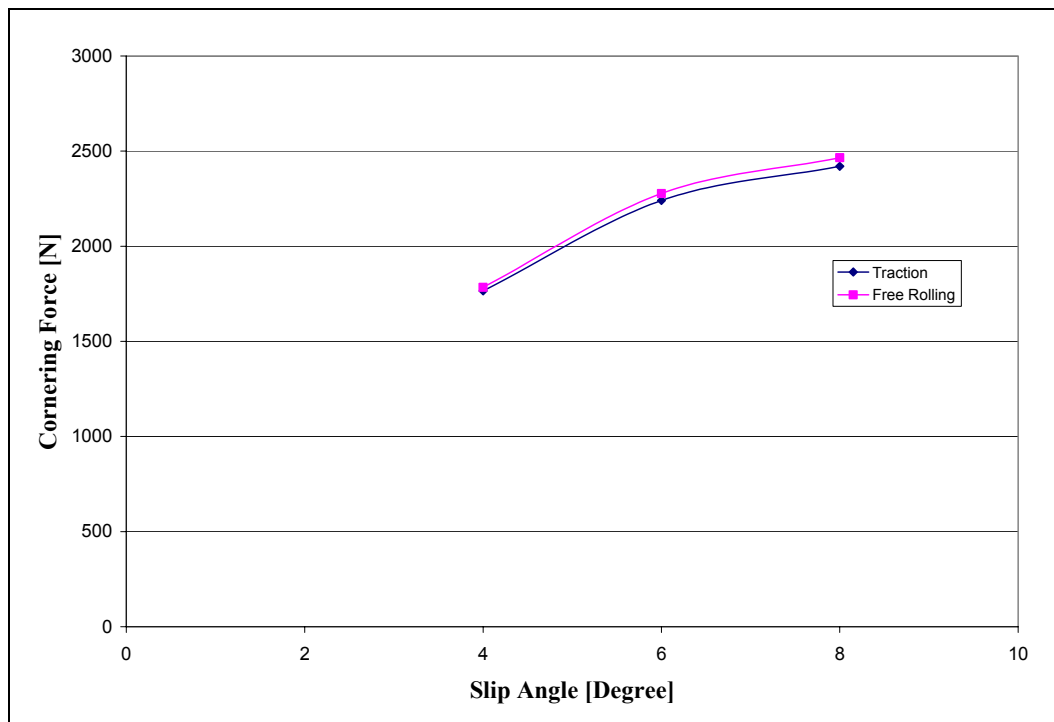

Figure 5.6 Cornering Force versus Slip Angle, Comparison for Traction and Free Rolling, 3000 N

For free rolling, cornering force values are slightly higher than traction rolling. This is expected and due to decreasing portion of the road adhesion used for cornering when traction is applied to the tire. It should be noted that in the literature this effect has not received much attention.

5.2.2 Model with Truss Elements

5.2.2.1 Cornering Force Characteristics

The model, which uses truss elements to model textile, run for 2,4,6,8 and 10 degrees slip angles and 2000, 3000 and 4000 N vertical loads. With decreasing solution time, fine mesh is used to perform cornering analysis. Coarse model also used for comparisons Figure 5.8 shows vertical force versus displacement plot on drum for 180kPa inflation pressure.
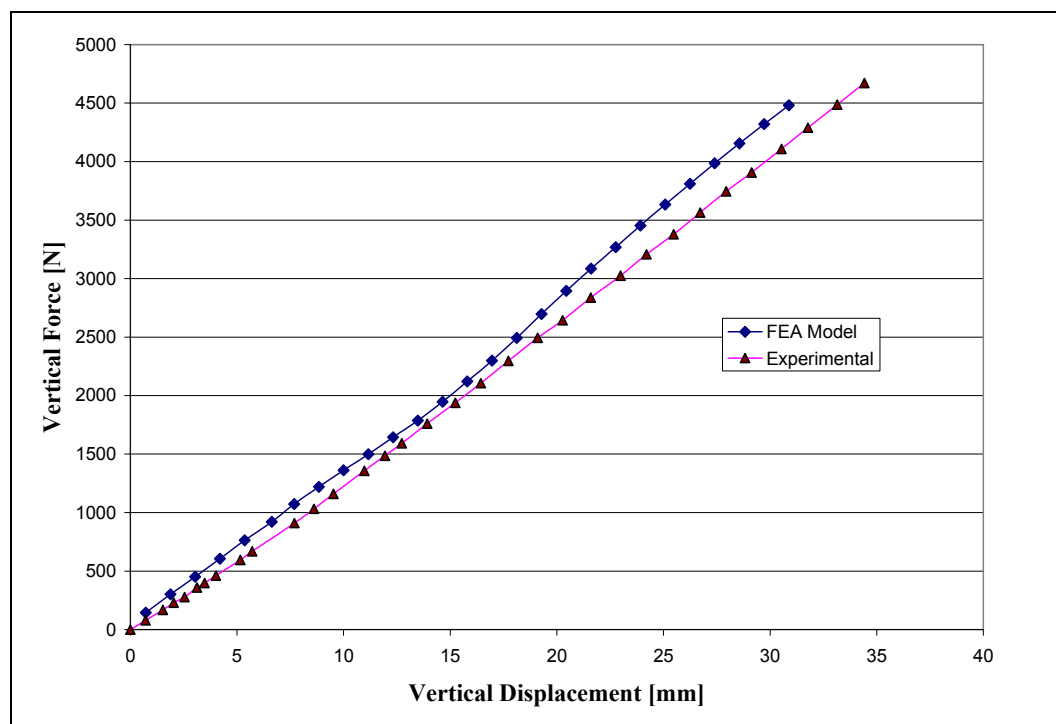

Figure 5.7 Vertical Force Versus Displacement for 180 kPa Inflation Pressure

When the change of vertical force with solution increment or tire rotation is investigated, it is observed that, for given initial vertical displacement, as the slip angle increases the vertical force on the tire drops. Since the contact patch moves laterally, the initial rim displacement does not keep the vertical force constant. As a result of this, for higher slip angles, cornering force saturates a steady state value for a vertical force less than initially set. Change of vertical force is more significant for 6 degrees slip angle and up. Figure 5.8 shows change of vertical force as well as cornering force buildup for 2 and 6 degrees slip angles for comparison. 250 solution increments correspond to 180 degrees rotation of the tire.
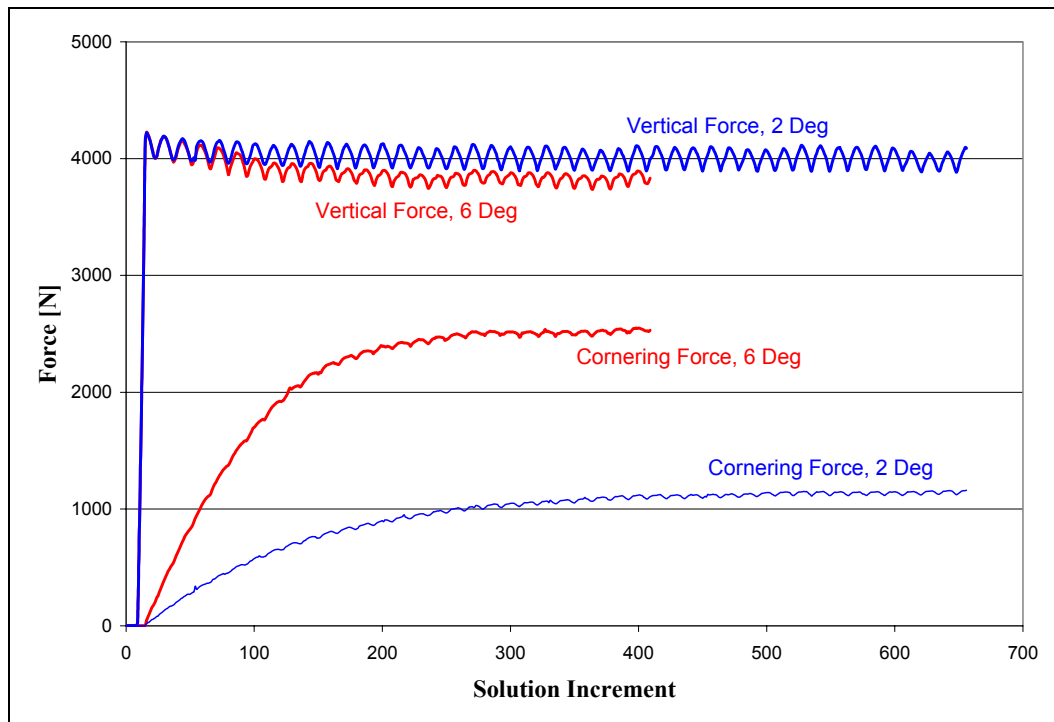

Figure 5.8 Change of Vertical Force and Cornering Force for 2 and 6 Degrees Slip Angles .

For high slip angles, the model underestimates cornering force characteristics more. Reducing vertical force is one of the sources of this effect.

Cornering force values are obtained for smaller vertical forces than set values and plotted on graphs for set values, not corrected for the reduced values.

Figure 5.9 shows cornering force versus solution increment plot for 3000N vertical load and 2, 4, 6, 8 and 10 degrees slip angles, obtained with fine meshed model. When compared with Figure 5.8, due to fine mesh oscillations of plots are reduced.
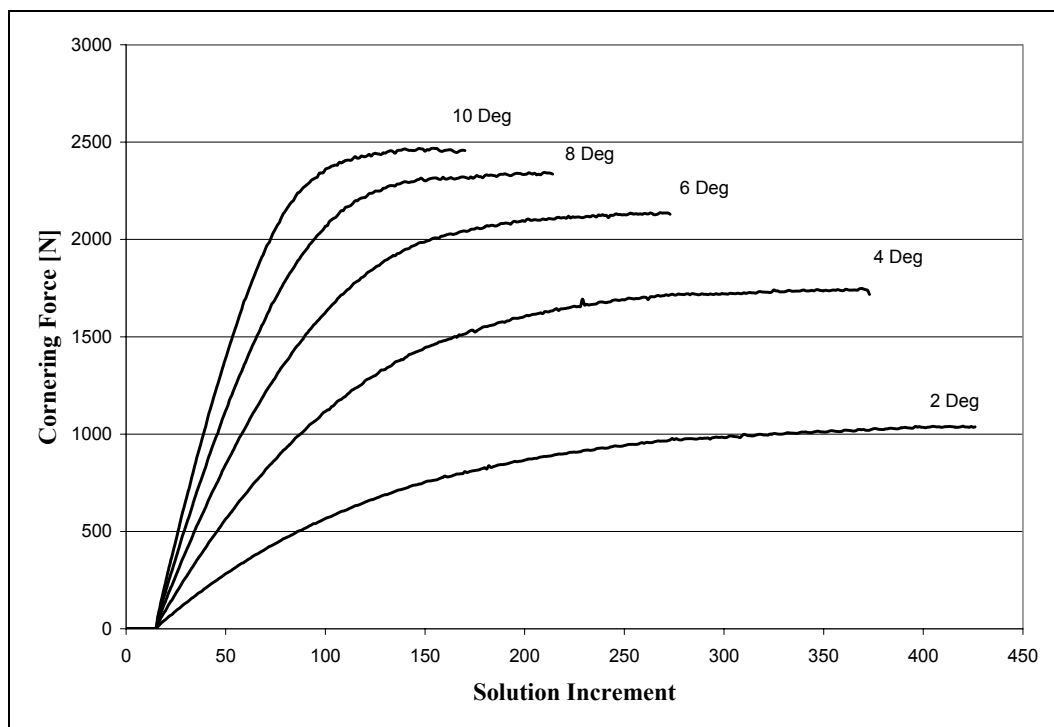

Figure 5.9 Cornering Force versus Solution Increments for 3kN Vertical Load and 2, 4, 6, 8 and 10 Degrees Slip Angles

Figure 5.10 shows top and front views of coarse meshed tire during cornering for 4000N vertical load and 6 degrees slip angle.
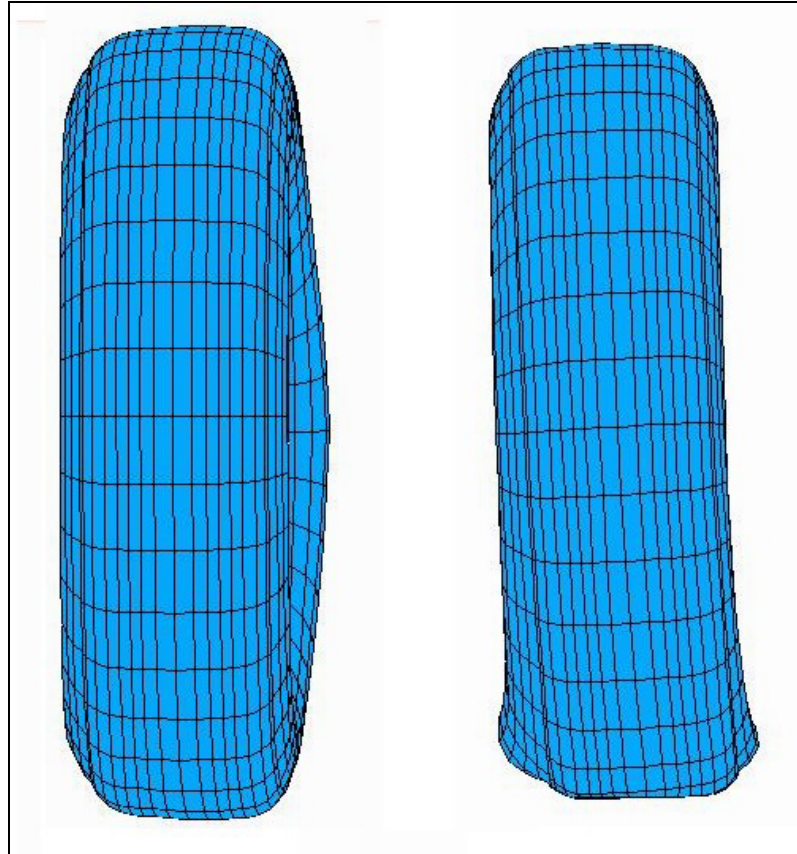
Figure 5.10 Top and Front Views of Cornering Tire, 4000N, 6 Degrees

Cornering force characteristics for 2000, 3000, and 4000 Newton vertical load and 2, 4, 6, 8 degrees slip angles and experimental results published by Tönük (1998) are given in Figure 5.11 together. In Figure 5.12, both experimental and calculated values are plotted for one of the characteristics (4000 N tire load) .

The model convergence is trouble free and half rotation of the tire is completed approximately in 4 hours on a P4 2.6 GHz processor, 1GB ram, 60 GB hard disk equipped computer.
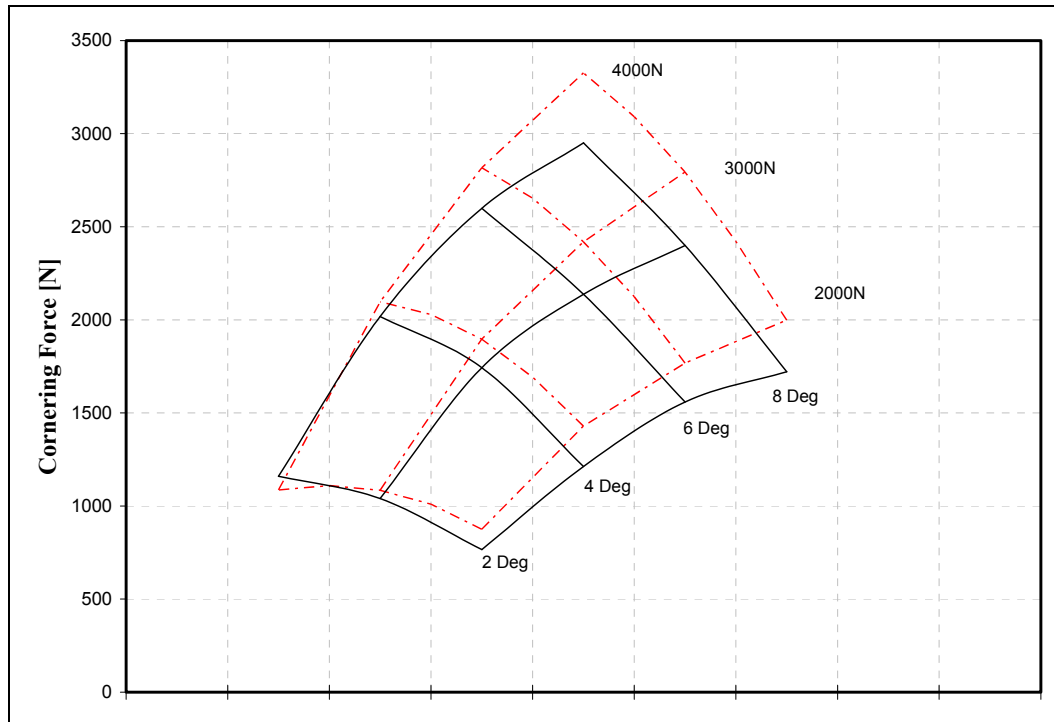
Figure 5.11 Cornering Force Characteristic Obtained by Truss Model (Red
dashed lines are Experimental Data Published by Tönük, 1998)

A comparison of Figures 5.5 and 5.11 readily indicates that in the case of
the model with truss elements, in spite of the extensive gains in computing time,
practically identical results have been obtained.

When buildup and saturation of cornering force plots are compared with
Figures 2.4, Koishi et al (1998), 2.5, Kabe et al (2000), 2.16, Rao et al (2002),
given in Chapter 2, it can be concluded that the calculations from the model in
the present study are more stable. This indicates that the model is superior to
previous models in literature with respect to accumulation of errors during
calculations. It should be noted also that the plots given in these publications
indicate stable results only up to a few degrees of slip angles and even at slip
angles as low as 3 degrees, convergence is not guaranteed.
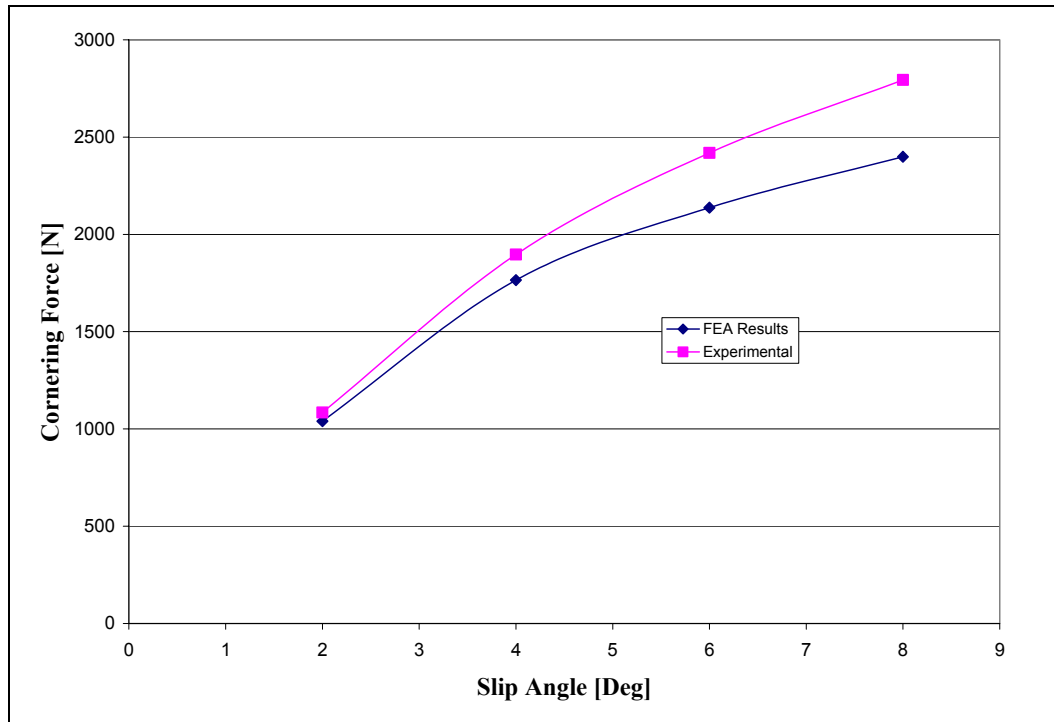
Figure 5.12 Change of Cornering Force with Slip Angle for 3000N Vertical Load and 180kPa Inflation Pressure, Finite Element and Experimental Data by Tönük, 1998

5.2.2.2 Stress State of Textile Belts During Cornering

Because of limitations of MARC, bilinear material behavior of textile could not be modeled as explained in Chapter 4. To see the amount of error introduced, stress state of textile belts are examined for different vertical load and slip angle combinations. Stresses on textile belts for different conditions in vector form are given in Figures 5.13 through 5.17. Lengths and directions of vectors indicate whether the element is in tension or compression and the magnitude of the stress. Arrows pointing out shows tension while arrows pointing to the elements shows compression. Truss elements carry load only in longitudinal direction and no bending capability, so the stresses are in the direction of the

133

elements. The stresses shown in the figures are also color coded, red for the larger and blue for smaller stresses.
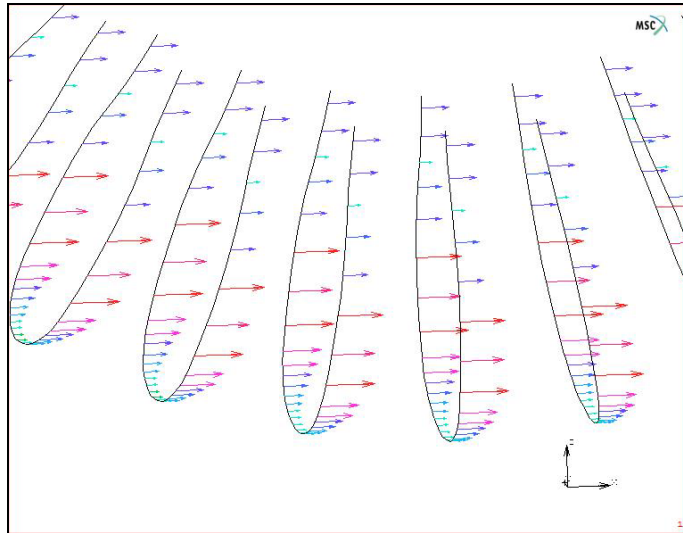
Figure5. 13 Stress Distribution on Textile For 180kPa Inflation Pressure

Figure5. 14 Stress Distribution on Textile around Contact Patch For 2000N
Vertical Load, 180kPa Inflation Pressure
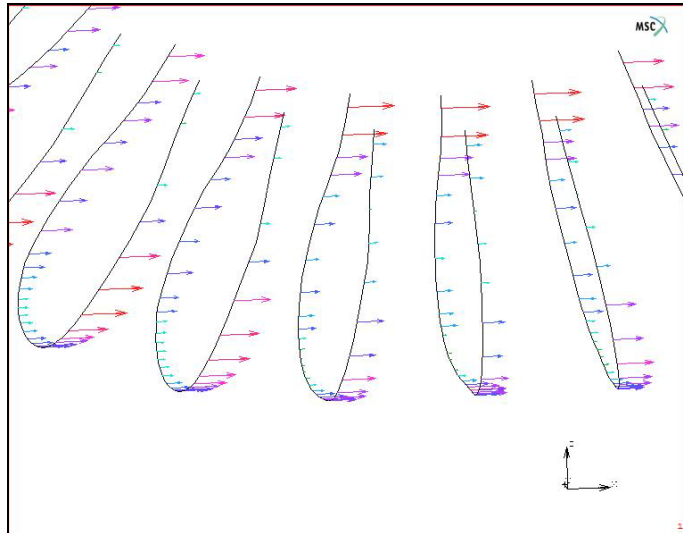
Figure5. 15 Stress Distribution on Textile around Contact Patch During Steady State Cornering for 2000N Vertical Load and 6 Degrees Slip Angle
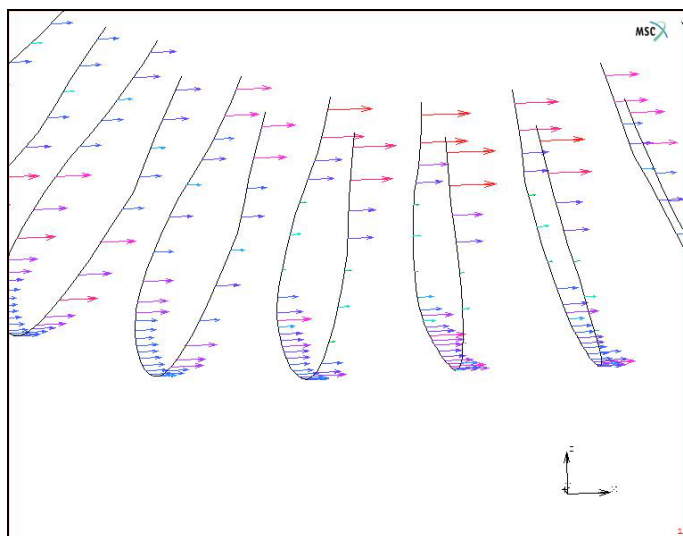
Figure5. 16 Stress Distribution on Textile around Contact Patch For 4000N Vertical Load, 180kPa Inflation Pressure
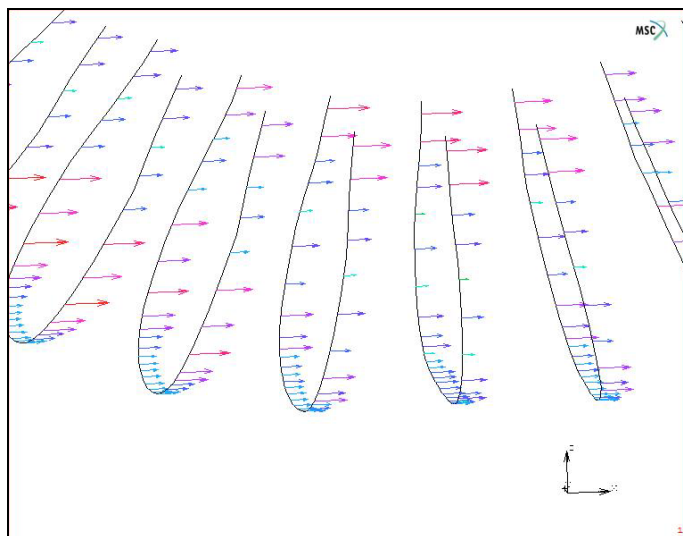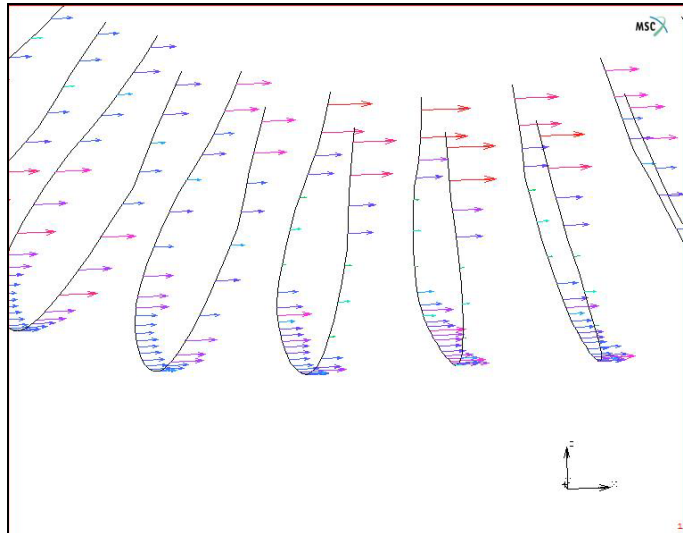
Figure5. 17 Stress Distribution on Textile around Contact Patch During Steady State Cornering for 4000N Vertical Load and 6 Degrees Slip Angle

For medium loads, pre tensioned textile mostly keeps in tension. For high loads and high slip angles, textile goes in to compression for some locations near contact patch.

5.2.2.3 Self Aligning Torque

Because of the special behavior of the node, as explained in Chapter IV, holding rotational degree of freedom of the tire-rim assembly, it is preferred to record the moment on the rim as the self aligning torque. For 4000 N vertical load, self aligning torque versus slip angle plot is given in Figure 5.18. For 2000 N vertical load, self aligning torque versus slip angle plot is given in Figure 5.19.

Self aligning torque increases until medium slip angles and starts to drop as the slip angle increases for 4000 N vertical load. For 2000 N vertical load, self aligning torque is almost constant and for 2, 4 and 6 degrees slip angles.
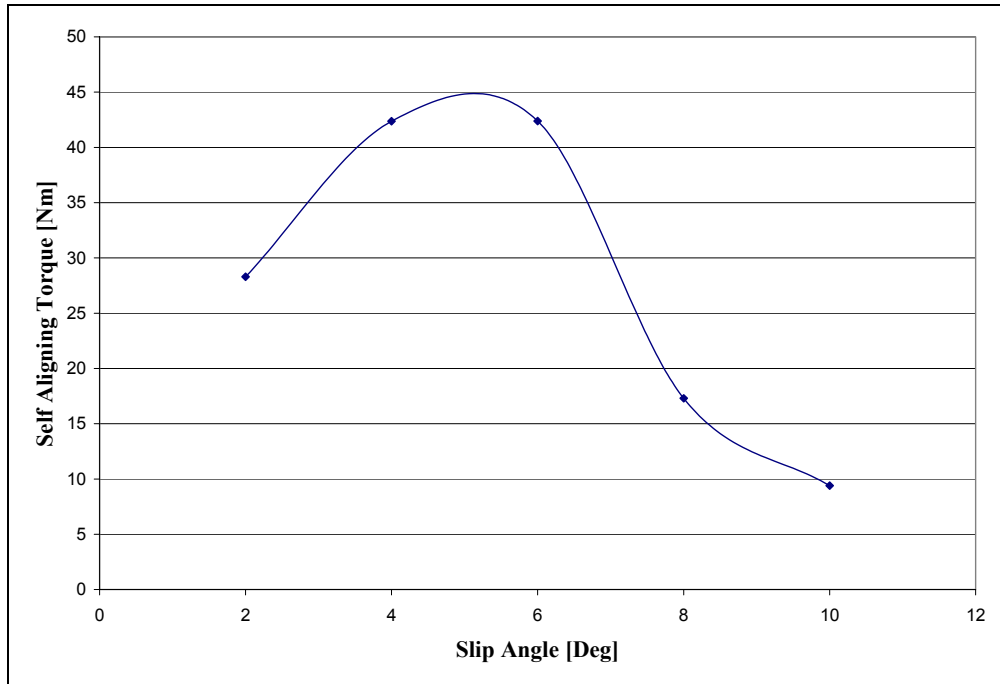
Figure5. 18 Self Aligning Torque versus Slip Angle, 4000 N vertical load
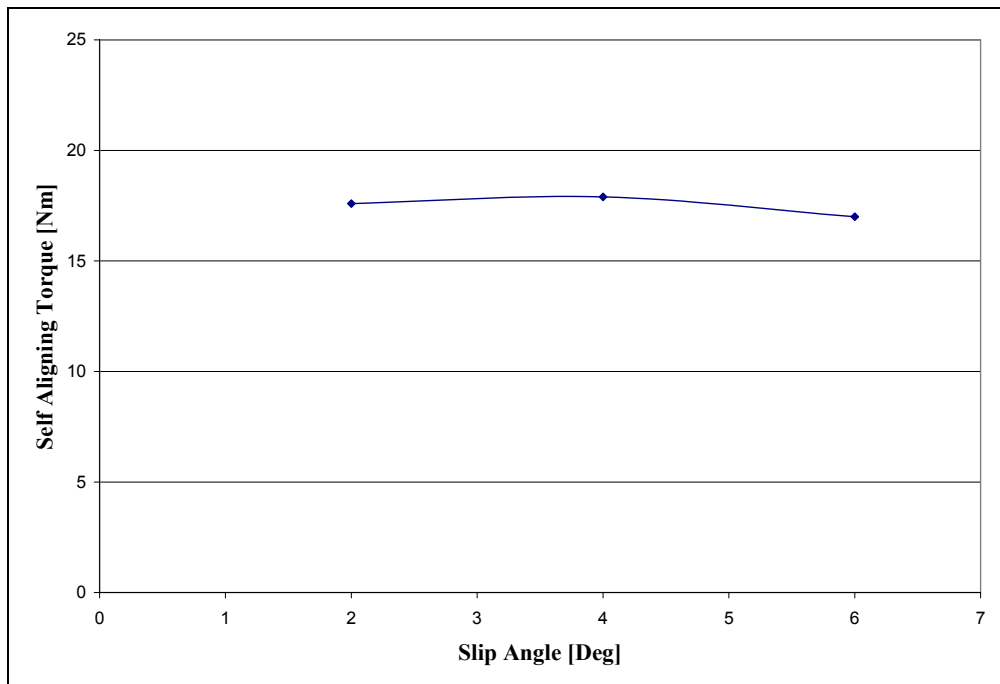
Figure5. 19 Self Aligning Torque versus Slip Angle, 2000 N vertical load

137

5.3 Tire on the Road

Tire cornering analysis is performed on a drum and for different slip angle vertical load combinations performance of the tire is compared. Tire under normal operating conditions rotates on a somewhat flat surface. To compare the cornering force characteristics obtained with the realistic operating conditions, the coarse tire model is run on a flat surface. Slip angle is set by applying road velocity in longitudinal and lateral directions. Tire models are also rotated for 3 complete turns on flat surface to control stability of solution.

Figure 5.20 shows top view of cornering tire on road surface for 4000 vertical load and 4 degrees slip angle. Front view of the same instance is given in Figure 5.21.
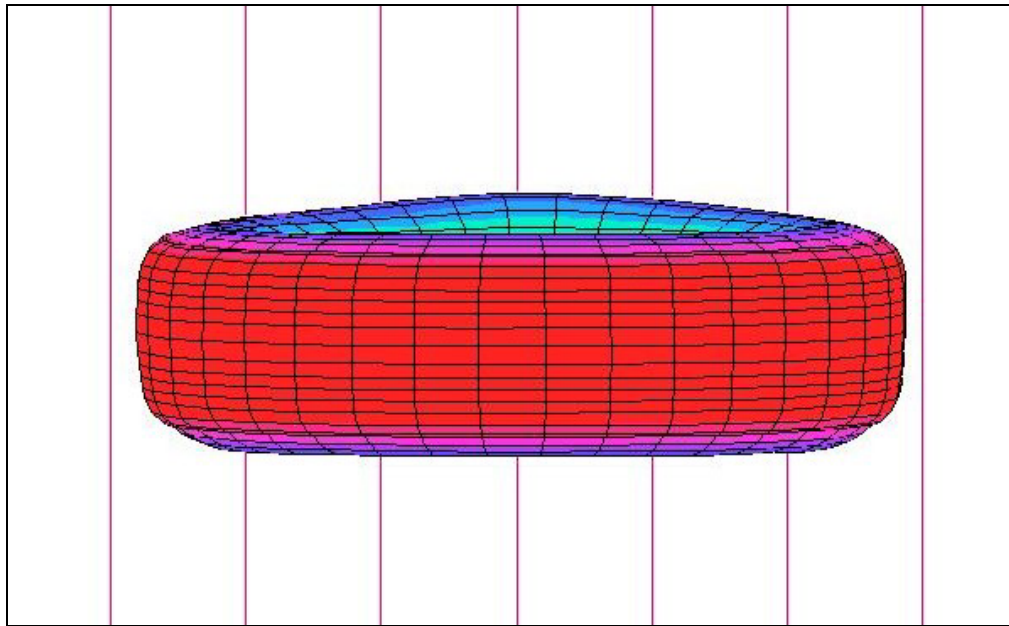
Figure5. 20 Tire Cornering on Road Surface, 180kPa, 4000N, 4 Degrees Slip Angle, Top View.
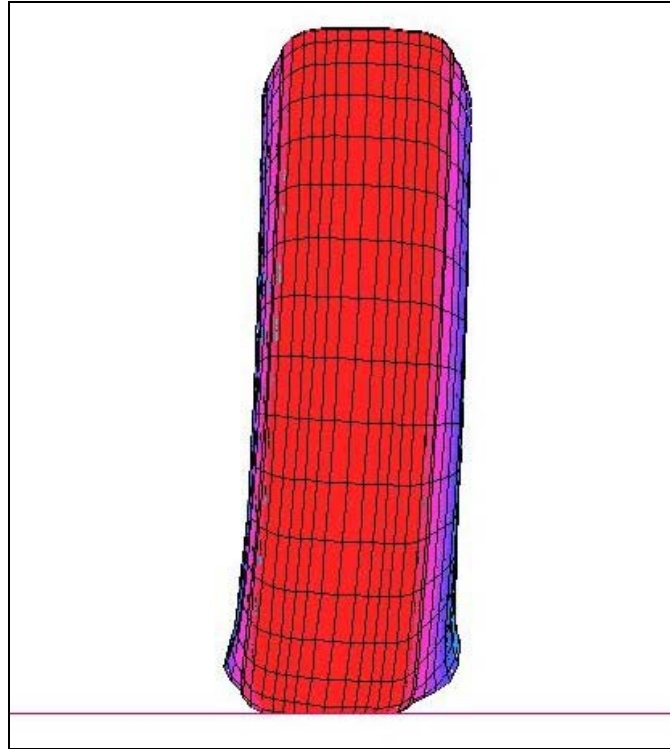
Figure5.21 Tire Cornering on Road Surface, 180 kPa, 4000 N, 4 Degrees Slip Angle, Front View.

Figure 5.22 shows comparison of build up of cornering force on drum and flat surface. It can be concluded from Figure 5.22 that, cornering force builds up faster on flat surface and reaches a higher steady state value. Drum model gives lower estimate for cornering characteristics.
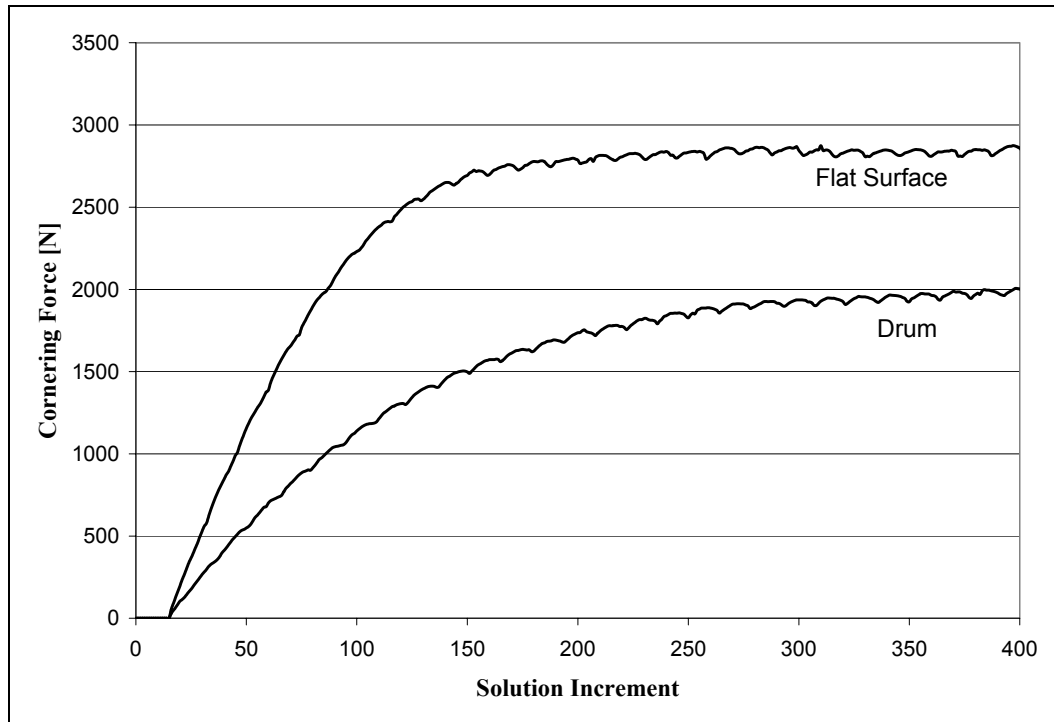
Figure5. 22 .Cornering Force versus Solution Increment Plot of Drum and Flat
Surface, 4000N, 4 Degree Slip Angle, 180kPa Inflation Pressure

5.3.1   A Case Study on the Road

For a vertical load of 4000 N, road surface is moved to rotate the tire.
First the road surface is moved in one direction to give the tire a slip angle. After
half rotation of the tire, road surface is moved in opposite direction at the same
speed and tire is made one complete rotation and direction of road movement
changed to opposite direction again and tire made half rotation. Figure 5.23
shows change of cornering force during the tire motion on the road surface.
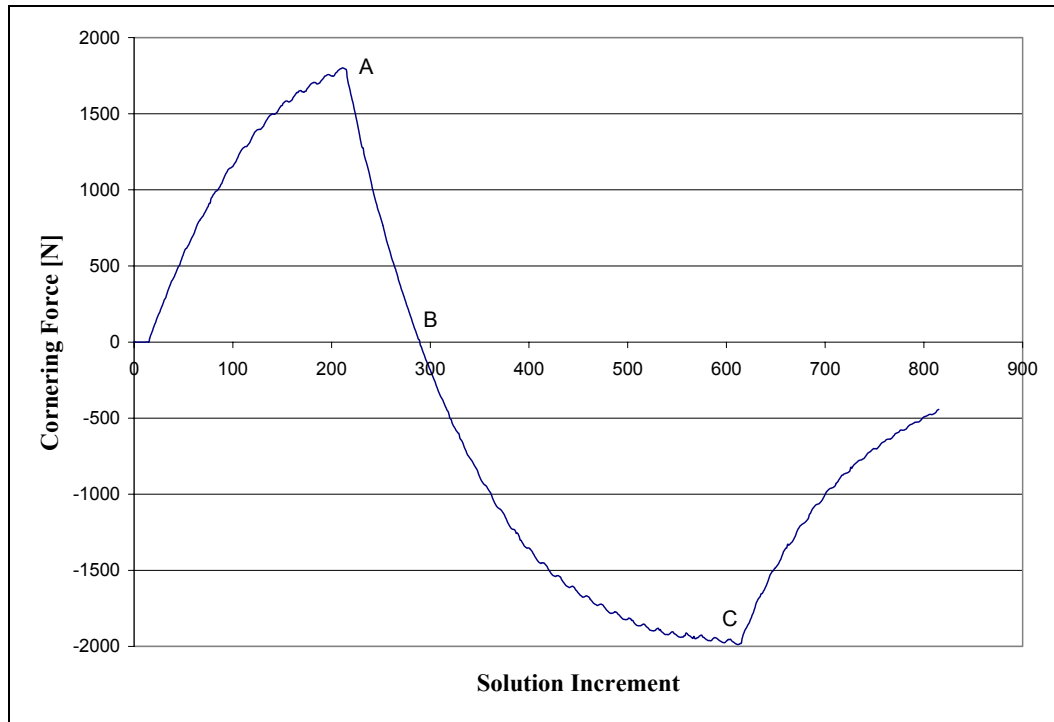
Figure5. 23 Variation of Cornering Force as the Tire Rolls on the Road

For maximum, zero and minimum values of the cornering force, (corresponding to points A, B and C on Figure 5.23) deflected shape of the tire is given in Figure 5.24.

It is noted that the calculations give very clear cornering force variations with a minimum magnitude of oscillations leaving no doubt on the actual results. Actually the oscillations in this study are related to the mesh density rather than the stability of calculations and accumulation of errors.

It can be concluded here that the proposed model can meet the requirements set at the beginning of the study.
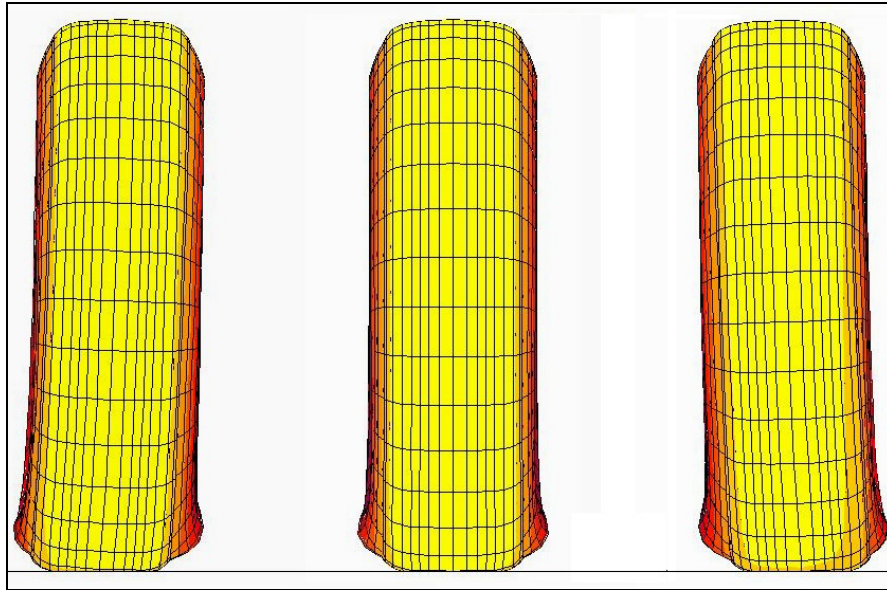
Figure5. 24 .Deflected Shapes of the Tire on the Road for Points A, B and C of

Figure 5.23

CHAPTER 6
CONCLUSION

The application of the Finite Element Modeling and Analysis to research related to pneumatic tires has been quite numerous, starting just after the maturity of the Finite Element Method as a general tool of analysis. There appeared a rather large number of publications in this subject. These applications, however, mainly covered static and dynamic variations of footprints, pressure distributions, stresses, and so on. The cornering force characteristics of pneumatic tires, on the other hand, have received attention only recently and the number of published studies in this particular area is still very small. One of the first of such studies was carried out in the Mechanical Engineering Department of the Middle East Technical University by Tönük, 1998. Tönük's Ph. D. thesis which was later published, Tönük and Ünlüsoy 2001, has been the starting point of this study. The aims of this study, therefore, are based on the results and experiences of the previous study and are directed towards the development of a new model in accordance with the suggestions for future work.

6.1 A new Tire Model

The existing tire model examined and improvements are implemented. Other tire finite element models in the literature are surveyed and modeling techniques are compared.

Drum, which the tire is in contact when rotating, is modeled as a rigid body. This reduces solution time considerably and increases accuracy. A rigid body in Marc is an analytical entity and is not included in the solution like

deformable elements. When a rigid body is represented as an analytical surface, the normal is recalculated at every iteration based upon the current position. This leads to a more accurate solution and faster convergence.

Rebar elements, which used to model cord reinforced rubber has some limitations and deficiencies. Rebar elements do not carry bending and share the same connectivity with the rubber matrix. For the same location, two elements, one for rubber matrix and one for rebar exist. Rebars are oriented for each element, and the orientation should be updated at each solution increment which requires additional computational effort. The last solved increment is considered to orient rebar's directions and positions. This introduces an error to the solution. As the deformation of the tire increases, the error accumulation increase, and for larger slip angles system becomes unstable before the steady state solution is obtained. To solve this problem, combined rubber cord properties are used. Calculated properties are assigned to continuum elements. Solution time is reduced and stability of the system is obtained.

Tire models with different element types are compared for solution time point of view. Layered continuum elements avoid calculating combined properties of plies oriented in different angles but increases solution time. For tread plies and body ply, calculated orthotropic material properties are oriented with a user subroutine. For body plies, a new approach is proposed and this procedure is avoided by using truss elements in reinforcement directions. Doing this drastically reduced the solution time, and allowed using finer mesh to obtain solution in a reasonable time. Truss elements carry only tension or compression, and do not have bending capability. Stress state of the truss elements are closely observed, and for small to medium slip angles and vertical loads, it is noted that, textile pre-tensioned with pressure keeps in tension for all the time. For high slip angles, some of the reinforcements go under small compression. Avoiding orientation of directions of body plies drastically reduced the solution time. A

144

complete carpet plot of the cornering force characteristics can now be obtained on a standard PC configuration in about a week.

6.2 Cornering Study with the New Tire Model

The tire model converged easily and quickly for all slip angle vertical load combinations quite accurately. Tire cornering force characteristics are observed up to 10 degrees slip angle. Effect of traction on cornering characteristics is studied. The analysis is extended to the calculation of self-aligning torque with changing slip angle during the cornering study.

Results of the cornering force analysis are compared with the experimentally obtained data, and concluded that the accuracy of simulation from the proposed tire model is better than that stated in the published studies so far.

The proposed model can be successfully applied to a specific tire and used to study for cornering characteristics for all range of slip angles and tire loads. Even with a coarse mesh, tire rotates more than two complete revolutions after steady state cornering is reached giving an idea of the stability of solution and the amount of error accumulation.

6.3 Recommendations for Future Study

Generic material properties are used to study the sample tire. Each tire in the market has been built up of with different processes and materials, which directly affects the performance. Rubber is not a standard material and properties heavily depend on the process.

Composite theory has many assumptions and sometimes depends on the material properties used. Researchers in composite industry, correlate their calculations for specific applications with tests. Some of the authors obtained

145

cord reinforced rubber properties by tests for use in tire models. For industrial applications, calculated properties of the cord-reinforced rubber should be correlated with tests.

APPENDIX

PROGRAM PARAMETERS

Load Case "Inflate"	
Load Case Type	Static
Non Positive Definite	On
Proceed When Not Converged	Off
Iterative Procedure	Full Newton-Raphson
Cont. of Initial Stress to Stifness	Full
Maximum Number of Recycles	10
Stepping Procedure	Fixed
Number of Steps	5
Convergence Testing	Relative
Convergence Criteria	Residual Force
Relative Force Tolerance	0.1
Load Case "Press Drum"	
Load Case Type	Static
Non Positive Definite	On
Proceed When Not Converged	Off
Iterative Procedure	Full Newton-Raphson
Cont. of Initial Stress to Stifness	Full
Maximum Number of Recycles	10
Stepping Procedure	Fixed
Number of Steps	10
Convergence Testing	Relative
Convergence Criteria	Residual Force
Relative Force Tolerance	0.1
Load Case "Press Drum"	
Load Case Type	Static
Non Positive Definite	On
Proceed When Not Converged	Off

Iterative Procedure	Full Newton-Raphson
Cont. of Initial Stress to Stifness	Full
Maximum Number of Recycles	20
Stepping Procedure	Fixed
Number of Steps	250 to 750
Convergence Testing	Absolute
Convergence Criteria	Residual Force
Max. Absolute Residual Force	20N
Contact Parameters	
Friction Type	Coulomb for Rolling
Method	Nodal Force
Relative Sliding Velocity	0.01
Increment Splitting	Allowed
Seperation Criteria	Force
Seperation Force	1 N
Distance Tolerance	0
Distance Tolerance Bias	0
"Tire" Contact Body Type	Deformable
"Drum" Contact Body Type	Rigid
"Drum" Rigid Body Control	Velocity
"Rim" Contact Body Type	Rigid
"Rim" Rigid Body Control	Load
Distance Tolerance Bias	0
Analysis Options	
Large Displacement	On
Follower Force	On
Elasticity Procedure	Large Strain-Total Lagrange
Solver	Direct Profile
Analysis Dimension	3D

REFERENCES

Akkerman R., J. Huétink, P.N. van der Helm, 1995, "Finite elements and volumes in a Euler-Lagrangian formulation - artificial dissipation versus limited flux schemes", proceedings Complas '95, D.R.J. Owen, E.Onate and E. Hinton, p 2307-2318.

Bai, X., Gall, R., 2000, "Tire Modal Analysis by Finite Element Method", The 19th Annual Meeting and Conference on Tire Science and Technology", Akron, Ohio

Breig, W.F. , 1991, "Finite Element Analysis of Spiral Utilizing Laminate Theory", Dayco Technical Center, Springfield, MO.

Carlson, C.R., Gerdes, J.C., 2002, "Nonlinear Estimation of Longitudinal Tire Slip Under Several Driving Conditions", Standford University, Standford.

Casanova, D., Sharp, R.S., Symonds, P., 2001, "On the Optimisation of the Longitudinal Location of the Mass Centre of a Formula One Car for two Circuits", Whiteways Technical Centre, Chipping Norton, UK.

Chamis, C. C., 1985, "Simplified Composite Micromechanics Equations for Hygral, Thermal, and Mechanical Properties", SAMPE Quarterly, April.

Chang, Y., 2002, "Nonliner FEA Rotating Tire Modeling For Transient Response Simulations", PhD Thesis in Mechanical Engineering, Pennsylvania State University.

Clark, S. K. ,1983, "Theory of the Elastic Net Applied to Cord-Rubber Composites", Rubber Chem. And Technology, 56, 2, 372-389.

Darnell, I.M., 2001, "An Efficient Three-Dimensional Tire Model For Predicting Spindle Loads", PhD Thesis in Applied Mechanics, The University of Michigan.

Dihua, G., Jin, S., Yam, L.H., 2000, "Establishment of Model For Tire Steady State Cornering Properties Using Experimental Modal Parameters", Vehicle System Dynamics, Vol.34, pp 43-56.

Duthoit,J., 1999, " A Micromechanics Based Method For Strength Prediction of Unidirectional Laminae- Approach for a Nonlinear Rubber Based Lamina", MSc Thesis, Virginia Polytechnic Institute and State University, Virginia.

Duvernier,M., 2002, "Tyre Modelling for NVH Engineering in ADAMS", Michelin Tyre Company.

Gerspacher,M., O'Farrell, C.P., 2000, "Tire Compound Materials", KGK Kautschuk Gummi Kunststoffe 53. Jahrgang, Poland.

Ghoreishy, M. H. R., 2001, "Finite Element Analysis of a 6.45-14 Bias Tire Under Contact Load", Iranian Polymer Journal, Vol 10, pp 53-58, Tehran.

Gim,G., Choi,Y., 2001, "Role of Tire Modeling on the Design Process of a Tire and Vehicle System", Hankook Tire Co., Korea ADAMS Users Conference 2001.

Gipser, M., 2000, "FTire, A New Fast Tire Model for Ride Comfort Simulations", Esslingen University of Applied Sciences, Germany.

Hanley,R., Crolla,D.,2000 "Tyre Modeling for Misuse Situations", FISITA World Automotive Congress, Seoul.

Hanley,R., Crolla,D.,2000 "Tire Impact Modeling", Tire Technology International.

Hathaway, R., 2001, "Vehicle Dynamics", Unpublished Lecture Notes, Mechanical Engineering Department,Western Michigan University

Hauke,M., Hanley,R., Crolla,D.,2001 "Tire FE Modeling for Misuse Situations", SAE 2001-01-0748, SAE World Congress, Detroit.

Herrmann, LR., 1965. "Elasticity Equattions for Incompressible and Nearly Incompressible Materials by a Variational Theorem". AIAA Journal, 3, pp. 1896-2000.

Invention & Technology, American Heritage of, 2001, Volume 16 / Number 4, pp. 28-41.

Kabe, K., Koishi, M., 2000, "Tire cornering Simulation Using Finite Element Analysis", Journal of Applied Polymer Science, Vol 78, 1566-1572.

Kennedy,K., 2002, "Finite Element Tire Models Drive the Development of a Virtual Proving Ground", Indiana, Personal Contact.

Koishi,M. , Kabe, K. , Shiratori, M., 1998, "Tire Cornering Simulation Using an Explicit Finite Element Analysis Code", Tire Science and Technology, TSTCA, Vol26, No.2, April-June 1998, pp. 109-119.

Koishi, M., Okano, T., 2000, " A new Computational Procedure to Predict Transient Hydroplaning Performance of a Tire", The 19th Annual Meeting and Conference on Tire Science and Technology", Akron, Ohio

Korkmaz, H., 1999, "Development of a Preprocessor for Finite Element Analyis and a Postprocessor for Experimental Analysis of Pneumatic Tires", Master Thesis, Mechanical Engineering Department, Middle East Technical University, Ankara

Kulikov, G.M, Grigolyuk, E.I, 1988, "Analysis Of Pneumatic Tires", International Centre for Scientific and Technical Information Publications, Moscow.

Kulikov, G.M, Grigolyuk, E.I, 1993, "Methods of Investigation of Multilayered Composite Shells Concerning Mechanics of Pneumatic Tires", International Centre for Scientific and Technical Information Publications, Moscow.

Kulikov, G.M.,1996,"Computational models for multilayered composite shells with application to tires", Tire Science and Technology, Vol. 24, N 1. P.11-38.

Lacombe, J., 2000, "Tire Model For Simulations Of Vehicle Motion On High And Low Friction Road Surfaces", Proceedings of the 2000 Winter Simulation Conference,Orlando

Lamers,E.A.D., Akkerman, R., 2000, "Modelling Of Multi Layer Fabric Reinforcedthermoplastic Laminates",Department of Mechanical Engineering, University of Twente, Enschede.

Longoria, R.G., "Basic Turning Models and Simulations" Unpublished Lecture Notes, Department of Mechanical Engineering, University of Texas at Austin.

Mancosu, F., Savi,D., Speziari,D., "Tyre Models", 2001, 2nd International Colloquium On Vehicle Tyre Road Interaction, Florance.

Marvalova, B., Nam,T.H., 2000, "Identification Of Material Parameters And Deformation Analysis Of An Inflated Cylindrical Membrane Of Composite With Rubber Matrix Reinforced By Textile Cords",

Marvalova,B., 2001, "Prediction Of Elastic Properties Of Textile Reinforced Composites", Technical University of Liberec, Halkova

Marvalova,B., 2001 "Identification Of Orthotropic Hyperelastic Material Properties Of Cord-Rubber Cylindrical Air-Spring", 39th International Conference of Experimental Stress Analysis, Tabor, Czech Republic.

Miller, S.L., Youngberg, B., Millie, A., Gerdes, J.C., Schweizer, P., 2001, "Calculating Longitudinal Wheel Slip and Tire Parameters Using GPS Velocity", Proceedings of the American Control Conference, Arlington, VA June 25-27.

MSC.Marc, 2000, User Manuals Volume A, Theory and User Information

MSC.Marc, 2000, User Manuals Volume C, Program Input

MSC.Marc, 2000, User Manuals Volume B, Element Library

MSC.Marc, 2000, User Manuals Volume D, User Subroutines

Niu, Michael C.Y, "Composite Airframe Structures" ISBN 962-7128-06

Noor, A.K., Andersen, C.M., Tanner, J.A, 1987, "Exploiting Symmetries in The Modeling and Analysis of Tires", Computer Methods in Applied Mechanics and Engineering, 63, 37-81, North Holland.

Olatunbosun, O. A., Burke, A. M., 1997, "Material Property Derivation for Finite Element Modeling of Tires", Presented at the 16th Annual Meeting of the Tire Society.

Olatunbosun, O. A., Burke, A.M., 2002, "Finite Element Modeling of Rotating Tires in Time Domain", Tire Science and Technology, TSTCA, Vol. 30. No.1., January-March 2002, pp 19-33.

Pelc,J. , 2000, "Material Modeling in Cord Rubber Structures", KGK Kautschuk Gummi Kunststoffe 53. Jahrgang, Nr. 10/2000 Poland.

Rao, K.V.N, Kumar, R.K., Bohara, B.C., Mouli, C.P., 2002, "Dynamic Analysis Of Tyre Cornering Behavior Using Explicit Finite Element Code", Proceedings of Twenty First Southeastern Conference On Theoretical And Applied Mechanics, Orlando, Florida.

Rao, K.V.N, Kumar, R.K., Bohara, B.C., Mouli, C.P., 2003, "Transient Finite Element Analysis of Tire Dynamic Behavior", Tire Science and Technology, TSTCA, Vol. 31, No. 2 April-June, pp. 104-127

Shiraishi,M., Iwasaki,N,Saruwatari,T., Hayashi, K., 2002, " Developing FE-Tire Model Library For Durability and Crash Simulations"", 7th International LS DYNA Users Conference, Michigan.

Tangorra, G., 1971 " Simplified Calculations for Mutli-Ply Cord Rubber Sheets as a combination of Cord Rubber Laminates", Proceedings, International Rubber Conference of 1969 Moscow

Tanner, J. A., 1996a. "Computational Methods for Frictional Contact with Applications to the Space Shuttle Orbiter Nose-Gear Tire, Comparisons of Experimental Measurements and Analytical Predictions". NASA Technical Paper 3573.

Tanner, J. A., 1996b. "Computational Methods for Frictional Contact with Applications to the Space Shuttle Orbiter Nose-Gear Tire, Development of Frictional Contact Algorithm". NASA Technical Paper 3574.

Tönük, E., Ünlüsoy, Y. S., 1995a. "Simple Analytic Tire Models for Vehicle Dynamic Simulations, Part I: Models" (in Turkish). 7th National Machine Theory Symposium, İstanbul pp. 606-615.

Tönük, E., Ünlüsoy, Y. S., 1995b. "Simple Analytic Tire Models for Vehicle Dynamic Simulations, Part II: Benchmarking" (in Turkish). 7th National Machine Theory Symposium, İstanbul pp. 616-623.

Tönük, E. ,1998. "Computer Simulation of Dynamic Behavior of Pneumatic Tires", Ph. D. Thesis, Mechanical Engineering Department., Middle East Technical University, Ankara

Tönük, E. Ünlüsoy, Y. S., 2001, "Prediction of Automobile Tire Cornering Force Characteristics by Finite Element Modeling and Analysis", Computers and Structures.

Ünlüsoy, Y. S. , 1993. "Automotive Engineering II". Unpublished Lecture Notes.

Ünlüsoy, Y. S. , 2000. "Vehicle Dynamics". Unpublished Lecture Notes.

Vossberg, S.M., Ford, J.L., 1998, "Fundementals of Cord Rubber Laminate Behavior with Applications to Tire Behavior and FEA Analyses", Presented at the 1998 Conference of Tire Science and Technology, Akron.

Wake, William Charles 1969, The analysis of rubber and rubber-like polymers, by William C. Wake, New York, Wiley Interscience 47191701

Zhang,F., Wan,Z., Du, X.,2002, "Mechanical Properties of Nylon Cord–Rubber Composite Subjected to Biaxial Tensile Loads" , Center for Composite Materials, Harbin Institute of Technology,Harbin, China

CURRICULUM VITAE

Mehmet Akif Erşahin is born in Manisa on August 13, 1970. He graduated from Kayseri Science Highschool at 1987. He received his B.Sc. degree in 1993 and M. Sc. degree in 1996 in the Mechanical Engineering Department, Middle East Technical University. He worked as a research assistant in the same Department from 1993 to 2000. Since March 2000, he is working as Technical Manager of Design Group at Environmental Tectonics Coorparation at Southampton, PA, USA. His main areas of work are finite element analysis of steel structures, design and analysis of composite structures, computer aided design and manufacturing, and hydraulic power circuits.